NO_X Reduction Using an Electrochemical Cell with NO_X adsorbents

Shao, Jing

Publication date:
2013

Document Version
Publisher's PDF, also known as Version of record

NO_x Reduction Using an Electrochemical Cell with NO_x adsorbents

PhD Thesis

Jing Shao

Department of Energy Conversion and Storage

Technical University of Denmark

May 2013

Preface

This thesis is submitted to the Technical University of Denmark as a partial fulfillment of the requirements for the degree of Ph.D. The thesis at hand is the product of three-year work conducted at Department of Energy Conversion and Storage, Technical University of Denmark. The Ph.D. study was supervised by senior researcher Kent Kammer Hansen and the daily work was carried out in the Gas purification work group. The Ph.D. project was financed by the Danish Strategic Research Council under contract no. 09-065186.

First and foremost, I would like to thank my fantastic supervisor Kent Kammer Hansen for all the help, guidance, and encouragement throughout my Ph. D. study and for always being available for questions and discussions.

I would like to thank my lovely colleagues in the Gas Purification Group for making my time at Risø a really great experience. A special thanks to Marie Lund Traulsen for being my social mentor and for giving me so much help with the work and the daily life.

Thank all the technical staffs for helping me with setups and equipments. A special thanks to Ole Hansen, Jens F. S. Borchsenius, and Henrik Henriksen for being so helpful and patient.

I would like to thank my mother for always giving me the warm understanding and support. Last, I want to thank my husband Youkun, for his love, care, and encouragement during the last three years.

Abstract

This thesis studied the electrochemical cells modified by NO_x adsorbents for the NO_x reduction under O_2-rich conditions. The structure of a multilayer electrochemical cell with a NO_x adsorption layer was optimized by removing a yttria-stabilized zirconia (YSZ) cover layer coated on a Pt/Ni/YSZ electrode. It was found that the NO_x removal properties of the electrochemical cell were dramatically enhanced through this optimization, which was attributed to the extensive release of selective reaction sites for NO_x species and a strong promotion for NO_x reduction from the interaction of the directly connected adsorption layer with the electrode.

Ag and $(La_{0.85}Sr_{0.15})_{0.99}MnO_3$ (LSM) were investigated as electrode materials to substitute for Pt and Ni. Selective NO_x reduction in the presence of excess O_2 could be achieved for both Ag and LSM/$Ce_{0.9}Gd_{0.1}O_{1.95}$ (CGO) electrodes by modifying the electrodes with NO_x adsorbents. Performances of 82% NO_x conversion with 7.7% current efficiency and 100% N_2 selectivity for the Ag electrode, and of 85% conversion with 4% current efficiency and 74% N_2 selectivity for the LSM/CGO electrode were achieved in 1000 ppm NO and 8-10% O_2 at 500 °C with the addition of a K-Pt-Al_2O_3 adsorption layer.

The effects of the NO_x adsorbents on the electrode processes were characterized by electrochemical impedance spectroscopy (EIS). The impedance analysis revealed that the NO_x adsorbents greatly enhanced the electrode activity, mainly contributed by the promotion of adsorption, surface diffusion, and transfer of NO_x and O_2 species at/near the triple phase boundary region, and the formation of intermediate NO_2. Severe degradation was observed on both electrodes following long-term operation, caused by the corrosion of the Ag electrode covered by a nitrate melt, or associated with a profound change in the microstructure for the LSM/CGO electrode.

Two different approaches to modify the electrochemical cell with NO_x adsorbents, adding a Ba-Pt-Al_2O_3 adsorption layer on top of the electrode or impregnating of the BaO into the electrode, were studied on a LSM/CGO symmetric cell. A comprehensive comparison between the two approaches was provided based on systematic investigations, including conversion measurements, degradation tests, microstructure observations, and impedance characterization. It was found that both approaches significantly increased the activity and selectivity of NO_x reduction on the LSM/CGO symmetric cell, by enhancing the adsorption and storage of NO_x species, or by providing reaction sites for direct nitrate

reduction. Cells with adsorption layers exhibited a superior performance at low temperatures (350 and 400 °C) and at low voltages (1.5 to 2 V) due to the NO oxidation ability of the Pt catalyst, although its performance was relatively poor at elevated temperatures and voltages due to the impedance of the diffusion of NO_x to the reaction sites by the adsorption layer. The presence of a strong NO oxidation catalyst was important for lowering the operating temperature and minimizing the power consumption of the electrochemical cell. Square-wave (SV) polarization balanced the trapping and reduction rates of NO_x species on the electrochemical cells, further improving the NO_x reduction activity relative to that observed under direct current (DC) polarization.

Abstrakt

I denne afhandling er elektrokemiske celler modificeret med NOx-adsorptionsmaterialer til NOx-reduktion under iltrige forhold blevet undersøgt. Strukturen af en multilags elektrokemisk celle med et NOx-adsorptionslag blev optimeret ved at fjerne et yttriastabiliseret zirkonia (YSZ) dæklag på en Pt/Ni/YSZ-elektrode. Det blev konstateret, at reduktion af NOx vha. af den elektrokemiske celle blev øget vha. denne optimering. Dette blev tilskrevet frigivelse af selektive reaktionssites for NOx-specier og en stærk promovering af reduktionen af NOx grundet direkte kontakt mellem adsorption lag og elektroden.

Ag og $(La_{0.85}Sr_{0.15})_{0.99}MnO_3$ (LSM), blev undersøgt som elektrodematerialer til erstatning for Pt og Ni. Selektiv reduktion af NO_x under netto oxiderende forhold kunne opnås for både Ag- og LSM/$Ce_{0.9}Gd_{0.1}O_{1.95}$ (CGO)-elektroder ved at modificere elektroderne med NO_x-adsorptionsmaterialer. En ydeevne på 82% NO_x-omdannelse med 7,7% strømudbytte og 100% N_2-selektivitet for Ag-elektroden, og 85% omdannelse med 4% strømudbytte og 74% N_2-selektivitet for LSM/CGO-elektroden blev opnået i 1000 ppm NO og 8-10% O_2 ved 500°C med tilsætning af et K-Pt-Al_2O_3 adsorptionslag.

Virkningerne af NO_x-adsorptionsmaterialer på elektrodeprocesserne blev undersøgt vha. af elektrokemisk impedansspektroskopi (EIS). Impedansanalysen viste, at NO_x-adsorptionsmaterialer forbedrede elektrodeaktiviteten betydeligt, primært ved at fremme adsorption, overflade diffusion, og overførsel af NO_x- og O_2-specier på/ved tre-fasegrænsen, og gennem dannelsen af mellemproduktet NO_2. Kraftig degradering blev observeret på begge elektroder efter langvarig drift, forårsaget af korrosion af Ag elektrode pga. smeltet nitrat, eller pga. en markant ændring i mikrostrukturen i LSM/CGO-elektroden.

To forskellige metoder til at ændre den elektrokemiske celle med NO_x-adsorptionsmaterialer, enten ved at tilføje et Ba-Pt-Al_2O_3-adsorptionslag oven på elektroden eller ved imprægnering af BaO i elektroden, blev undersøgt på en LSM/CGO symmetrisk celle. En omfattende sammenligning mellem de to metoder blev foretaget gennem systematiske undersøgelser, herunder omsætningsmålinger, degraderingstest, mikrostrukturobservationer, og impedanskarakterisering. Det blev konstateret, at begge tilgange signifikant øgede aktiviteten og selektiviteten mod NO_x-reduktion på en LSM/CGO symmetrisk celle ved at forbedre adsorption og lagring af NO_x-arter eller ved at danne reaktionssites for direkte reduktion af

nitrat. Celler med adsorptionslag udviste en overlegen ydeevne ved lave temperaturer (350° og 400° C) og ved lave spændinger (1,5 til 2 V) pga. Pt's evne til at oxidere NO, selv om dens ydeevne var relativt ringe ved forhøjede temperaturer og spændinger på grund af diffusion af NO_x til reaktionsstederne ved adsorption laget. Tilstedeværelsen af en stærk NO oxidationskatalysator var vigtigt for at sænke driftstemperaturen og minimere effektforbruget af den elektrokemiske celle. Square-wave (SV) polarisering balancerede adsorption- og reduktionsaktiviteten for NO_X-arter på de elektrokemiske celler, hvilket yderligere forbedrede NO_X-reduktionaktiviteten i forhold til hvad der blev observeret under jævnstrømspolarisering (DC).

Table of Contents

Chapter 1 Introduction

1.1 NO_x emission from diesel engine exhaust

Diesel engines offer superior fuel efficiency compared to gasoline engines (45% vs. 30%, respectively). Widespread use of diesel engines could lower the fuel consumption of transport vehicles, reducing emissions of greenhouse gases and decreasing dependencies on petroleum fuels.[1] In Europe, around 50% of new cars are sold with a diesel engine.[2] In the USA and Japan, diesel engines only accounts for approximately 3% and 0.4%, respectively, of the car sales.[3, 4] One of the technical obstacles to broad implementation of diesel cars is the inherent difficulty of removing nitrogen oxides (NO_x) from diesel exhaust. Unlike conventional gasoline exhaust, which is almost oxygen-free due to the stoichiometric combustion process, diesel exhaust contains excess oxygen from combustion at high air-to-fuel ratios (Table 1.1).[5] This oxygen-rich environment deactivates the traditional three-way-catalysts used to reduce NO_x with CO or hydrocarbons, making the removal of NO_x extremely challenging.

Table 1.1 Example of exhaust compositions and conditions for diesel engines and gasoline engines.[5]

Exhaust components And conditions	Diesel Engines	Gasoline Engines
NO_x	350-1000 ppm	100-200 ppm
Hydrocarbon	50-330 ppm C	20,000-30,000 ppm C
CO	300-1200 ppm	1-3%
CO_2	7%	10-13%
O_2	10-15%	0.2-2%
H_2O	1.4-7%	10-12%
SO_x	10-100 ppm	~20 ppm
Particulate Matter	65 mg m^{-3}	
Temperatures	r.t.-650 °C	r.t.-1000 °C
Space Velocity	30,000-100,000 h^{-1}	30,000-100,000 h^{-1}
Air-to-Fuel	~26	~14.7

The concentration of NO_x in diesel exhaust is normally in the range of 300 to 1000 ppm, depending on the type of engine and the driving conditions, which is typically significantly higher than that in gasoline exhaust. NO_x is the collective name for the compounds of nitric oxide (NO) and nitrogen dioxide (NO_2).

NO is usually the dominant species of NO_x in exhaust gases (90-95%)[6] and can be produced during the combustion process in three ways:[7] 1) thermal NO, formed from oxidation of atmospheric nitrogen; 2) prompt NO, formed by reaction of atmospheric nitrogen with hydrocarbon radicals in fuel-rich regions of the flames; and 3) fuel NO, formed from oxidation of nitrogen bound in the fuel. For diesel engines, thermal NO is the main source of NO emission due to the lean combustion conditions. The process of thermo-NO formation can be described by the Zeldovich mechanism:[8]

$$N_2 + O = NO + N \quad (1.1)$$

$$N + O_2 = NO + O \quad (1.2)$$

NO_2 is a secondary product, mainly formed by oxidation of NO with hydroperoxide redicals in cooler regions of the flames (< 800 °C) during combustion processes(Eq. 1.3) [9–11] or by the equilibrium of NO/NO_2 when the exhaust gases are vented after combustion (Eq. 1.4).[12]

$$NO + HO_2 = NO_2 + HO \quad (1.3)$$

$$2NO + O_2 = 2NO_2 \quad (1.4)$$

NO_x is detrimental to human health[13] and contributes to the formation of acid rain,[14] the generation of photochemical smog,[15] and the depletion of the protective stratospheric ozone layer.[16] For these reasons, increasingly stringent limitations have been imposed worldwide on NO_x emissions from mobile sources (Table 1.2).[17] Since the emerging standards are below what industry can achieve by adjusting diesel engines, the use of NO_x control systems are required to meet these tighter limit on NO_x emissions.[18]

Table 1.2 Emission standards for diesel passenger cars in Europe and US.[17]

Europe	Implementation Year	NO_x (g km^{-1})	US	Implementation Year	NO_x (g $mile^{-1}$)
Euro 4	2005	0.25	Tier 1	1997	1.0
Euro 5	2009	0.18	Tier 2 Bin 5	2007	0.07
Euro 6	2014	0.08			

1.2 NO_x control technologies

The process for removal of NO_x from exhaust gases is to 'unfix' the molecules of NO_x back to N_2 at temperature lower than 700 °C, where NO_x species are thermodynamically unstable, yet kinetically extremely stable.[12, 19] The direct catalytic decomposition without added any reductant was considered to be the most advantageous means for NO_x removal, however, its NO_x conversion in diesel exhaust is too low to be of practical use. One solution is to promote catalytic reduction with the addition of reductants, which are currently the main means of NO_x removal from diesel exhaust. These include selective catalytic reduction (SCR), NO_x storage and reduction (NSR), and lean NO_x catalysts (LNC). This work is based on another option: electrochemical NO_x reduction, which consisted of the use of electrical power (electrons) to replace the reductants and reduce NO_x to N_2 at the polarized electrodes of a solid state cell. Both SCR and NSR have been commercialized. The LNC and electrochemical NO_x reduction are currently under development. Each of these technologies will be described in detail in the following sections.

1.2.1 Selective catalytic reduction (SCR)

The selective catalytic reduction (SCR) process has been used in stationary applications, such as power plants and generators, for decades. The application of SCR in automotive vehicles started on heavy-duty trucks in 2003 and has spread to most diesel passenger cars today.[20] The SCR employs the catalysts which are able to catalyze the selectively reduction of NO_x to N_2 with ammonia added into the exhaust stream, as showing in equations 1.5 and 1.6.[21–23]

$$4NO + 4NH_3 + O_2 = 4N_2 + 6H_2O \quad (1.5)$$

$$2NH_3 + NO_2 + NO = 2N_2 + 3H_2O \quad (1.6)$$

The source of ammonia can be liquid or gaseous ammonia or liquid urea which decomposes in the exhaust stream to ammonia. For the mobile applications, a 32.5 wt% urea solution is used for the reason of toxicity and safety. Recently, a solid ammonia storage and delivery system has been developed by Amminex, which stores ammonia inside a solid $SrCl_2$ cube, which has a volume density similar to that of liquid ammonia, and releases gaseous ammonia when heated.[24]

The catalysts used for SCR in industry are mainly TiO_2-supported WO_3/V_2O_5 or MoO_2/V_2O_5. These catalysts can operate in the temperature range of 200 to 500 °C, but deactivate quickly if exposed to temperatures above 600 °C.[18, 25] Metal-exchanged zeolite catalysts have been proposed as a new type of SCR catalyst to broaden this temperature window, with most of the attention focused on Fe- and Cu-zeolites.[26]

The SCR process achieves the highest deNO_x efficiency (>90%) among the current NO_x control technologies, but also has some drawbacks.[20] The use of ammonia requires the installment of an on-board storage and delivery system and an electronic control module to meter out the ammonia, which increases the initial cost and introduces problems related to storage, transport management, and development of a distribution network. Ammonia is toxic; any extra ammonia in the exhaust gas will became a secondary pollutant, which increases the complexity of the required on-board system to ensure an accurate measurement and dosing of ammonia.

1.2.2 NO_x storage and reduction (NSR)

The NO_x storage and reduction (NSR) process is operated via cyclic switching of the state of the engine between lean- and rich-modes. The NSR catalysts adsorb and store NO_x during the lean-mode until the storage sites are saturated; a rich spark is imposed afterwards to introduce rich exhaust to the catalysts to reduce the stored NO_x to N_2 using the surplus fuel or incompleted combustion products (hydrocarbon or CO) in the exhaust. NSR is currently the leading technology for smaller lean-burning passenger cars in Europe and is of interest in applications with limited space or in which urea usage is difficult.[20, 27] The NSR catalysts typically consist of 1-3 wt% Pt with 10-20 wt% K or Ba dispersed over an Al_2O_3 support.[25] The reaction mechanism of NSR is represented in figure 1.1.[28]

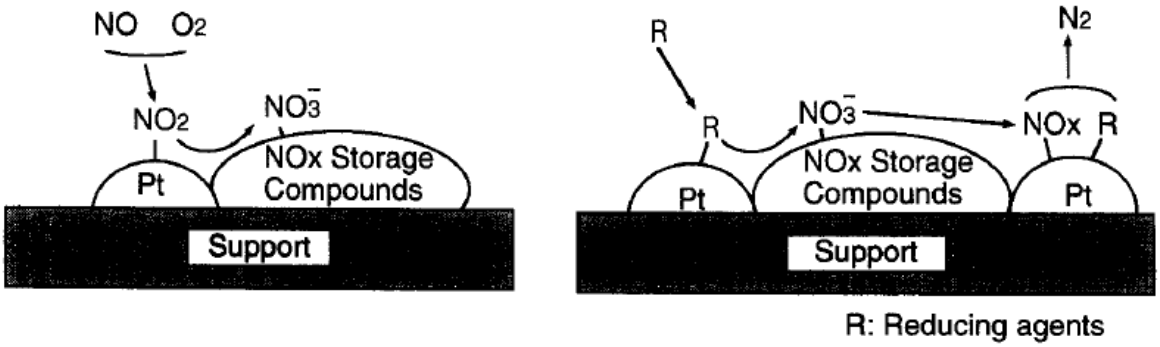

Figure 1.1 NO_x storage and reduction mechanism of NSR catalysts.[28] (reprint permit from Elsevier 2013)

The deNO_x efficiency of NSR catalysts is usually 70-80% under realistic conditions.[20] Chief drawbacks of this technology are the low resistance against sulfur poisoning and the requirement of a sophisticated, adaptive control system to control the state of the engine.[25]

1.2.3 Lean NO_x catalysts (LNC)

Lean NO_x catalysts (LNC), also known as hydrocarbon-selective catalytic reduction (HC-SCR), utilize fuel as the reductant and potentially cheap catalysts such as Ag/Al_2O_3 and Cu-zeolites.[29] But the reductant has to be dosed continually, unlike with NSR where the reductant is needed merely during the rich-burn phase. Thus, the fuel penalties are relatively high (6%). Another drawback is that there is a restricted temperature window for LNC, typically 350 - 450 °C, only within this window can significant NO_x reduction be achieved. Under real operating conditions, the deNO_x efficiency of LNC is usually below 40%.[27, 30]

1.3 Electrochemical NO_x reduction

Electrochemical NO_x reduction is an attractive alternative for lean NO_x control compared to the aforementioned technologies. No reductants, other than electrons, are needed in this approach, thus eliminating the requirement of installing a secondary storage and delivery system for reductants or a complicated control system to switch the state of the engine inside the vehicle. The principle of electrochemical NO_x reduction is illustrated in figure 1.2. The NO_x species are reduced to nitrogen gas

and oxygen ions at the cathode under a negative polarization. Oxygen ions are transported through the ionically conductive electrolyte to the anode, where they are oxidized to oxygen. In an oxygen-rich environment, a competitive reaction of O_2 reduction will take place on the cathode, as showing in equation 1.7.

$$O_2 + 4e^- = 2O^{2-} \tag{1.7}$$

Based on theoretical calculations, it is possible to selectively reduce NO_x rather than O_2 by tuning the electrical potential and choosing suitable cathode materials.[31] In real diesel exhaust, the concentration of oxygen can be hundreds of times higher than that of NO_x, it is therefore essential to have a highly selective cathode for NO_x reduction otherwise the oxygen side reaction will consume most of the electrical power supplied to the cell.

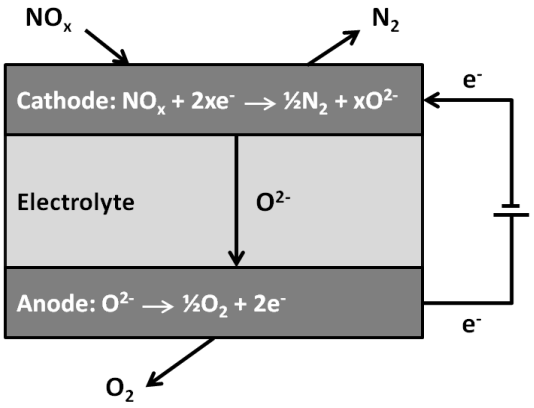

Figure 1.2 Illustration of the principle for the NO_x reduction on a solid state electrochemical cell.

The concept of electrochemical NO_x reduction was first proposed by Pancharatnam et al. in 1975 on a zirconia-based electrochemical cell using porous Pt or Au electrodes.[32] Significant conversion of NO to N_2 was observed at applied voltages higher than 1.0 V in a gas atmosphere containing no O_2 from 600 to 800 °C. As Au has no catalytic activity for NO decomposition, the authors suggested that the reaction did not occur on the electrode but on the surface of the electrolyte, which contained F-centers formed by partial reduction of zirconia at high voltages. The reaction sequence was suggested as follows:

$$V_O^{\cdot\cdot}(s) + 2e^- \text{ (cathode)} \leftrightarrow V_O^x(s)(F - \text{center}) \tag{1.8}$$

$$NO + V_O^x(s) \rightarrow N - O_O^x(s) \tag{1.9}$$

$$NO + N - O_O^x(s) \rightarrow N_2O + O_O^x(s) \quad (1.10)$$

$$N_2O + V_O^x(s) \rightarrow N_2 + O_O^x(s) \quad (1.11)$$

$$O_O^x(s) + V_O^{\cdot\cdot}(b) \leftrightarrow V_O^{\cdot\cdot}(s) + O_O^x(b) \quad (1.12)$$

where (s) denotes the surface and (b) the bulk of the electrolyte. In a later study by Gür and Huggins on Pt point electrode,[33] it was confirmed that F-centers generated on the surface of the electrochemically reduced zirconia were the reaction sites for NO reduction at large overpotentials.

Since then, research efforts have been focused on increasing the selectivity of NO_x reduction relative to O_2 reduction by exploring suitable electrode materials and optimizing the electrode structure. The reaction mechanism has also been studied. Several reaction paths were proposed based on different electrodes and polarization conditions. The electrode materials that have been investigated can be broadly divided into three categories: metals, metal oxides, and combination of metals and metal oxides.

1.3.1 Metals

Hibino et al. did a series of studies on the electrochemical activities of Pd, Rh, Au, and Pt electrodes for NO removal in an oxidizing atmosphere on a yttria-stabilized zirconia electrolyte (YSZ)[34–36] or a samaria-doped ceria (SDC) electrolyte in the temperature range of 400 to 800 °C.[37] It was shown that the removal of NO could be achieved in the presence of excess O_2 on an electrochemical cell. Pd and Pt were found to have higher electrocatalytic activities than Rh and Au.[35] However, the activity and selectivity towards NO reduction decreased significantly with increasing oxygen concentration and the maximum current efficiency was below 2.5% in 750 ppm NO with 1% O_2 at 800 °C on a Pd electrode.[35, 37] Further, Hibino et al. suggested that NO was reduced at the cathode rather than on the electrolyte surface (F-centers). Later, the authors investigated the mechanism of NO decomposition on the electrochemical cell using solid electrolyte potentiometry (SEP).[36] It was found that the electrode, having poorer oxygen pumping properties, exhibited higher current efficiency for NO decomposition. The co-existence of H_2O enhanced the NO reduction due to the formation of H_2 through electrolysis. The co-existence of CO_2 did not influence the NO reduction process because it was not electrolyzed. It was also observed that applying AC voltages rather than DC voltages lower than 6 V could promote the NO_x reduction and avoid severe degradation of the cell.[35]

Walsh et al. performed a detailed kinetic study on Pt[38] and Ir[39] electrodes using an YSZ electrolyte at temperatures between 500 and 600 °C. The Pt electrode showed no performance for NO reduction in the presence of O_2, whereas the Ir electrode showed a limited selectivity towards NO reduction with a ratio of these two reaction rates (NO/O_2) lower than 1.6. The selectivity was found to increase with decreasing temperature. The following mechanism was proposed for reaction on the Ir electrode by the authors:

$$\mathrm{NO\,(g)} + \mathrm{(s)} \rightarrow \tfrac{1}{2}\mathrm{N_2(g)} + \mathrm{O_{ad}} \tag{1.13}$$

$$\mathrm{O_2} + \mathrm{(s)} \leftrightarrow 2\mathrm{O_{ad}} \tag{1.14}$$

$$\mathrm{O_{ad}} + \mathrm{S_{e-e}} \leftrightarrow \mathrm{O_{e-e}} + \mathrm{(s)} \tag{1.15}$$

$$\mathrm{O_{e-e}} + \mathrm{V_O^{\cdot\cdot}} \leftrightarrow \mathrm{O_O^x} + \mathrm{S_{e-e}} + 2\mathrm{h^{\cdot}} \tag{1.16}$$

where $S_{e\text{-}e}$ denotes a site at the interface between the electrode and electrolyte.

Hansen studied the electrochemical reduction of NO and O_2 on point electrodes of Au and Pt in the temperature range of 400 to 600 °C.[40] It was shown that Pt was more active towards O_2 reduction than towards NO reduction, except at 400 °C when the activities of the NO and O_2 reactions were almost the same. Au was nearly inactive towards NO reduction. These results indicated that the electrode materials have to be catalytically active in order to reduce NO electrochemically.[41]

1.3.2 Metal oxides

The use of metal oxides for electrochemical NO reduction was reported for the first time in 1990.[42] An electrochemical cell consisted of transition-metal electrodes and a YSZ electrolyte, removed up to 91% of NO in the presence of 8% O_2 in the temperature range of 650 to 1050 °C. However, no detailed information about the composition of the electrode materials was provided.

Later, Reinhardt et al. studied $La_{0.8}Sr_{0.2}MnO_3$ electrodes on a YSZ electrolyte for reactions with O_2, NO, and NO_2 in the temperature range of 500 to 900 °C. A dramatic increase in current density of O_2 reduction was observed when NO or NO_2 were present with oxygen, which has been explained as a contribution of a parallel electrode reaction between NO and NO_2 proceeding much faster than that of

O_2 reduction. However, as no gas analysis was undertaken in this study, it is also possible that the current increase with the addition of NO_x can be attributed to the reduction of NO_x itself.

Hansen et al. performed a series of studies on the electrochemical properties of metal oxides for NO reduction using cone-shaped electrodes, including NiO,[40] CuO,[43] and the perovkites $La_{1-x}Sr_xMnO_3$ (x=0.05-0.5),[44] $La_{0.6}Sr_{0.4}Fe_{1-x}Mn_xO_3$ (x=0.0-1.0)[45], and $La_{0.85}Sr_{0.15}CoO_3$,[46] as well as the spinels Co_3O_4 and Cu_2CrO_4,[44] between 300 and 600 °C. The results of cyclic voltammetry analysis showed that Cu was more active towards NO reduction than O_2 reduction, whereas NiO was almost inactive towards NO reduction. The Co_3O_4 spinel exhibited no selectivity towards NO reduction and the Cu_2CrO_4 spinel showed activity only for NO oxidation but not NO reduction. For the perovskites, it was concluded that the redox capacity for the NO bond breaking and the oxygen vacancies for the adsorption and incorporation of oxygen species were crucial for the activity of the electrodes towards NO reduction. Among the various perovskites investigated, LSM15 showed the most promising performance for selective NO reduction.

Simonsen et al. and Bræstrup et al. also investigated the spinel oxides for electrochemical reduction of NO and O_2 using cone-shaped electrodes.[47–51] Various metal oxides have been examined, among which $CuFe_2O_4$, $NiFe_2O_4$, La_2CuO_4, $MgFe_2O_4$, and $NiCr_2O_4$ showed a higher activity towards NO reduction than towards O_2 reduction. Especially the $MgFe_2O_4$ spinel, which had almost no activity towards O_2 reduction but a high activity for NO reduction.[50] However, when the Fe in $MgFe_2O_4$ was partly substituted by Mn to increase the electronic conductivity, the NO reduction activity was decreased.[51]

Washsmen et al. tested a $La_{0.8}Sr_{0.2}Co_{0.9}Ru_{0.1}O_3$ cathode on a YSZ electrolyte for electrochemical reduction of NO_x at 750 °C.[52] The cathode achieved a complete conversion of NO_x in an atmosphere containing 500 ppm NO, approximately 3% O_2, 2.4% CO, and 9% CO_2, but the current efficiency was lower than 2%.

Hwang et al. studied perovskite-based thin film electrodes on YSZ electrolytes for NO reduction.[53, 54] The $LaCoO_3$ thin film was found to be able to reduce up to 40% of NO in the presence of 2% O_2 from 600 to 800 °C at applied voltages above 2 V, but the current efficiency was lower than 1.5% and decreased with increasing temperature.[54] The LSM and LSM/YSZ composite thin film electrodes could also decompose NO in the presence of 2% O_2 at 600 °C. The addition of YSZ promoted the NO reduction

relative to that observed on pure LSM at applied currents larger than 300 mA, but inhibited the NO reduction at currents below 300 mA.[53] The following mechanism was proposed by the authors to explain this observation: as the triple-phase boundaries (TPBs) increased by adding YSZ, more oxygen needed to be pumped out before the reaction of NO could start. Once O_2 had been sufficiently removed, the increased TPBs provided more reaction sites for efficient NO_x reduction.

Finally, Werchmeister et al. analyzed perovskite-based electrodes in a NO_x containing atmosphere using electrochemical impedance spectroscopy (EIS) and demonstrated that NO_2 was an important reaction intermediate for electrochemical NO_x reduction on LSM, LSF, and LSCF electrodes.[55–57] Furthermore, the authors performed a NO_x conversion measurement on a porous LSM/gadolinia doped ceria (CGO) cell stack from 250 to 400 °C.[58] It was found that the deNO_x performance of the cell stack was enhanced by the impregnation of ceria or doped ceria, but the selectivity towards NO reduction under oxygen-rich conditions needed to be improved further as the current efficiency was only 1% in 1000 ppm NO with 5% O_2 at 400 °C.

1.3.3 Combination of metals and metal oxides

In 1996, Nakatani et al. coated $La_{1-x}Sr_xCoO_3$ on a dense Pd electrode and observed an improvement of NO reduction due to this coating.[59] The Pd electrode was sintered at high temperatures to form a dense layer on the electrolyte in order to decrease the TPB region and inhibit O_2 reduction. In a later study by the same group,[60] several metal oxides were added onto dense Pd electrodes and among them, RuO_2 was reported to increase the activity most. Replacement of Pd with Ag could further increase the performance and decrease the operation temperature. A 31.9% NO conversion with 11.8% current efficiency was achieved at 500 °C in 1000 ppm NO with 6% O_2. However, RuO_2 is highly carcinogenic and is therefore not suitable for practical applications.

Park et al. studied NO decomposition on a Pt cathode covered by a La_2SnO_7/YSZ composite in 2004.[61] The deNO_x efficiency was observed to be higher on the coated Pt cathode compared to the pure Pt cathode. The NO conversion was 80-87% at 700 °C on the coated Pt cathodes, but the maximum current efficiency was 3% when 2% O_2 was present and decreased to 1.3% when 4% O_2 was present. Minimum currents to initiate NO decomposition were required when O_2 was present in the gas atmosphere, indicating the preference for O_2 adsorption of the reaction sites.

Bredikin et al. proposed the covering of a Pt cathode by a mixture of YSZ and NiO for NO_x reduction under lean conditions.[62–64] It was shown that adding the NiO/YSZ layer enhanced the selectivity reduction of NO versus O_2 reduction, most significantly when the layer was sintered at the highest temperature (1450 °C). Microstructural observation revealed that the NiO/YSZ layer was quite dense after being sintered at such high temperatures, but a nano-porous structure was formed during operation. The NiO in the NiO/YSZ interface region was reduced to Ni under polarization, which generated numerous nano-Ni grains (10-50 nm) and nano-pores inside the oxide layer (Eq. 1.17).[65]

$$\mathrm{NiO} + \mathrm{V_O^{\cdot\cdot}} + 2\mathrm{e^-} \rightarrow \mathrm{Ni} + \mathrm{O^{2-}} \tag{1.17}$$

The performance enhancement by adding the oxide layer was suggested to be due to the oxide layer impeding the direct penetration of O_2 molecules to the TPB and the nano-Ni particles providing selective reaction sites for NO molecules. The NO molecules adsorbed and decomposed on the nano Ni-grains, oxidizing them to NiO (Eq. 1.18 and 1.19). The NiO was reduced back to Ni through reaction 17 to regenerate Ni grains continuously throughout cell operation.[65]

$$\mathrm{NO} + \mathrm{Ni} \rightarrow \mathrm{NO} - \mathrm{Ni} \tag{1.18}$$

$$2\mathrm{NO} - \mathrm{Ni} \rightarrow 2\mathrm{NiO} + \mathrm{N_2} \tag{1.19}$$

The optimum NiO loading of this layer was found to be 35 vol%.[66] Control of oxide layer composition was able to enhance the activity towards NO reduction at lower operation voltages but could not improve the selectivity. Substitution of the Pt cathode by a Pt/YSZ composite cathode further decreased the operation voltage by improving the diffusion of oxygen ions from the NiO/YSZ layer to the electrolyte.[67] The best performance was observed on a cathode with a YSZ volume slight less than 50%, but again the composition optimization did not improve the selectivity.[68] Later, a YSZ cover layer (2-3 μm) was added to the surface of the NiO/YSZ layer, which was shown to be able to increase the activity as well as the selectivity.[69, 70] The improvement was attributed to a suppression of O_2 adsorption by the dense YSZ layer and an increase of the amount of nano-Ni located in the NiO/YSZ interface region. The multilayered cathode using an YSZ electrolyte achieved approximately 30% NO_x conversion with 10% current efficiency at 475 °C in 1000 ppm NO with 2% O_2. The effect of the ionic conductivity of the electrolyte on NO_x reduction was investigated by Hamamoto et al.[71] It was found

that increasing the ionic conductivity of the electrolyte lowered the operating temperature but decreased the current efficiency.

In general, all the aforementioned studies on electrochemical NO_x reduction followed the pattern of choosing selective electrode materials and/or densifying the electrode layers to increase the selectivity for NO_x reduction. Although several materials have been found to be more electrochemically active towards NO_x vs. O_2, using these materials alone did not give satisfactory deNO_x performance in the presence of excess O_2. Densification of the electrodes increased the selectivity of NO_x reduction by significantly suppressing the competing O_2 reduction. However, the activity of NO_x reduction was suppressed simultaneously as the amount of reaction sites was reduced and the gas diffusion was impeded by this densification. The desirable method should be able to improve both the selectivity and activity of NO_x reduction relative to O_2 reduction.

1.4 Electrochemical NO_x reduction with NO_x adsorbents

In 2008, Hamamoto et al. proposed a new type of electrochemical cell using a multilayered cathode and a NO_x adsorption layer.[72] The multilayered cathode was almost identical to that developed by Bredikin et al. The adsorption layer coated on the top of the cathode was made of a typical NSR catalyst. It was demonstrated that the introduction of a NO_x adsorption layer greatly improved both the activity and selectivity of the electrochemical cell towards NO_x reduction under O_2-rich conditions. An approximately 80% NO_x conversion and 17% current efficiency was achieved on the cell with a K-Pt-Al_2O_3 adsorption layer at 500°C in 1000 ppm NO with 2% O_2, compared to a 20% NO_x conversion and 5% current efficiency on the cell without the adsorption layer. In later work by the same group in 2011, the NO_x adsorbents were introduced to the electrochemical cell by another method: impregnation.[73] The NO_x storage material BaO was infiltrated into a Pt/Ni/CGO cathode covered by an LSM electrode. Effective NO_x decomposition was realized on such a cell at low temperatures (< 300 °C) in the presence of 10% O_2 but with a lower current efficiency. It was calculated that an electrode area of about 0.9 m^2 was required to remove 500 ppm NO from the exhaust gas from a 1.6 L engines at 400 °C.[65] Yoshihara et al. reported the simultaneous removal of NO_x and particulate matter (PM) by an electrochemical reactor in 2010.[74] The electrodes were made of a composite of Ag and YSZ (or CGO) mixed with BaO. It was confirmed that the addition of BaO was essential for NO_x reduction. During the tests using real diesel exhaust, 97% of

the PM and 74% of the NO_x were reduced with a fuel penalty of 2.4% to 9.0%. Traulsen et al. recently reported a series of studies on electrochemical NO_x reduction using LSM/CGO or LSF/CGO electrodes impregnated with NO_x storage compounds (K_2O, MnO_x, and BaO).[75–77] The LSM/CGO electrode with BaO impregnation showed a promising performance of 61% NO conversion and 8% current efficiency at 400 °C in the presence of 10% O_2. In the following section, the materials related with electrochemical NO_x reduction with NO_x adsorbents will be discussed in more detail.

1.4.1 Electrode materials

1.4.1.1 Pt

Pt is a good catalyst for NO oxidation, and is also capable of catalyzing the reduction of NO_x by CO or hydrocarbons under O_2-free conditions. As a cathode material in electrochemical cells, Pt shows a higher activity for O_2 reduction than for NO_x reduction and thus has no selectivity towards NO_x reduction in the presence of excess O_2. The amount of Pt added to the cathode needs to be higher than 30 vol% to form a continuous frame, which is much more than that typically used in NSR catalysts (0.02 vol% or 3.5 g Pt per L).[78] For practical applications, the use of Pt as cathode material is cost prohibited.

1.4.1.2 Ni

Ni has been the main anode material used in solid oxide fuel cells (SOFCs) for decades, primarily due to its known performance and economic benefits. In the case of deNO_x cells, NiO was used to prepare the NiO/YSZ layer of the multilayered cathode and was subsequently reduced to Ni during cell operation. The electrical potential for reduction of NiO to Ni is calculated to be approximately -0.85 V vs. air at 500 °C using FactSage.[79] According to the studies by Bredikin et al., new grains of Ni or NiO were observed in the NiO/YSZ and NiO/NiO interface boundaries at applied voltages above 1.0 V. The nano-Ni grains formed in the NiO/YSZ layer were proposed as selective reaction sites for NO_x reduction (Eq. 1.18 and 1.19).

The adsorption of NO on Ni has been studies by femtomole adsorption calorimetry. The results showed that NO adsorbs both dissociatively and molecularly on the Ni surface and there is a threshold coverage

at which a switch in the adsorption mode takes place.[80–83] This is different from the Pt (100) surface where NO only adsorbs molecularly.[81]

The main problem with Ni as the cathode material is the volume expansion. During cell operation, a redox cycle between Ni and NiO is proceeding continuously at the cathode. At high applied voltages (> 2.5 V), this reaction will spread from the interface of NiO/YSZ to deep inside the NiO grains, resulting in large volume changes.[70] In theory, the bulk volume of a fully dense NiO grain should reduce by 40.9% upon reduction to Ni and expand by 69.2% upon oxidation back to NiO.[84] Consequently, the microstructure of the cathode is severely deteriorated by these redox reaction, leading to a significant degradation in the deNO_x performance.[84]

1.4.1.3 LSM

LSM is widely used as a material for cathodes in SOFCs, due to its decent electronic conductivity, high catalytic activity, good thermal and chemical compatibility with a YSZ electrolyte, and high stability when operating at high temperatures (> 800 °C).[85] Extensive studies have been performed on LSM as an O_2 reduction electrode. It is generally accepted that the reaction sites for O_2 reduction are confined to the TPB as the oxygen diffusion in LSM is quite low; for the $La_{1-x}Sr_xMnO_3$ (x = 0.15-0.25), the diffusion coefficient of oxygen was reported to be about 10^{-12} cm^2 s^{-1}.[85–87] In addition to O_2 reduction, LSM has shown attractive performance for electrochemical NO reduction. LSM15, where the strontium dopant is present at 0.15 mol% (x = 0.15), exhibited the highest activity towards NO reduction among the various LSM compositions (x = 0.05 to 0.5).[44] The LSM15/CGO cell with BaO impregnation showed a high selectivity for NO_x reduction in the presence of excess O_2.[77]

NO_2 has been demonstrated to be a reaction intermediate for NO_x reduction on the LSM cathode, which was proposed to be formed catalytically from the oxidation of NO. In this reaction, LSM was suggested to act as a heterogeneous catalyst,[55] which seems plausible as LSM has shown good catalytic activity towards NO oxidation and is a potential substitute for Pt as a NSR catalyst.[88]

1.4.1.4 Ag

Ag is one of the most investigated metallic materials for the electrochemical reduction of oxygen because of its high catalytic activity, excellent electronic conductivity, and lower cost compared with other precious metals (Pt, Pd, etc.). As described in the previous sections, reports on an Ag catalyst for the electrochemical reduction of NO_x have been rare. The pure Ag[60] or Ag/YSZ cathodes[74] were inactive for NO_x reduction under lean-burning conditions. With a RuO_2 coating or adding a NO_x storage compound, a high NO_x conversion can be achieved on a Ag-based cathode in the presence of excess O_2.[60, 74] However, detailed characterizations of the cathode and an in-depth analysis on the electrode processes are missing.

1.4.2 Electrolyte materials

YSZ is commonly used as the electrolyte material for high temperature SOFCs (700-1000 °C). For lower temperature operation, CGO is proposed as the electrolyte material as it has higher ionic conductivity than YSZ below 600 °C.[89] In electrochemical deNO_x, the electrolyte may be partially reduced on the cathode side when subjected to large voltages. In the case of YSZ as the electrolyte, partial reduction of zirconia produces F-centers on the surface of the electrolyte, which are suggested to be the reaction sites for NO reduction. However, in the case of CGO as the electrolyte, the reduction of ceria generates electronic conductivity in the electrolyte frame, resulting in current leakage inside the cell.[90] The current leakage was reported to decrease the current efficiency on a deNO_x cell with an electrically reduced thin CGO electrolyte.[73] Thus, it is necessary to prevent this current leakage for highly effective NO_x reduction.

1.4.3 NO_x adsorbents

NO_x adsorbents comprised NSR catalysts or sorbate components of NSR catalysts. The NSR catalysts typically consisted of 1-3 wt% noble metals and 10-20 wt% alkali- or alkaline-earth elements distributed over a support with high surface area (eg. Al_2O_3).[25, 28, 91, 92] Noble metals are capable of catalyzing the oxidation reaction of NO to NO_2. Most of the NO_x in exhaust gases is NO. Empirical evidence shows that NSR catalysts sorb NO_2 more effectively than NO, or NO_2 may be a necessary precursor for the NO_x trapping process at the alkali- or alkaline-earth components.[25] Among various noble metals being

investigated, Pt is the most active one for NO oxidation[93–95] and has been the primary oxidation catalyst choice for NSR to date. Alkali- or alkaline-earth components work as the storage or trapping sites of NO_x in the NSR catalysts. The exact mechanism of the trapping process is still being debated, but it is generally accepted that nitrate is the dominant species of NO_x storage (Eq. 1.20), although nitrite may also be observed under certain conditions (Eq. 1.21).[25, 91] The basicity of the alkali- or alkaline-earth components is demonstrated to be directly related to their NO_x trapping performance. At 350 °C, the performance of the storage components of NSR were found to decrease in the order of K > Ba > Sr ≥ Na > Ca > Li > Mg.[96] Thus, most of the studies used Ba or K as the storage components of the NSR catalysts.

$$\mathrm{BaO} + 2\mathrm{NO_2} + \mathrm{O_2} \rightarrow \mathrm{Ba(NO_3)_2} \tag{1.20}$$

$$2\mathrm{BaO} + 4\mathrm{NO_2} \rightarrow \mathrm{Ba(NO_3)_2} + \mathrm{Ba(NO_2)_2} \tag{1.21}$$

As real exhaust gases contain significant amounts of CO_2, H_2O, and CO, the effect of these gas species on the NO_x trapping ability of the NSR catalysts has been studied.[25, 28, 91, 97–99] The presence of CO_2 and H_2O decreases the rate of NO_x trapping, nitrate formation, or stability on the catalysts. CO competes against NO_x for the sorption sites with a high selectivity. However, it is well established that the NSR catalysts can efficiently remove NO_x species (90% conversion) in real exhaust gases,[25, 28] which indicated that the effects of CO_2, H_2O, and CO are not crucial for the NO_x trapping ability of the catalysts. The main challenges left for the application of NSR catalysts are low resistance to sulfur poisoning from fuel or lube oil, and thermal degradation induced by periodic desulfurization operation.[25, 100, 101]

When applied in electrochemical NO_x reduction, the NO_x adsorbents are not used in the same way as in NSR catalysts. The NSR catalysts operate through a periodic switch from lean to rich conditions in order to decompose the nitrate formed during lean operation conditions and subsequently reduce the released NO_x using surplus fuels under rich condition. In the electrochemical cell, the decomposition of nitrate is induced by the concentration gradient of NO_x species across the adsorption layer or the applied electrical potential near the interfacial region. The reduction of NO_x is not accomplished near the trapping sites in the adsorption layer, but rather inside the electrode layer, which means the NO_x species need to diffuse through the adsorption layer to the reaction sites in the electrode. Therefore,

the adsorption and desorption properties of the NO_x adsorbent in the vicinity of the reaction sites may play an important role in NO_x decomposition.[72, 73]

1.5 Thesis objectives and outline

Modification of the electrochemical cells using the NO_x adsorbents has been shown to be an effective way to increase both the activity and selectivity of the cells towards NO_x reduction under O_2-rich conditions. However, several issues remained unsolved:

-The multilayered cathode combined with a NO_x adsorption layer so far exhibited the highest current efficiency reported in the literature. The structure of this cathode is complicated and is initially developed to be used without the addition of an adsorption layer. It is uncertain whether the structure of this cathode is optimal for operating with the adsorption layer.

-The multilayered cathode in the previous study contained a large amount of noble metal Pt and reactive material Ni. Electrode materials with reduced cost and improved stability are needed for practical applications.

-The modification of the electrochemical cell with NO_x absorbents can be achieved in two different ways: adding an adsorption layer on top of the electrode or impregnating the storage components into the electrode. It is not clear which way is preferable for NO_x reduction because a meaningful comparison between the two approaches cannot be obtained from the previous studies based on various electrode materials, various cell structures, and various NO_x adsorbents.

-The reaction mechanism behind the performance improvement by this modification is not well understood.

The aforementioned questions can be concisely summarized as:

-What is the optimal structure of a cathode with an additional adsorption layer?

-What are the suitable electrode materials for the electrochemical cell with the NO_x adsorbents?

-Which approach is better to modify the electrochemical cell with the NO_x adsorbents?

-How does the modification improve the performance of the electrochemical cell?

To answer these questions, the following studies have been performed in this project:

First, the structure of the multilayered cathode has been optimized by eliminating the YSZ cover layer.

Second, LSM and Ag have been evaluated as cathode materials of the electrochemical cells coated with a NO_x adsorption layer.

Third, the two approaches to modifying the electrochemical cells with the NO_x adsorbents have been compared using a fully ceramic LSM/CGO cell.

Finally, the electrode processes and the effect of modification with the NO_x adsorbents on these processes have been investigated by impedance spectroscopy.

Accordingly, the content of this thesis is arranged as follows:

Chapter 1 introduces the significance of lean NO_x control, the development of lean NO_x control technologies, and includes a literature review of electrochemical NO_x reduction.

Chapter 2 describes the experimental instruments and techniques used in this work.

Chapter 3 concerns the structure optimization of the multilayered cathode.

Chapters 4 and 5 describe the exploration of Ag and LSM as cathode materials for the electrochemical NO_x reduction with the NO_x adsorption layers and the impedance analysis of the electrode processes.

Chapters 6-8 include the comparison of the two approaches for modifying the electrochemical cells with NO_x adsorbents and the investigation of reaction mechanism by impedance characterizations.

Chapter 9 summarizes the research results and gives some recommendations for future research.

Chapter 2 Experimental

2.1 Cell fabrication

The cells were supported on a 200-300 μm thick dense electrolyte. The electrodes were screen printed or brush painted onto both sides of the electrolyte. The NO_x adsorbents were introduced into the cells in two ways: coating an adsorption layer on top of the electrodes or impregnating the storage compounds into the electrodes. The details of preparation procedure can be found in chapters 3-8.

2.2 Preparation of NO_x adsorption layers

Table 2.1 Comparison of the two kinds of alumina powder as the support materials of the adsorption layer.

Properties	Particle size (nm)	Specific surface are (m^2 g^{-1})	Microstructure after sintering	Adhesion with the electrode
α-Al_2O_3	40-80	~180	Agglomeration	Poor
α-Al_2O_3	100-300	8-10	Homogeneous	Good

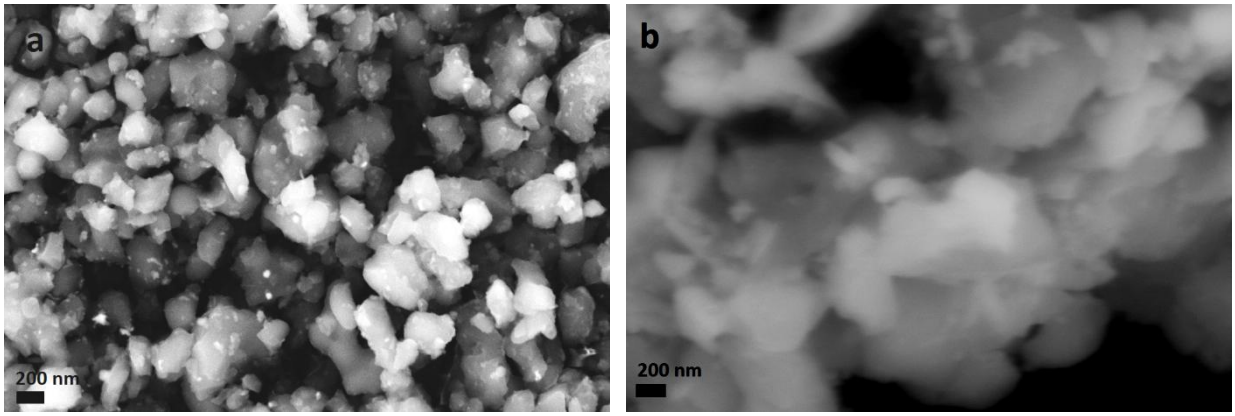

Figure 2.1 SEM image of the Ba-Pt-Al_2O_3 powder made of the two kinds of alumina powder, a) with particle size of 100-300 nm, and b) with particle size of 40-80 nm.

The adsorption layers consisted of nano-sized Pt and K or Ba supported on Al_2O_3 powders. Two kinds of alumina powders were examined as the support materials for the adsorption layer, as showing in table 2.1 and figure 2.1. The alumina powder with a particle size of 40-80 nm have quite a high surface area, which may benefit the dispersion of the active components (Pt, and K or Ba) over the alumina support.

However, severe agglomeration was observed with this type of alumina powder after sintering. Additionally, the adhesion of the resulting adsorption layer to the electrode was too poor to use in testing. In contrast, the adsorption layer made from the larger grain alumina powder (100-300 nm) exhibited a homogenous microstructure and a good adhesion to the electrode layer. Therefore, the alumina powder with a particle size of 100-300 nm was chosen for preparing the adsorption layers.

Two types of adsorption layers were prepared in this work: the Pt-K-Al_2O_3 layer and the Pt-Ba-Al_2O_3 layer. The K-Pt-Al_2O_3 layer consisted of 3 wt% Pt and 10 wt% K supported on Al_2O_3 powder, which is the same as that used for electrochemical NO_x removal by Hamamoto et al.[72] For the Pt-Ba-Al_2O_3 system, which has not yet been reported for used in electrochemical applications, the starting composition was chosen to be 1 wt% Pt with 20 wt% Ba as in the studies on NSR catalysts. However, measurements on the electrochemical cells showed the Pt-Ba-Al_2O_3 layer with this composition could not effectively promote NO_x conversion under O_2-rich conditions (chapter 5). One possible reason could be that the Ba component was overloaded in the adsorption layer as the Al_2O_3 support used in this work had a smaller surface area than that used in typical NSR catalysts. Excessive loading may decrease the density of exposed Ba sites as the particles become larger rather than more numerous, or reduce the number of exposed Pt sites due to steric hindrance or coverage by the Ba component.[25] The composition of the Pt-Ba-Al_2O_3 adsorption layer was subsequently adjusted by decreasing the Ba loading to 10 wt% and increasing the Pt loading to 3 wt%. The addition of this adsorption layer was demonstrated to be able to improve the NO_x removal performance of the electrochemical cell significantly under net-oxidizing conditions (chapters 6 and 7).

2.3 Test set-up

The apparatus used to test the electrochemical cells is illustrated in figure 2.2. The apparatus was placed inside a furnace and connected to a Gamry Reference 600 potentiostat. The cells were mounted between two alumina tubes containing channels for gas flow and measurement probes. Two pieces of Au mesh were placed on both sides of the cell as current collectors and contacted with the measurement probes. The electrochemical performance of the cells was measured by recording the current and monitoring the composition change in the outlet gas at applied voltages. The gas

composition was analyzed by chemiluminescence (Model 42i HL, Thermo Scientific, USA) for NO, NO_2 and NO_x and mass spectrometry (Omnistar GSD 301, Pfeiffer Vacuum, Germany) for N_2, N_2O, and O_2.

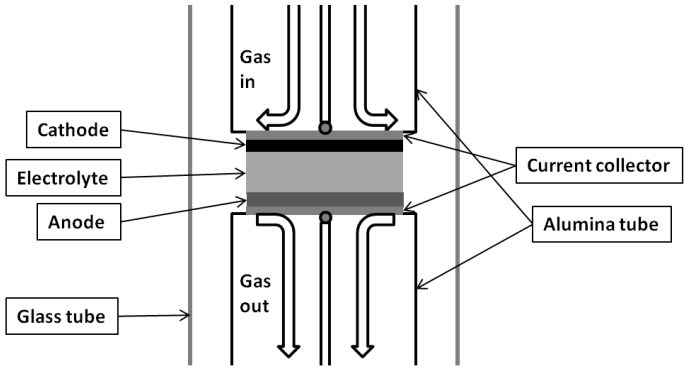

Figure 2.2 Sketch of the test setup for electrochemical cells.

2.4 Impedance characterization

Electrochemical impedance spectroscopy (EIS) was used to characterize the electrodes in this work. A Gamry Reference 600 potentiostat was used to measure the impedance spectra. The obtained impedance spectra were modeled with equivalent circuits using ZView software.[102] The individual elements of the circuits can be related to physical, chemical, or electrochemical processes. Thus, deconvolution of the impedance spectra can give valuable information about the processes contributing to the polarization resistance of the electrodes and the influence of the presence of the NO_x adsorbents on these processes.

2.5 Analysis of gas composition

2.5.1 Mass spectroscopy

The mass spectrometer (MS) works by ionizing chemical compounds to generate charged molecules or molecular fragments and then detecting the ions as a function of mass-to-charge ratio. The MS can be used for determining the structure of gas molecules or for measuring the composition of a gas mixture.

In other words, it has both qualitative and quantitative uses. In this work, the MS was employed for monitoring the change in concentrations of N_2, N_2O, and O_2 species in the outlet. The equipment was carefully calibrated using "standard" gases with accurate concentrations in advance of the measurement.

2.5.2 Chemiluminescence NO_x analysis

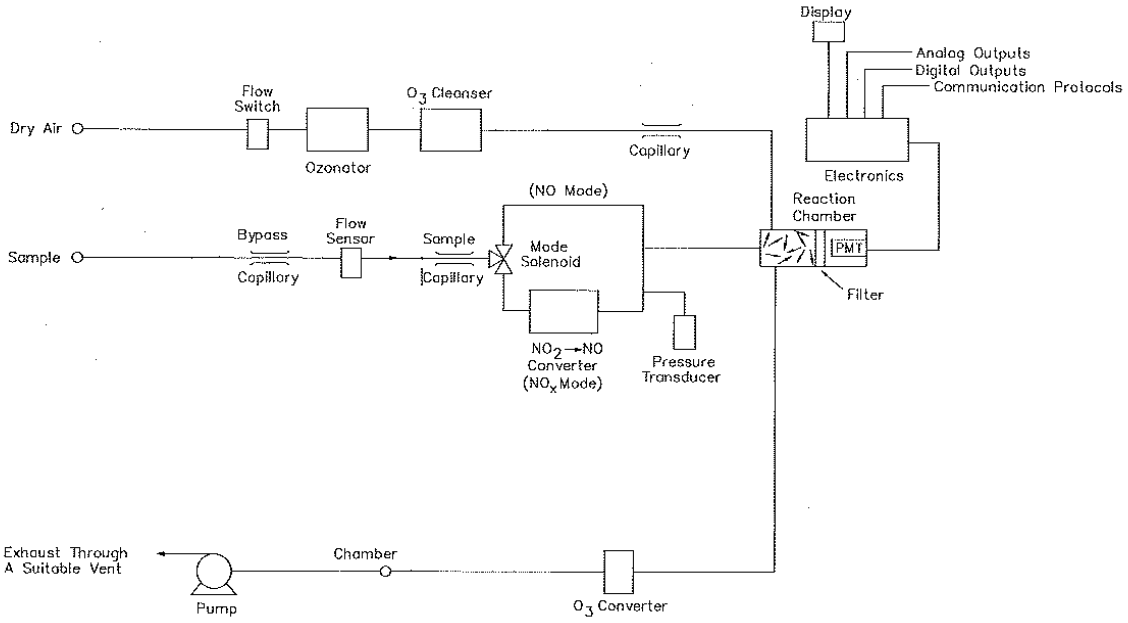

Figure 2.3 Chemiluminescence NO_x analyzer flow schematic.[103]

A chemiluminescence NO_x analyzer was used to measure the concentrations of NO_x species. A sketch of the components in a chemiluminescence analyzer is shown in figure 2.3.[103] The analyzer utilizes the chemiluminiscent reactions between nitric oxide (NO) and ozone (O_3) to produce optical emissions (luminescence) and then measures the intensity of the luminescence to determine the concentration of NO. The reactions are shown in the following equations:

$$NO + O_3 \rightarrow NO_2^* + O_2 \quad (2.1)$$

$$NO_2^* \rightarrow NO_2 + hv \quad (2.2)$$

where the raised asterisk (*) denoted the excited state.

For detection of NO_2, the sample gas is directed to a convertor, in which the NO_2 is converted to NO. By comparing the signal measured under these conditions with that when the convertor is bypassed, the concentration of NO_2 can be determined.

Chapter 3 Structure optimization of the multilayered cathode with a NO_x adsorption layer

This chapter is the manuscript "Optimization of an electrochemical cell with an adsorption layer for NO_x removal" accepted for publication in the Journal of Solid State Electrochemistry.

Abstract

The structure of a multilayer electrochemical cell with an adsorption layer was optimized by removing an yttria-stabilized zirconia cover layer. It was found that the NO_x removal properties of the electrochemical cell were dramatically enhanced through the optimization, especially under conditions of low voltage, intermediate temperature, and high O_2 concentration. The pronounced increase in activity and selectivity for NO_x decomposition after removing the ytrria-stabilized zirconia cover layer was attributed to the extensive release of selective reaction sites for NO_x species and a strong promotion for NO_x reduction from the interaction of the directly connected adsorption layer with both the Pt and catalytic layers. The optimized electrochemical cell may provide a promising solution for NO_x emission control.

3.1 Introduction

Lean burn engines can greatly improve fuel economy, however, the amount of NO_x emission also increases under lean conditions and cannot be removed by the traditional three-way catalyst due to the O_2-rich environment.[104] NO_x is dangerous for both human beings and the environment, causing heath problems,[13] acid rain, and depletion of the protective ozone layer.[14, 15] Government regulations to limit NO_x emission are becoming increasingly more stringent in many countries.[17] Therefore, there is high demand to find an effective method to reduce NO_x emission from lean burn engine exhaust. The electrochemical reduction of NO_x using a solid oxide cell is an attractive technique for lean burn exhaust gas after treatment because it requires no additional reducing agents other than electrons and has the potential to form only N_2 and O_2.[41, 65] The challenge of this technique is to achieve both high

selectivity and activity towards NO_x reduction in the presence of excess O_2. Thus, a lot of research effort has been made on searching suitable electrode materials and optimizing the cell structure.[41, 65]

Recently, Hamamoto et al. proposed a new type of electrochemical cell with a multilayer cathode and a NO_x adsorption layer or a NO_x adsorbent for the NO_x removal.[72, 73, 105] It was reported that the introduction of a NO_x adsorption layer greatly improved both the activity and selectivity of the electrochemical cell towards NO_x reduction.[72, 105] Figure 3.1 shows a sketch of such a cell with an adsorption layer for NO_x decomposition.[72]

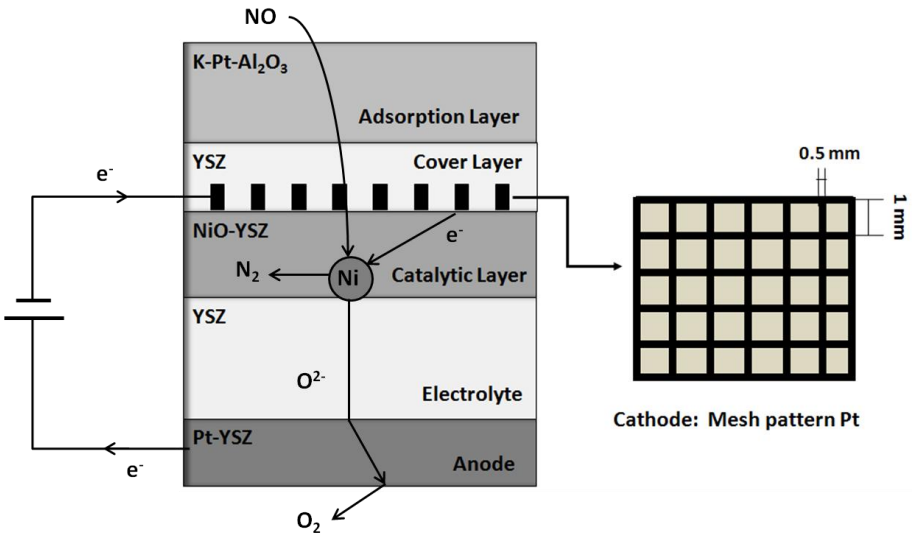

Figure 3.1 A sketch of the electrochemical cell with a multilayered cathode and a NO_x adsorption layer for removal of NO_x.[72]

During the cell operation, the external voltage was applied between the mesh-patterned Pt cathode and the Pt| yttria stabilized zirconia (YSZ) anode, which led to the polarization of the YSZ electrolyte and the reduction of NiO to nano-Ni grains in the vicinity of NiO|YSZ interfacial regions in the catalytic layer.[65, 69–72, 106] The self-assembled nanopores and nano-Ni particles in the catalytic layer were suggested to provide a highly selective reaction site for NO_x reduction[65, 69–71, 80–83, 106] and also suppress the unwanted reaction of oxygen decomposition.[63, 67] The adsorption layer, coated on the cathode side of the electrochemical cell, was made of a traditional NSR (NO_x storage and reduction) catalyst that is normally used to trap and reduce NO_x through a cyclic switch between lean and rich conditions.[25] It was previously proposed[72] that an additional adsorption layer could provide a NO_x-rich atmosphere to the reaction sites in the NiO|YSZ catalytic layer to promote NO_x reduction. A YSZ cover layer was deposited on the top of the catalytic layer in order to increase the NO_x selectivity, because it was stated

that the YSZ upper layer led to inhibit the O_2 decomposition on the open surface of the catalytic layer and increase the amount of nano-Ni grains in the interface region of YSZ|NiO.[65, 69, 70]

However, for the electrochemical cell itself, the cathode with a YSZ cover layer was developed before the adsorption layer has been introduced.[63–65, 67, 69–71, 106] Although on a cell without the adsorption layer, the deposition of a YSZ upper layer led to improve NO_x selectivity,[65, 69, 70] after adding the adsorption layer, we believe the presence of the YSZ cover layer will be harmful to NO_x decomposition. First, the diffusion of NO_x gas from the adsorption layer to the reaction sites in the catalytic layer should be severely impeded by the intervening YSZ layer, which could in turn inhibit the desorption of the NO_x stored in the adsorption layer. Second, a promotion effect for NO_x removal may be generated at the interface of the adsorption layer and the Pt layer or catalytic layer because the adsorption and desorption properties of the NO_x adsorbent in the vicinity of the reaction site may play an important role in NO_x decomposition.[72, 105] But this positive effect cannot be utilized with the YSZ cover layer because it blocks the direct contact between the adsorption layer and the other layers. Therefore, in this study, we modified the structure of the electrochemical cell by removing the YSZ cover layer to make the cell better cooperate with the adsorption layer.

3.2 Experiment

3.2.1 Cell preparation

A schematic diagram of the electrochemical cell with a YSZ cover layer can be found in figure 3.1. The cell was supported on a 200-μm layer of YSZ (8% Y_2O_3-doped ZrO_2) electrolyte with a multilayer cathode and a Pt|YSZ anode. An adsorption layer was applied to the surface of the cathode. Here, two kinds of electrochemical cells were prepared and tested for comparison: one with a YSZ cover layer, named S1; the other one without a YSZ cover layer, named S2. Other than the YSZ cover layer, all the other parts of these two cells were fabricated in the same way. The preparation procedure of S1 is described below as an example.

The catalytic layer was made by screen printing a composite paste of 55 mol% NiO–45 mol% YSZ (8% Y_2O_3-doped ZrO_2) on a 5 x 5 cm YSZ tape. Then, the NiO|YSZ layer was sintered at 1,450 °C for 5 hours. A net-shaped Pt layer was screen printed over the NiO|YSZ layer and calcined at 1,250 °C for 1 hour. A YSZ

(8% Y_2O_3-doped ZrO_2) cover layer was later screen printed over the Pt layer and sintered at 1,450 °C for 3 hours. The Pt|YSZ paste (TR-7070, Tanaka Kikinzoku) was subsequently screen printed on the other side of the YSZ tape and sintered at 1,400 °C for 1 hour. Finally, the adsorption layer was coated by dripping several drops of an adsorbent solution on the top YSZ cover layer. The adsorbent solution was made by mixing 10 wt% adsorbent and 10 wt% Pluronic 123 surfactant (BASF) in water. The adsorbent was composed of 10 wt% K and 3 wt% Pt supported on Al_2O_3 powder. The adsorption layer was first dried at 110 °C for 12 hours, followed by heating at 600 °C for 1 hour. The preparation was similar to that of Hamamoto et al.[72] After the preparation, the large cell (5 x 5 cm) was laser cut into several small round cells with diameters of 14 mm.

3.2.2 Electrochemical test

For the electrochemical test, S1 and S2 were examined under the same conditions. The cells were set in a quartz tube reactor[58] inside a furnace and connected to a Gamry Reference 600 potentiostat. The cells were polarized under -1.5 to -4.5 V for a certain period in the temperature range of 375–500 °C, with 25 °C intervals. The gas composition was 1,000 ppm NO and 0%- 8% O_2 in a balance gas of Ar with a flow rate of 2 L/h, maintained by Brooks mass flow controllers. The outlet gas composition was monitored throughout the test. The NO, NO_2 and NO_x concentration were measured by chemiluminescence (Model 42i HL, Thermo Scientific). The N_2 and N_2O were measured by mass spectrometry (Omnistar GSD 301, Pfeiffer Vacuum). No N_2O was detected in all the tests.

3.2.3 Microstructure characterization

The microstructure and element composition of the cells before and after the test were investigated by scanning electron microscopy (Zeiss Supra 35) and energy dispersive spectroscopy (EDS). The cells were broken manually and the cross-section was polished and coated with carbon. In order to distinguish different elements on the cross-section, all the images were recorded with the backscattered detector.

3.3 Results

The performance of the electrochemical cell can be evaluated by its activity and selectivity toward NO_x reduction. The activity of the cell can be represented by the NO_x conversion rate, a percentage of the NO_x decomposed compared with the total NO_x content. The selectivity can be evaluated by current efficiency (CE), a ratio of the current consumed by NO_x reduction (I_{NO}) to the total current (I_{tot}) flowing through the cell. I_{NO} is calculated using Faraday's law, as shown in equation 3.1. The current consumed by O_2 reduction is calculated by subtracting I_{NO} from I_{tot}.

$$I_{\mathrm{NO}} = z \times v \times \Delta \mathrm{NO_x} \times F \tag{3.1}$$

$$I_{\mathrm{O_2}} = I_{\mathrm{tot}} - I_{\mathrm{NO}} \tag{3.2}$$

ΔNO_x is the amount of NO_x decomposition; z is the charge change of N from NO_x to N_2 (for NO, z = 2; for NO_2, z = 4), v is the total flow rate, and F is Faraday's constant. Because NO_2 concentration varies with O_2 concentration and temperature and it is usually lower than 30% of the total NO_x concentration, we calculated CE as the minimum by assuming all of the NO_x were NO (z = 2), in order to simplify the calculation and compare our results with the literature.[72]

3.3.1 Dependence of NO_x removal properties on O_2 concentration

The dependence of NO_x removal properties of S1 (with the YSZ cover layer) and S2 (without the YSZ cover layer) on O_2 concentration is shown in figures 3.2 and 3.3. The cells were polarized under -2.5 V at 450 °C in 1,000 ppm NO and different O_2 concentrations with balance Ar. The concentration of O_2 was varied from 0 to 8%. The results reported by Hamamoto et al.[72] on an electrochemical cell with a YSZ cover layer, which has the same structure with S1, was also listed as a reference. The reference results, which were the best reported in the literature, were measured under the same polarization voltage (-2.5) but at a higher temperature (500 °C).

It was observed that without O_2, both S1 and S2 could decompose NO_x with quite high activity and selectivity. After O_2 was introduced, the activity of S1 sharply fell to less than 40% while the activity of S2 only slightly decreased from 100% to greater than 85%; the current efficiencies of S1 and S2 both dropped to approximately 16%, but the CE of S2 became increasingly higher than that of S1 with

increasing O_2 concentrations. Because S1 and S2 were prepared and tested under the same conditions, the difference in their performance could be ascribed to the presence of the YSZ cover layer, which strongly supported the great improvement in NO_x removal properties by removing the YSZ cover layer. In comparing the results of this work with that of the reference, the NO_x conversion rate of S1 was obviously lower than that of the reference cell. Because S1 should have the same structure as the reference cell, we assumed that the deviation might be caused by the difference of the raw material and some other preparation details, which have not yet been clearly identified. Other than the YSZ cover layer step, the cell S2 was prepared exactly in the same way as S1. Thus, if there was any negative effect on the structure brought by the preparation other than the YSZ cover layer, it should be equally present on S2. However, S2, showed a much higher NO_x conversion rate than the reference cell. The current efficiency of S2 was slightly lower than that of the reference cell under low O_2 concentrations, but became increasingly higher than the latter with increasing O_2. Moreover, because the results of S2 were recorded at 50 °C lower than that in the reference [72], it indicated that by removing the YSZ cover layer, better performance could be achieved at a lower temperature, which further demonstrated that the modification of the structure was successful.

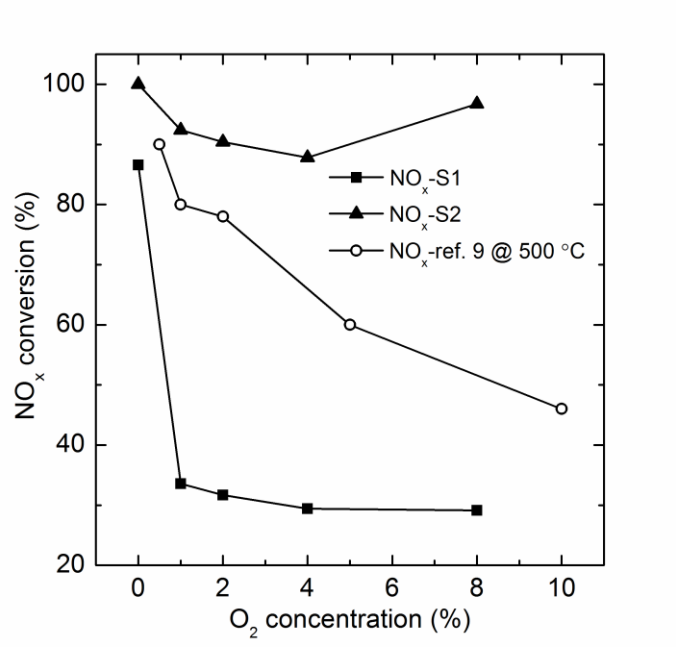

Figure 3.2 Activity of different cells toward NO_x decomposition at various O_2 concentrations and 1,000 ppm NO with balance Ar under -2.5 V at 450 °C (S1: with a YSZ cover layer, S2: without a YSZ cover layer).

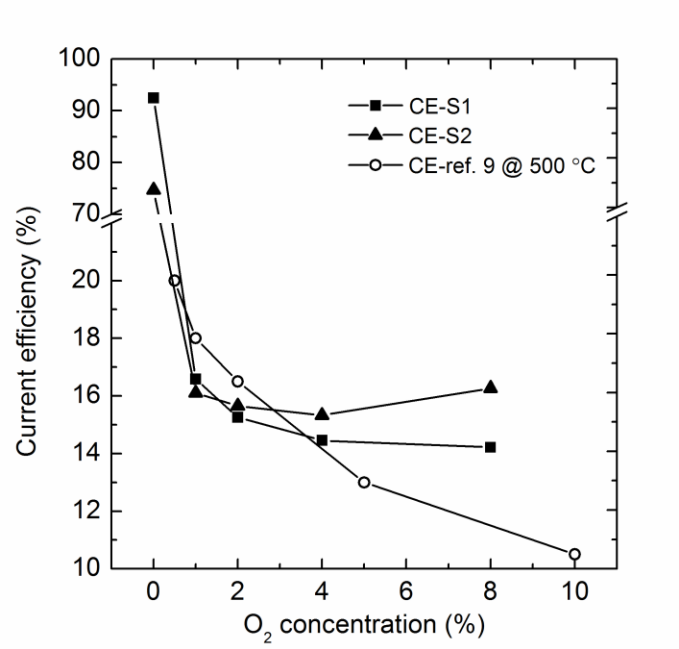

Figure 3.3 Selectivity of different cells toward NO_x decomposition at various O_2 concentrations and 1,000 ppm NO with balance Ar under -2.5 V at 450 °C (S1: with a YSZ cover layer, S2: without a YSZ cover layer) .

There was an unusual increase of the activity and selectivity of S2 in 8% O_2. The reason has not yet been identified, but it should not be ascribed to a measurement error because the result was reproducible. One possible reason for the promotion of NO_x conversion under higher O_2 concentration was the larger ratio of NO_2 to NO because NO_2 was a stronger oxidant and proposed as an intermediate for NO reduction on the LSM|CGO electrode.[55] However, it was unclear why the promotion was only revealed on S2 when 8% O_2 was present.

3.3.2 Dependence of NO_x removal properties on temperature

Figure 3.4 shows the performance of S1 and S2 for NO_x decomposition at different temperatures under -2.5 V in 1,000 ppm NO and 2% O_2 with balance Ar. It was observed that S2 gave a greatly higher activity for NO_x decomposition than S1 over the entire temperature range and completely removed all the NO_x at 475 and 500 °C. Meanwhile, S1 decomposed less than 50% NO_x under the same conditions.

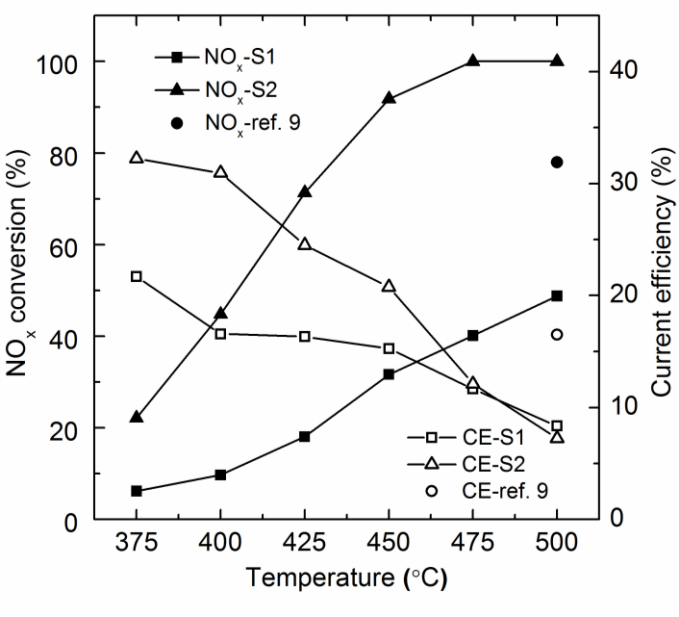

Figure 3.4 NO_x removal properties of different cells as a function of temperature under -2.5 V in 1,000 ppm NO and 2% O_2 with balance Ar (S1: with a YSZ cover layer, S2: without a YSZ cover layer).

The selectivity of S2 was also markedly higher than that of S1 at lower temperatures, but fell close to that of S1 at 475 °C and slightly lower at 500 °C. S2 lost the advantage of selectivity over S1 at high temperature, as it was approaching the limit for NO_x conversion. At 450 °C, the NO_x conversion of S2 achieved 92%, so with additional temperature increases, there was little room for further increases in NO_x conversion. At 475 °C, S2 completely decomposed all the NO_x in the system. The I_{NO} had reached the maximum and could not increase further at elevated temperatures. Under these conditions, the increased activity of the system at high temperatures resulted in increased O_2 reduction rather than NO_x reduction. As a result, the decline in selectivity of S2 was magnified at high temperatures. This result indicated that S2 might have the potential to give a higher selectivity at high temperature when a larger amount of NO_x is presented. It is noteworthy that S2 showed a similar NO_x conversion (8.5% lower) and a far greater CE (48.5% higher) at as low as 425 °C compared with the reference cell at 500 °C.[72]

3.3.3 Dependence of NO_x removal properties on polarization voltage

Figure 3.5 shows the NO_x removal properties at various voltages at 450 °C in 1,000 ppm NO and 2% O_2 with balance Ar. S2 reduced near 50% NO_x under voltage as low as -1.5 V and completely removed all the NO_x from -3.5 to -4.5 V, while the NO_x conversion of S1 was below 50% over the entire voltage range.

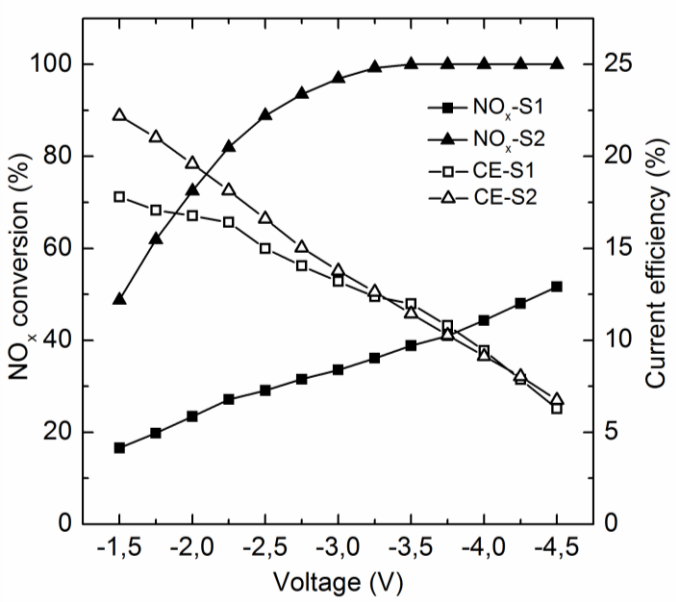

Figure 3.5 NO_x removal properties of different cells as a function of voltage at 450 °C in 1,000 ppm NO and 2% O_2 with balance Ar (S1: with a YSZ cover layer, S2: without a YSZ cover layer).

The selectivity of S2 was increasingly higher than that of S1 with voltage decreasing below -2.5 V. Above -2.5 V, the CE of S2 decreased to values near that of S1. In the case of S2, the NO_x conversion increased rather linearly by increasing the voltage up to -2.5 V, while eventually reached a steady state above -3.5 V, which behavior could be an evidence of a diffusion controlled process taking place. Specifically, in the range of -2.5 and -3.5 V, the process could be likely a mixed controlled behavior, limited both by the mass transfer of NO_x species towards the electrode or product species from the electrode, and by charge transfer or surface adsorption/desorption processes depended on the change of voltage.

However, it is needed to point out that the application of voltage higher than -3.5 V resulted in a 100% conversion of NO_x species present in the gas mixture. Therefore, even though the absolute value of the applied voltage increased, the NO_x conversion could not further be increased, since NO_x species in the system have been already completely reduced by S2. For sample S1, with YSZ cover layer, it seems not to be a simple diffusion controlled behavior, although the diffusion of NO_x species to the electrode should be seriously impeded by the YSZ cover layer. One possible explanation is that not only the diffusion of NO_x species was impeded, but also the other processes related with the electrochemical reduction of NO_x were affected by the existence of YSZ cover layer.

3.3.4 Selectivity towards N_2 formation

On both S1 and S2, the amount of N_2 formation measured by mass spectrometer was quite close to that calculated from NO_x decomposition (see equation 3.4). The N_2 selectivity (η, see equation 3.3) was approximately 90% under all the test conditions. Taking into account the N_2 formation calculated for sample S2 at different O_2 concentrations as an example (table 3.1), it was found that the selectivity towards N_2 formation was as high as 91.5% without O_2; While in presence of O_2, the N_2 selectivity decreased slightly below 90%. Besides, no N_2O was detected by mass spectrometry in all the tests. Therefore, it is concluded that both S1 and S2 have high selectivity towards N_2 formation.

Table 3.1 Selectivity towards N_2 formation on sample S2, without YSZ cover layer, in 1,000 ppm NO with various O_2 concentrations with balance Ar under -2.5 V at 450 °C.

O_2 concentrations / %	N_2 formation (ΔN_2) /ppm	NO_x decomposition (ΔNO_x) /ppm	N_2 selectivity (η)[a] /%
0	455	995	91.5
1	403	919	87.7
2	396	899	88.1
4	388	869	89.3
8	411	939	87.5

[a] N_2 selectivity (η) is calculated as in equation 3.3, according to the decomposition reaction of NO_x to N_2 as showing in equation 3.4:

$$\eta = 2 \times \Delta N_2 / \Delta NO_x \quad (3.3)$$

$$2NO_x \rightarrow N_2 + xO_2 \quad (3.4)$$

In summary, compared with the sample with the YSZ cover layer, the sample without a YSZ cover layer gave much higher activity for NO_x decomposition under all the tested voltages, temperatures and O_2 concentrations, providing better selectivity at low voltage (-1.5 to -2.75 V), intermediate temperature (375−450 °C) and high O_2 concentrations (4−8%). Therefore, by removing the YSZ cover layer, the NO_x removal properties of the electrochemical cell with an adsorption layer could be dramatically enhanced under harsh conditions.

3.4 Discussions

3.4.1 Reasons for activity enhancement

According to systematic research[65, 69–71, 106] on the NiO|YSZ catalytic layer by Bredikhin and colleagues, it is believed that there are two reaction sites for NO and O_2 molecules in the catalytic layer.

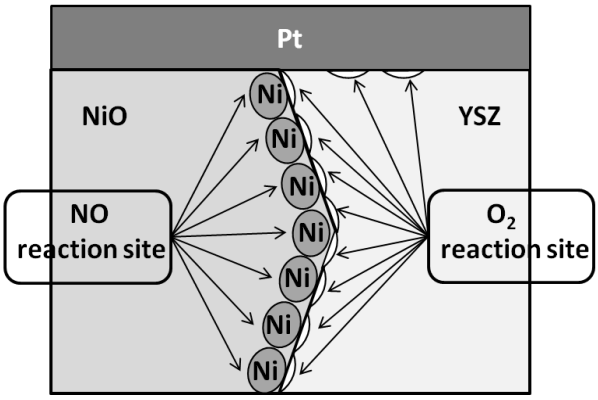

Figure 3.6 Schematic representation of the reaction sites for NO and oxygen gases in the catalytic layer.[65, 69–71, 106]

As schematically shown in figure 3.6, one is the F-center near the three phase boundaries of YSZ|Pt|gas or YSZ|Ni|gas, which is dominated by O_2 reduction in O_2-rich environment. The other is the nanosized Ni particle generated by reducing NiO under cell operation, which was suggested to preferably adsorb and decompose NO in the presence of O_2,[80–83] thus providing an effective reaction site for the selective reduction of NO_x. The reaction mechanism can be modeled by the following equations.

For O_2 reduction:

$$V_{\ddot{O}}(YSZ) + O_2 + 4e^- \rightarrow 2O_O^{2-}(YSZ) \quad (3.5)$$

For NO reduction:

$$Ni + NO \rightarrow Ni - NO \quad (3.6)$$

$$2Ni - NO \rightarrow 2NiO + N_2 \quad (3.7)$$

$$NiO + V_{\ddot{O}}(YSZ) + 2e^- \rightarrow Ni + O_O(YSZ) \quad (3.8)$$

In this study, one of the major reasons for the enhancement of NO_x reduction activity by removing the YSZ cover layer was thought to be the increase in active reaction sites for NO_x reduction. This assumption was corroborated by the microstructure observation and EDS analysis results of the NiO|YSZ layer.

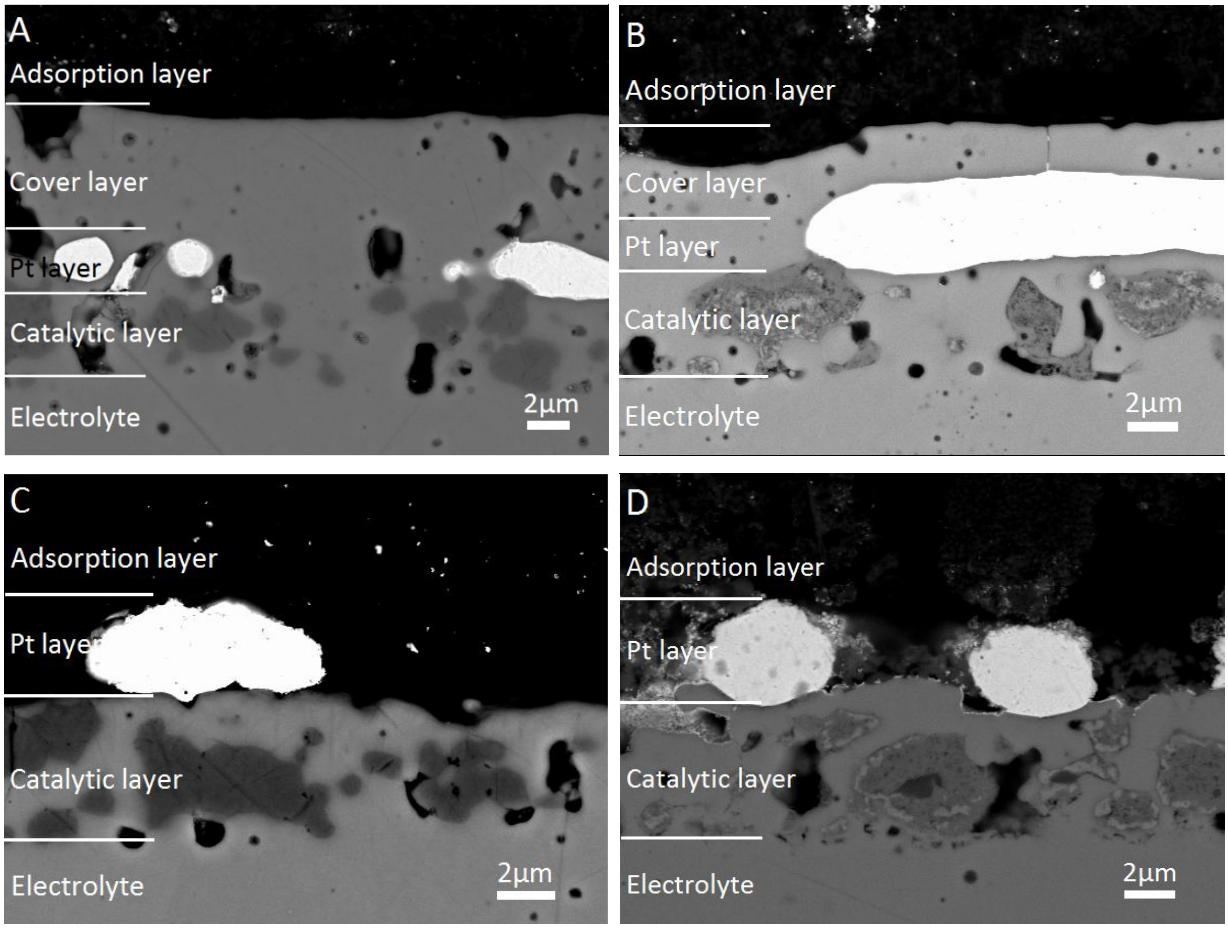

Figure 3.7 Microstructure images for the cathodes of different cells before and after testing. The images show: A: S1 cathode before testing, B: S1 cathode after testing, C: S2 cathode before testing, D: S2 cathode after testing (S1: with a YSZ cover layer; S2: without a YSZ cover layer).

Figure 3.7 shows the microstructure images for the cathodes of S1 and S2 before and after measurement. It can be clearly seen that there were nanoparticles and nanopores generated in the NiO|YSZ catalytic layer after measurement, which was due to the reduction of NiO to Ni by the cell

operation. More importantly, it was found that there was a large amount of nano-Ni particles left on S1 compared to S2, which was confirmed by composition analysis by EDS in figure 3.8. It was previously demonstrated that because the oxidation of Ni by O_2 started at 350 °C,[84] most of the unconsumed Ni would be re-oxidized by O_2 during the cooling period without the protection of applied voltage.[107] In this work, both S1 and S2 were held in 2% O_2 at 500 °C for approximately 10 hours before cooling down. Therefore, the Ni particles should be almost fully re-oxidized unless they cannot be reached by O_2. Significantly more residual Ni in the catalytic layer of S1 indicated that the gas path to the nano-Ni grains was severely impeded or even blocked compared with that of S2, which led to a large loss of active sites for NO_x reduction. By removing the YSZ cover layer, a significant number of reaction sites for NO_x reduction could be released, greatly enhancing the NO_x reduction activity of S2.

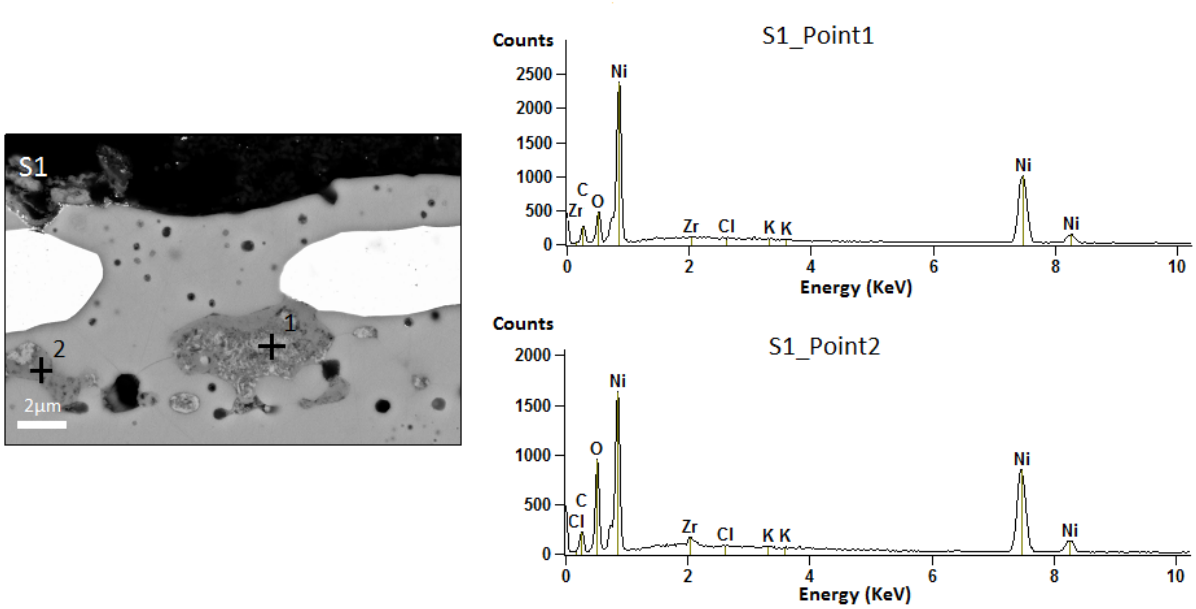

Figure 3.8 Microstructure image and EDS results for the NiO|YSZ catalytic layer of the cell (S1) with a YSZ cover layer after testing.

3.4.2 Reasons for selectivity increase

In addition to the activity enhancement for NO_x reduction, the O_2 reduction also increased after removing the YSZ cover layer, because the suppression of O_2 adsorption and decomposition on the open surface of the catalytic layer by the YSZ layer was lost as well. On an electrochemical cell without an adsorption layer, omitting the YSZ cover layer resulted in a lower selectivity for NO_x reduction. However,

in the case with an adsorption layer, the cell without a YSZ cover layer showed much better selectivity under harsh conditions while simultaneously maintaining a high activity.

The difference was most likely due to the introduction of the adsorption layer. The adsorption layer on the electrochemical cell is made of an NSR catalyst (Pt-K-Al_2O_3) but is not used in the same way as an NSR catalyst.[25] The NSR catalyst is operated via cyclic switches between lean and rich conditions. NO_x gases are trapped and stored in the form of nitrate under lean condition. The nitrate is then induced to decompose by the switch to rich condition. The released NO_x species are reduced near the trapping sites by the reducing agents. While on the electrochemical cell, there is no gas switch to induce the decomposition of nitrate. The reduction of NO_x is not accomplished near the trapping sites in the adsorption layer, but rather inside the NiO|YSZ layer, which means the stored NO_x species has to be released by the decomposition of the nitrate (KNO_3 in this case) and then diffuse through the adsorption layer to the reaction sites in the NiO|YSZ layer. There are then two steps that likely become rather difficult by depositing an additional YSZ cover layer on the electrochemical cell.

One step is the diffusion of the released NO_x species from the storage sites to the reaction sites. With a YSZ cover layer in between, diffusion is severely impeded or even blocked, which has been demonstrated above. The other step is the decomposition of nitrate on the alkali component (KNO_3), which is the prestep for NOx release and, more importantly, regeneration of the NO_x storage sites to trap NO_x continuously. Thus, this step is vital to the overall efficiency of the adsorption layer. Because of missing the strong driving force from gas switch, the decomposition of KNO_3 on the electrochemical cell with the YSZ cover layer can only be driven by the concentration gradient of NO_x species along the adsorption layer, which should be comparatively weak and insufficient. Consequentially, the adsorption layer was incapable of trapping NO_x as effectively as possible.

Correspondingly, by removing the YSZ cover layer, the aforementioned two steps can be significantly affected in a positive way. Firstly, the diffusion of NO_x species from the trapping sites to the reaction sites could becomes unobstructed, which would in turn benefit the adsorption and desorption of NO_x species inside the adsorption layer. Secondly, by removing the YSZ cover layer, the KNO_3 on the trapping sites near the interface between the adsorption layer and the Pt layer was able to be directly decomposed by the negative polarization applied during the operation, which was essentially impossible with the presence of YSZ cover layer because it covered nearly the whole interface between these two

layers. According to the research on molten potassium nitrate (KNO_3), the decomposition of KNO_3 starts at a potential of -0.65 V (vs. $Ag|Ag^+|NO_3^-$) on a Pt cathode at 340 °C.[108] Because the electrochemical cell was polarized under the voltage from -1.5 to -4.5 V and operated above the melting point of KNO_3, after removing the YSZ cover layer, the decomposition of KNO_3 on the interface should be easily achieved while the electrochemical cell is running. As a result, the trapped NO_x species could be effectively released and reduced on the reaction sites nearby. The trapping sites of the adsorption layer were able to be quickly regenerated near the interfacial area.

Figure 3.9 shows the microstructure pictures and EDS analysis results for the interface of the adsorption layer and cathode of S1 and S2 after testing. On S2, many tiny Pt particles accumulated around the Pt surface bared in the adsorption layer, and a thin Pt layer deposited on the open surface of the YSZ nearby. On S1, a similar phenomenon was only observed on the Pt surface exposed to the adsorption layer through a few narrow gaps of the dense YSZ layer. It was reported that in the molten KNO_3 with the cathodic potential increasing to greater than -1.5 V, Pt was extensively oxidized to Pt oxide by the potassium peroxide formed through the accumulation of O^{2-} under continuous KNO_3 decomposition.[108] On a solid state fuel cell, it was reported that Pt could migrate via PtO_2 gas vaporized from the Pt current collector and be deposited around the TPBs (three phase boundaries) because the volatility of PtO_2 was comparatively higher among the Pt species.[109] Therefore, we concluded that the Pt particles accumulation and Pt layer deposition on our cells were caused by redistribution of Pt from the Pt layer through a mechanism of oxidation of Pt by the potassium peroxide, diffusion of gas phase Pt oxide, and subsequent decomposition or reduction of Pt oxide to Pt under negative polarization. It must be noted that the oxidation of Pt was not likely due to the reaction between Pt and O_2 or NO because in that case, the oxidation should be much weaker and should only be able to result in an extremely small amount of Pt migration. The intensive redistribution of Pt provided an evidence for the decomposition of KNO_3 by polarization at the interface of the Pt layer and adsorption layer. However, such benefits for KNO_3 decomposition were negligible on the cell with the YSZ cover layer because the electronic insulated layer extensively broke the connection between the Pt layer and adsorption layer. Moreover, it should be noted that by removing the YSZ cover, there was a possibility for the KNO_3 to be reduced directly to N_2 over the potassium trapping sites adjacent to Pt|YSZ|gas TPBs (three phase boundaries) under negative polarization. The reduction of NO_x through this short reaction path, as shown in equation 3.9, should be much more efficient than through a long

path of KNO_3 decomposition, NO_x diffusion to nano-Ni grains and finally NO_x reduction to N_2 over the Ni grains. Thus, the Pt|YSZ|gas TPBs could also work as the selective reaction sites for NO_x reduction rather than only being dominated by O_2 reduction if they remained connected with the adsorption layer. This effect might be one of the reasons for the selectivity improvement by removing the YSZ cover layer.

$$2KNO_3 + 10e^- \rightarrow K_2O + N_2 + 5O_O^{2-}(YSZ) \quad (3.9)$$

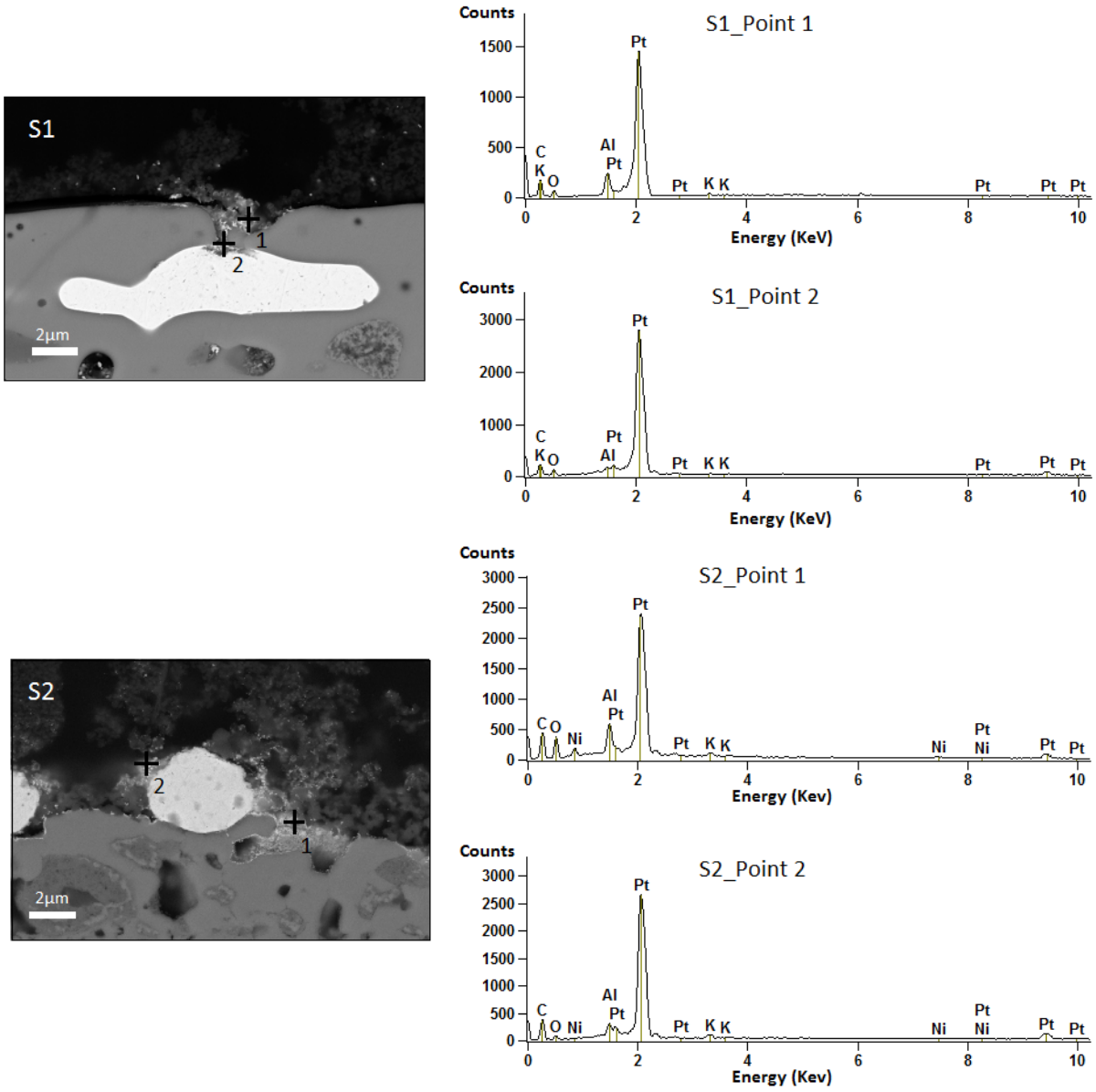

Figure 3.9 Microstructure images and EDS results for the Pt layer|adsorption layer interfaces of different cells after testing (S1: with a YSZ cover layer, S2: without a YSZ cover layer).

In summary, these two steps, diffusion of NO_x species and regeneration of NO_x trapping sites, which might limit the performance of the NSR adsorption layer on the electrochemical cell with a YSZ cover layer, were distinctly improved by removing the YSZ cover layer. These improvements gave rise to a much more efficient adsorption layer for NO_x trapping and smoother transport for the NO_x species to the reaction sites. Additionally, a short reaction path of direct reduction of KNO_3 to N_2 might be created at the interface of the Pt layer and adsorption layer. Combined, all of these positive effects could greatly promote the NO_x reduction and make it more pronounced than the increase of O_2 reduction. As a result, selectivity was not decreased, but rather increased by removing the YSZ cover layer.

3.5 Conclusions

By the optimization of removing the YSZ cover layer, the NO_x removal properties of an electrochemical cell with an adsorption layer was dramatically enhanced, especially under conditions of low voltage, intermediate temperature, and high O_2 concentration.

The large increase of NO_x decomposition activity was due to the extensive release of the reaction sites for NO_x reduction by removing the YSZ cover layer. The improvement of selectivity for NO_x reduction in spite of the increase of O_2 reduction was attributed to the interaction of the adsorption layer with the Pt layer and the catalytic layer strongly promoting the reduction of NO_x, which was specified as the following:

1. The diffusion of NO_x species from the adsorption layer into the reaction sites on the NiO|YSZ catalytic layer was greatly enhanced after optimization.

2. The trapping sites of the adsorption layer in the interfacial area of the Pt layer and adsorption layer were quickly regenerated by the decomposition of nitrite under negative potential.

3. The direct reduction of KNO_3 to N_2 could be realized over the Pt|YSZ|gas TPBs adjacent to the NO_x storage sites of the adsorption layer.

Through the structure optimization of removing the YSZ cover layer, an electrochemical cell with an adsorption layer was able to give good performance under harsh conditions, may providing a promising solution for NO_x emission control.

Acknowledgments

The author would like to acknowledge the financial support of the Danish Strategic Research Council under contract no. 09-065186. We are grateful to our colleagues at the Fuel Cell and Solid State Chemistry Division, Risø-DTU for help and discussion.

Chapter 4 Ag electrodes with a NO_x adsorption layer

This chapter is the manuscript "NO_x reduction on Ag electrochemical cells with a K-Pt-Al_2O_3 adsorption layer" accepted for publication in the Journal of the Electrochemical Society.

Abstract

Ag electrochemical cells with and without a K-Pt-Al_2O_3 adsorption layer were tested for NO_x reduction under oxygen-rich conditions. The effect of the addition of the adsorption layer on the electrochemical reduction of NO_x was investigated by a conversion measurement, an impedance analysis and a microstructure characterization. The blank Ag cell was incapable of converting NO_x to N_2 under any of the investigated conditions. In contrast, the Ag cell with an adsorption layer showed good NO_x reduction activity. An 82% NO_x conversion with 100% N_2 selectivity and 7.7% current efficiency was achieved at -1.25 V and 500 °C. An impedance analysis revealed that the adsorption layer promoted the adsorption and the surface diffusion of the NO_x species at or near the triple phase boundaries (TPBs) and the formation of NO_2. A severe degradation was also observed on the cell with the adsorption layer, which was caused by the corrosion of the Ag cathode and the subsequent migration of the Ag into the adsorption layer during the operation.

4.1 Introduction

Nitrogen oxides (NO_x), the collective reference for nitric oxide (NO) and nitrogen dioxide (NO_2), are detrimental to human health[13] and contribute to the formation of acid rain,[14] the generation of photochemical smog,[15] and the depletion of the ozone layer.[16] For these reasons, increasingly stringent limitations have been imposed worldwide on the NO_x emissions from vehicle exhaust.[17] Unlike conventional gasoline engine exhaust, which is almost oxygen-free due to the stoichiometric combustion process, diesel engine exhaust contains excess oxygen from a combustion with high air-to-fuel ratios.[88] This oxygen-rich environment deactivates the traditional three-way-catalysts, making the removal of NO_x rather difficult.[25] The most mature technologies for reducing NO_x under an oxygen-rich environment are the ammonia selective catalytic reduction (SCR) and the NO_x storage and reduction (NSR). The implementation of these technologies for mobile vehicles requires either an additional fluid

system of ammonia or sophisticated control strategies for the engine. [25] One attractive alternative process is the electrochemical removal of the NO_x using a solid state cell.[32, 33, 37] The principle of this technology is shown in figure 4.1.[57] With this approach, the NO_x are reduced to nitrogen at the polarized cathode, sparing the need to add any reducing agents or to change the operational state of the engine. Currently, this technology is limited by the low activity for selectively reducing the NO_x under the oxygen-rich conditions. [41]

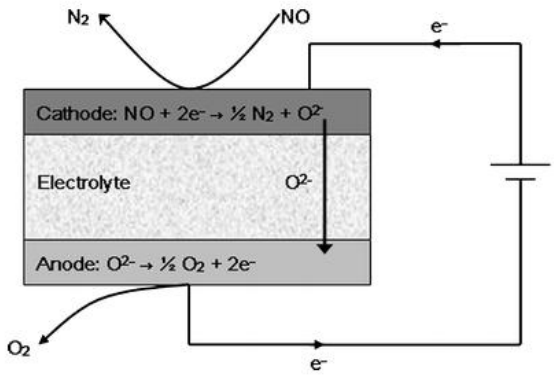

Figure 4.1 Sketch of the principle for the NO_x reduction on a solid state electrochemical cell. (*reprinted with permission from ref. 56; copyright 2012 Springer)*

An electrochemical cell using an Ag cathode with a K-Pt-Al_2O_3 adsorption layer was developed in this study to efficiently reduce the NO_x to N_2 in the presence of excess oxygen. The K-Pt-Al_2O_3 adsorption layer has been reported to improve the performance of an electrochemical cell for NO_x reduction by Hamanmoto et al.[72, 73] and our group.[110] The cathode material used in the literatures, NiO, has been suffering from the continuous redox reaction between NiO and Ni during the cell operation that would eventually deteriorate the cell structure.[84] With a high catalytic activity, an excellent electronic conductivity, and a decreased cost compared with other precious metals (Pt, Pd, etc.),[111–113] Ag is one of the most investigated electrode materials for the electrochemical reduction of oxygen. Reports on an Ag catalyst for the electrochemical reduction of NO_x have been rare. Iwayana and co-workers reported that an electrochemical cell using an Ag cathode with a RuO_2 cover layer reached a 30% NO_x conversion under oxygen-rich conditions,[60] but the use of the carcinogenic RuO_2 limited its applications. Yoshinobu et al. reported a high NO_x reduction rate (74%) for an electrochemical cell with an Ag/$Ce_{0.9}Gd_{0.1}O_{1.95}$(CGO10) cathode mixed with BaO using a real diesel engine exhaust,[74] but the detailed characterizations of the cell and a deep analysis on the electrode processes were missing.

In the present study, an electrochemical cell with an Ag cathode and a K-Pt-Al_2O_3 adsorption layer were investigated for NO_x reduction under oxygen-rich conditions. The Ag cell without an adsorption layer was also measured for comparison. Systematic impedance characterizations were performed to identify the processes for the electrochemical reduction of NO_x and to determine the effects of the adsorption layer on these processes. The cells were also investigated by scanning electron microscopy and energy dispersive spectroscopy both before and after testing.

4.2 Experimental

4.2.1 Cell preparation

The blank Ag cell consisted of a porous Ag cathode, a dense $Ce_{0.9}Gd_{0.1}O_{1.95}$(CGO10) electrolyte, and a Pt anode. The electrolyte was approximately 200 µm thick. The anodes were prepared by painting Pt paste (Ferro GmbH, Germany) on one side of the electrolyte and sintering at 900 °C for 1 hour. The Ag cathode was prepared by painting silver paste (Ferro GmbH, Germany) mixed with 20% by weight of graphite (Graphit Kropfmühl AG, Germany) as a pore former on the other side of the electrolyte and sintering at 700 °C for 1 hour. The active area of the cathode was 1.54 cm^2, the same as that of the anode. The thicknesses of the cathode and anode layers were both approximately 8 µm and 10 µm, respectively. The Ag cell with the adsorption layer was prepared by coating a K-Pt-Al_2O_3 layer on top of the cathode and sintering at 600 °C for 1 h. The amount of the adsorption layer coated on the cathode was approximately 8 $mgcm^{-2}$ with a thickness of approximately 50 µm. The adsorption layer consisted of 10 wt% K with 3 wt% Pt supported on Al_2O_3 nanopowders. The composition was identical to a normal NSR catalyst.[25] The preparation of the adsorption layer can be found elsewhere.[110] An Au wire was connected to the Ag cathode as the cell was coated with the adsorption layer.

4.2.2 Measurement of NO_x reduction

The cells were installed in a glass tube apparatus that was placed inside a furnace and connected to a Gamry Reference 600 potentiostat.[57] Before the conversion measurements, all the samples were pretreated in 1000 ppm NO with 10% O_2 in Ar at 350 °C for 2 to 4 h in order to remove the carbonates and hydroxides of potassium that potentially co-existed in the adsorption layers with the oxide. The cells

were polarized at various voltages (-0.25 to -2.0 V) at temperatures ranging between 200 and 500 °C. The gas used to test the cells consisted of 1000 ppm NO with 10 % O_2 in Ar maintained by Brooks mass flow controllers. The flow rate was fixed at 2 L/h. The outlet gas composition was monitored and recorded throughout the test using chemiluminescence (Model 42i HL, Thermo Scientific, USA) for NO, NO_2 and NO_x and mass spectrometry (Omnistar GSD 301, Pfeiffer Vacuum, Germany) for N_2, N_2O, and O_2. The blank cell and the cell with the adsorption layer were examined using the same conditions. Three replicates for the blank cell and two for the cell with the adsorption layer were tested, giving results with good reproducibility.

The NO_x conversion, the current efficiency (CE), and the N_2 selectivity (η) for the two types of cells were calculated to evaluate the NO_x reduction performance. The NO_x conversion was defined as the percentage of NO_x decomposed relative to the total NO_x content. The current efficiency is the ratio of the current consumed by the NO_x reduction (I_{NO}) to the total current (I_{tot}) flowing through the cell. The N_2 selectivity demonstrates the extent of the decomposed NO_x converted to N_2. The calculation of η, shown in equation 4.1, corresponds to the reaction for the decomposition of NO_x to N_2 as shown in equation 4.2.

$$\eta = 2 \times \Delta N_2 / \Delta NO_x \tag{4.1}$$

$$2NO_x = N_2 + xO_2 \tag{4.2}$$

4.2.3 EIS measurement

A Gamry Reference 600 potentiostat was used to measure the EIS data over a frequency range from $1x10^6$ to 0.001 Hz with 6 data points per decade with a 36 mV rms amplitude under an open circuit voltage. To define the electrode processes of the NO_x reduction and the effect of the adsorption layer on the processes, a series of variations in the experimental conditions were used during recording of the impedance spectra. The temperature was increased from 300 to 500 °C at 50 °C intervals. The concentrations of NO and O_2 were varied in the range of 0 - 5000 ppm and 0 - 15%, respectively. The flow rate increased from 2 L/h to 6 L/h.

4.2.4 Microstructure characterization

The microstructure and the element composition of the cells were investigated by scanning electron microscopy (Zeiss Supra 35) and EDS (energy dispersive spectroscopy). The cells were cracked manually and used directly for the SEM observations. The SEM images were recorded with a secondary electron detector with a 10 KeV acceleration voltage. For the EDS analysis, the acceleration voltage was increased to 15 KeV. To avoid the effect of surface irregularities and charging, the cross sections of the cells were fixed in epoxy, polished, and coated with carbon before being used for the EDS measurement.

4.3 Results

4.3.1 NO_x removal properties

To investigate the NO_x removal properties in an oxygen-rich environment, the blank Ag cells and the cells with a K-Pt-Al_2O_3 adsorption layer were tested in an atmosphere of 1000 ppm NO with 10% O_2. The temperature dependence of the cell performance was studied by testing the cells using a specific voltage for temperatures ranging of 200 - 500 °C. The results are shown in figures 4.2 and 4.3.

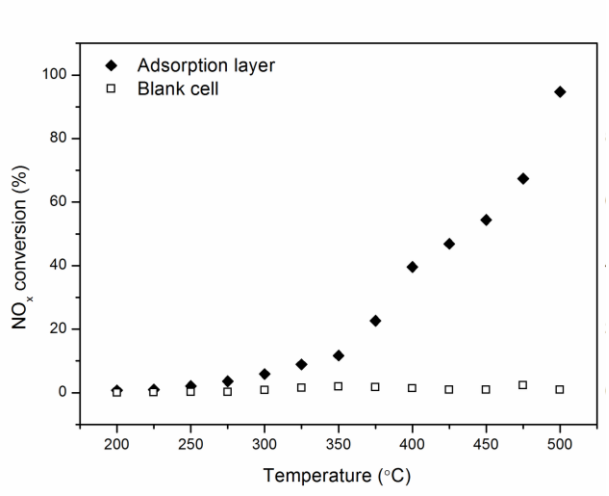

Figure 4.2 NO_x conversions for the blank cell and the cell with a K-Pt-Al_2O_3 adsorption layer at different temperatures in 1000 ppm NO with 10% O_2 under a polarization of -1.5 V.

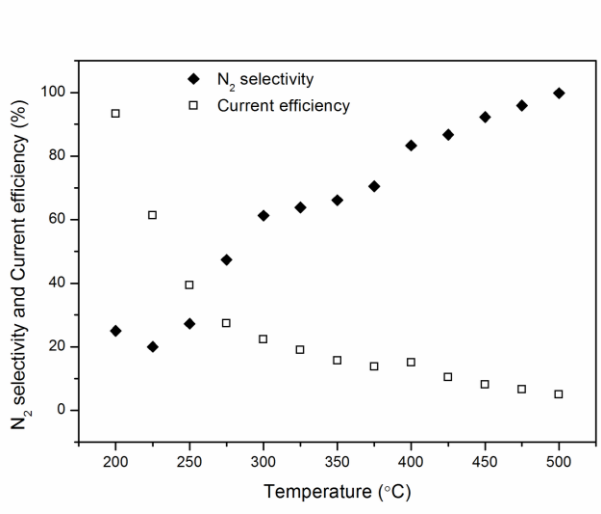

Figure 4.3 N_2 selectivity and current efficiency at different temperatures in 1000 ppm NO with 10% O_2 under a polarization of -1.5 V on the cell with a K-Pt-Al_2O_3 adsorption layer.

For the blank cell, the NO_x conversion fluctuated between 0% and 2% within the entire temperature range (figure 4.2). The conversion showed no temperature dependence and these variations could be considered to be within the experimental error. For the cell with a K-Pt-Al_2O_3 adsorption layer, the conversion of the NO_x started at temperatures as low as 275 °C, gradually increasing to 12% at 350 °C and finally reaching 95% at 500 °C. The selectivity for the N_2 formation on the cell with an adsorption layer increased with increasing temperature to levels that were greater than 80% above 400 °C, figure 4.3. The CE decreased with decreasing temperature with the lowest values being maintained above 5%.

The voltage dependence of the cell performance was studied by testing the cells at 500 °C with voltages varying from -0.25 to -2.0 V. The results are shown in figures 4.4 and 4.5. The conversion of NO_x to N_2 was negligible with the blank cell. For the cell with the adsorption layer, the NO_x conversion increased rather linearly from 0 to 82% with increasing voltages from -0.5 to -1.25 V, eventually reaching 100% at -2.0 V. The N_2 selectivity was maintained at 100% from -0.25 to -1 V, decreasing slightly for voltages exceeding -1.0 V. The CE increased with increasing voltages from 0 to -1.0 V, reaching a maximum value of approximately 12% at -1.0 V followed by a decrease for voltages exceeding -1.0 V. The decrease of CE above -1.0 V indicated that the increase in the activity of the NO_x reduction was less significant than that of the O_2 reduction, which could be explained by a mixed controlled behavior of the NO_x conversion under these conditions. Figure 4.4 shows that the increase of the NO_x conversion with increasing voltage

slowed down from -1.25 to -2.0 V as it approached a compete conversion of NO_x. From -1.25 to -2.0 V, the NO_x conversion on the cell was probably limited both by the mass transfer of NO_x species towards the electrode or product species from the electrode, and by charge transfer or surface adsorption/desorption processes depended on the change of voltage. A 60% NO_x conversion with a 12% CE and a 100% N_2 selectivity was achieved at the rather low voltage of -1.0 V.

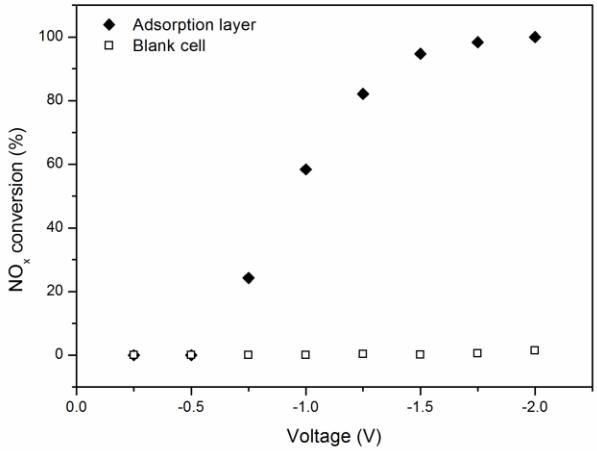

Figure 4.4 NO_x conversions for the blank cell and the cell with a K-Pt-Al_2O_3 adsorption layer under different voltages in 1000 ppm NO with 10% O_2 at 500 °C.

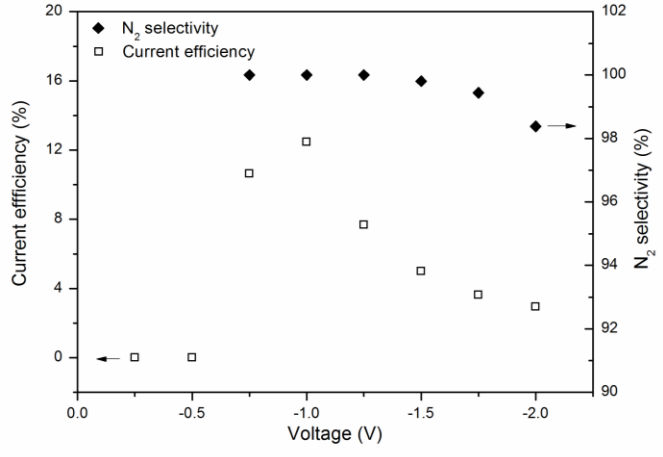

Figure 4.5 N_2 selectivity and current efficiency under different voltages in 1000 ppm NO with 10% O_2 at 500 °C for the cell with a K-Pt-Al_2O_3 adsorption layer.

The voltage dependence of the cell performance was studied by testing the cells at 500 °C with voltages varying from -0.25 to -2.0 V. The results are shown in figures 4.4 and 4.5. The conversion of NO_x to N_2 was negligible with the blank cell. For the cell with the adsorption layer, the NO_x conversion increased rather linearly from 0 to 82% with increasing voltages from -0.5 to -1.25 V, eventually reaching 100% at -2.0 V. The N_2 selectivity was maintained at 100% from -0.25 to -1 V, decreasing slightly for voltages exceeding -1.0 V. The CE increased with increasing voltages from 0 to -1.0 V, reaching a maximum value of approximately 12% at -1.0 V followed by a decrease for voltages exceeding -1.0 V. The decrease of CE above -1.0 V indicated that the increase in the activity of the NO_x reduction was less significant than that of the O_2 reduction, which could be explained by a mixed controlled behavior of the NO_x conversion under these conditions. Figure 4.4 shows that the increase of the NO_x conversion with increasing voltage slowed down from -1.25 to -2.0 V as it approached a compete conversion of NO_x. From -1.25 to -2.0 V, the NO_x conversion on the cell was probably limited both by the mass transfer of NO_x species towards the electrode or product species from the electrode, and by charge transfer or surface adsorption/desorption processes depended on the change of voltage. A 60% NO_x conversion with a 12% CE and a 100% N_2 selectivity was achieved at the rather low voltage of -1.0 V.

Overall, the conversion of NO_x to N_2 was negligible for the blank Ag cell at any of the tested conditions with the presence of excess O_2. With a K-Pt-Al_2O_3 adsorption layer, the NO_x reduction activity of the cell was significantly enhanced. By tailoring the applied voltage, a good NO_x conversion with a high selectivity towards both N_2 formation and current usage can be achieved using the cell with an Ag cathode and a K-Pt-Al_2O_3 adsorption layer.

4.3.2 Deconvolution of the impedance spectra

The impedance spectra were fitted with between 3 and 5 *RQ* elements (the resistance (*R*) and the constant phase element (*Q*) were connected in parallel) in series with a serial resistance (R_s) and an inductance (*L*). The inductance of the experimental apparatus was measured and held fixed during the fitting procedure. The impedance of the constant phase element can be written as,[114]

$$Z = \frac{1}{Y_0(j\omega)^n} \tag{4.3}$$

where Y_0 is a constant, j is an imaginary number, ω is the angular frequency, and n is the frequency exponent.

The equivalent capacitance (C_ω) of the constant phase element can be calculated according to the formula,[115]

$$C_\omega = \frac{(RY_0)^{1/n}}{R} \tag{4.4}$$

The summit frequency of the arc was calculated as follows,

$$f_{max} = (\frac{1}{2\pi})(RY_0)^{1/n} \tag{4.5}$$

The activation energy (E_a) of the individual processes was calculated according to the Arrhenius equation,

$$\delta = \delta_o e^{(-\frac{E_a}{k_B T})} \tag{4.6}$$

where δ is the electrical conductivity, δ_o is the pre-exponential factor, k_B is the Boltzmann's constant, and T is the absolute temperature.

Representative examples of the impedance spectra and their deconvolution for the blank Ag cell and the Ag cell with a K-Pt-Al_2O_3 adsorption layer are shown in figures 4.6 and 4.7.

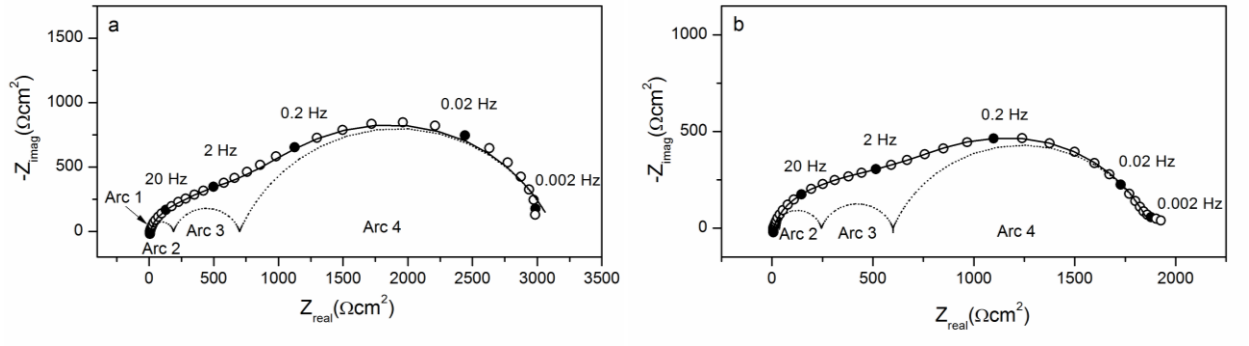

Figure 4.6 Deconvolution of the impedance spectra for the blank Ag cell in a) 1000 ppm NO + 10% O_2 and b) 1000 ppm NO in Ar at 500 °C under OCV. Note the different axis scales. The solid lines represent the fitting of the entire spectrum and the dashed lines represent the deconvolution of the individual processes. The frequency is shown for the data points marked with solid circles.

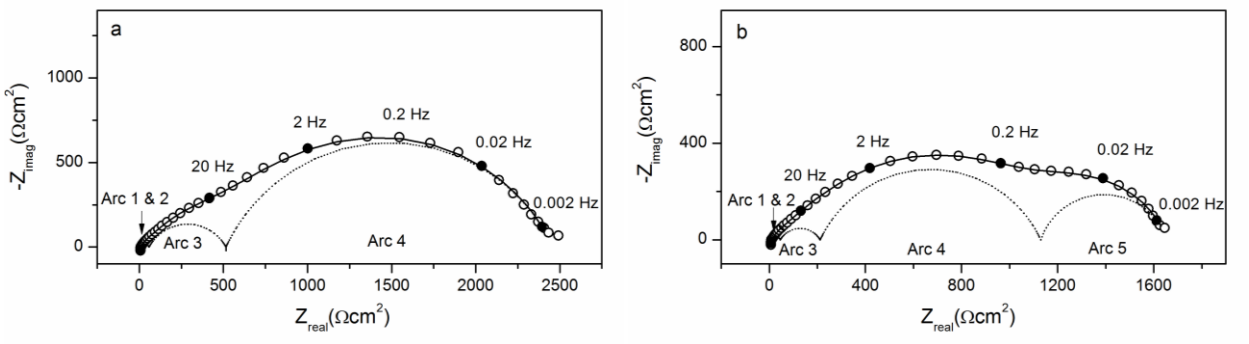

Figure 4.7 Deconvolution of the impedance spectra for the Ag cell with a K-Pt-Al2O3 adsorption layer in a) 1000 ppm NO + 10% O_2 and b) 1000 ppm NO in Ar at 500 °C under OCV. Note the different axis scales. The solid lines represent the fitting of the entire spectrum and the dashed lines represent the deconvolution of the individual processes. The frequency is shown for the data points marked with solid circles.

4.3.3 Effect of the adsorption layer on the EIS spectra

To define the effect of the adsorption layer on the electrode processes for the electrochemical reduction of NO_x, detailed EIS measurements were performed on the blank Ag cell and the cell with the adsorption layer. The characteristics of the different processes for the two types of cells are summarized in tables 4.1 and 4.2. The serial resistance (R_s), the total polarization resistance (R_p), and the polarization resistances of the individual processes (R_1 - R_4) for the two types of cells are compared in figures 4.8 and 4.9. The total polarization resistance (R_p) is the sum of the individual resistances (R_1+R_2+R_3+R_4). The values of the resistances were determined by fitting the impedance data using equivalent circuits. Four arcs were identified in the spectra for the blank cell, corresponding to processes 1 to 4 from the highest to the lowest frequency range, table 4.1. One additional arc was observed for the cell with the adsorption layer in an atmosphere of 1000 ppm NO above 400 °C, table 4.2. For processes 1 to 4, the addition of the adsorption layer decreased the activation energies and increased the summit frequencies without altering the dependences of each process on the temperature, the gas atmosphere, and the flow rate. In characterizing the effects on the resistances, the values of R_s for the two types of cells were similar, with the R_p of the cell with the adsorption layer increasingly lower than the resistances of the blank cell with decreasing temperature. In determining the resistances of the individual processes, the R_1 values of the cell with the adsorption layer were slightly lower than the values for the blank cell below 450 °C. The R_2 to R_4 values were consistently lower for the cell with an adsorption layer than for the blank cell. The differences of R_1 between the two types of cells were relatively small compared with the differences between those of R_2 to R_4. The decrease in the polarization resistance with the addition of the adsorption layer was primarily from the decrease in the resistances of processes 2 to 4.

Table 4.1 Characteristics of the processes contributing to the impedance of the blank Ag cell in atmospheres containing 0 - 5000 ppm NO and 0 - 15% O_2 in Ar from 300 to 500 °C. The activation energy (E_a) was calculated for the impedance data recorded in 1000 ppm NO with 10% O_2 in Ar.

Processes /Arcs	f_{max} (Hz)	C_ω (F cm^{-2})	R (Ω cm^2)	Characteristics
1	500 - 4 x 10^4	~ 5x10^{-7} independent of temperature and gas atmosphere	decreases with increasing temperature independent of gas atmosphere	independent of gas atmosphere E_a = 1.01 ± 0.05 eV
2	0.2 - 30	3x10^{-5} - 7x10^{-5} depends on the presence of O_2	decreases with increasing temperature depends on the presence of O_2	dependent on temperature and the presence of O_2 weak dependency on the variation of pNO E_a = 0.92 ± 0.10 eV
3	0.02 - 4	4x10^{-5} - 3x10^{-4} increases with increasing temperature	decreases with increasing temperature decreases with increasing pNO and pO_2	dependent on temperature and gas composition independent of flow rate E_a = 1.10 ± 0.13 eV
4	0.001 - 0.2	1x10^{-4} - 0.002 increases with increasing temperature and decreasing pO_2	decreases with increasing temperature decreases with increasing pNO and decreasing pO_2 increases with increasing flow rate	dependent on temperature, gas composition, and flow rate E_a = 1.11 ± 0.06 eV

Table 4.2 Characteristics of the processes contributing to the impedance of the Ag cell with a K-Pt-Al_2O_3 adsorption layer in atmospheres containing 0 - 5000 ppm NO and 0 - 15% O_2 in Ar from 300 to 500 °C. The activation energy (E_a) was calculated for the impedance data recorded in 1000 ppm NO with 10% O_2 in Ar.

Processes /Arcs	f_{max} (Hz)	C_ω (F cm^{-2})	R (Ω cm^2)	Characteristics
1	4 x 10^3 - 7 x 10^4	~ 1x10^{-7} independent of temperature and gas atmosphere	decreases with increasing temperature independent of gas atmosphere	independent of gas atmosphere E_a = 0.80 ± 0.06 eV
2	0.8 - 120	3x10^{-5} - 6x10^{-5} depends on the presence of O_2	decreases with increasing temperature depends on the presence of O_2	dependent on temperature and the presence of O_2 weak dependency on the variation of pNO E_a = 0.71 ± 0.06 eV
3	0.04 - 5	7x10^{-5} - 2x10^{-4} increases with increasing temperature	decreases with increasing temperature decreases with increasing pNO and pO_2	dependent on temperature and gas composition independent of flow rate E_a = 0.76 ± 0.03 eV
4	0.002 - 0.2	2x10^{-4} - 0.002 increases with increasing temperature and decreasing pO_2	decreases with increasing temperature decreases with increasing pNO and decreasing pO_2 increases with increasing flow rate	dependent on temperature, gas composition, and flow rate E_a = 0.82 ± 0.02 eV
5	0.001- 0.03	0.01 - 0.02	decreases with increasing flow rate	appears in 1000 ppm NO above 400 °C dependent on flow rate

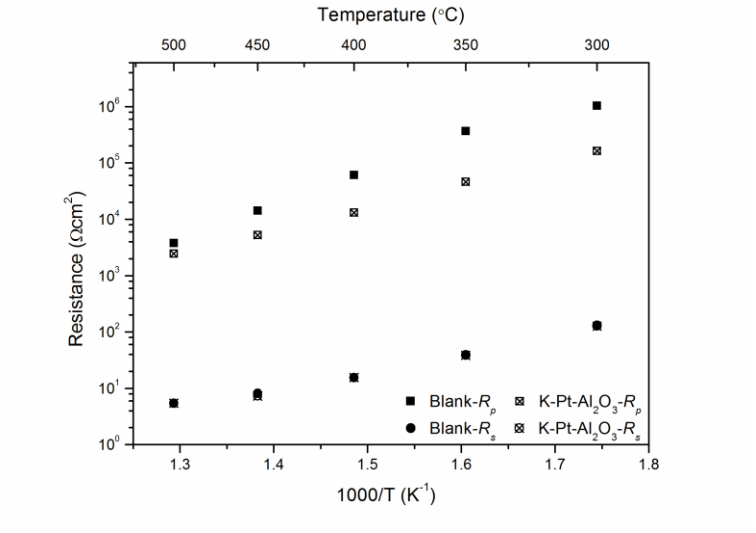

Figure 4.8 Serial resistances (R_s) and polarization resistances (R_p) of the blank Ag cell and the Ag cell with a K-Pt-Al_2O_3 adsorption layer in 1000 ppm NO with 10% O_2 in Ar as a function of the inverse temperature.

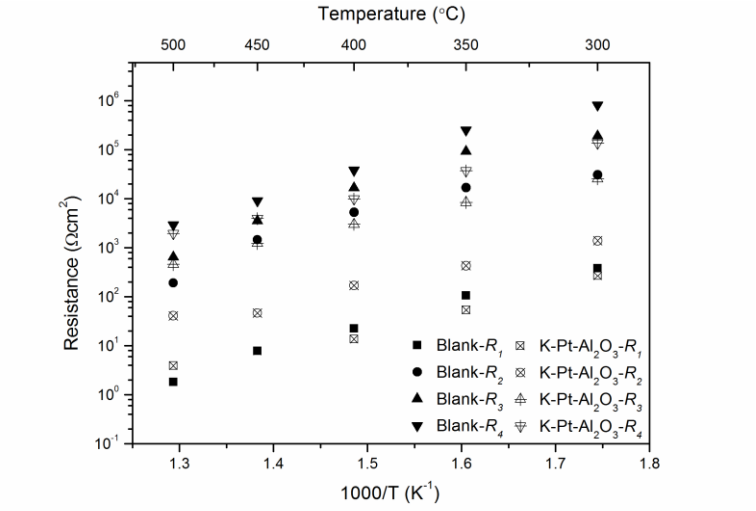

Figure 4.9 Polarization resistances of the individual processes (R_1 - R_4) for the blank Ag cell and the Ag cell with a K-Pt-Al_2O_3 adsorption layer in 1000 ppm NO with 10% O_2 in Ar as a function of the inverse temperature.

4.3.4 Microstructure and composition of the cathodes

Figure 4.10 shows the SEM pictures for the cathodes of the blank cell and the cell with a K-Pt-Al_2O_3 adsorption layer both before and after testing. For the Ag cathode in the blank cell, the effects of the testing conditions on the microstructure were negligible. For the cell with the adsorption layer, the amount of the Ag particles on the cathode was reduced, indicating a loss of the Ag on the cathode during operation. In the EDS analysis on the cell with the adsorption layer after the testing protocol (figure 4.11), a strong Ag peak was detected near the interfacial area between the adsorption layer and the Ag cathode, demonstrating a migration of the Ag from the cathode into the adsorption layer.

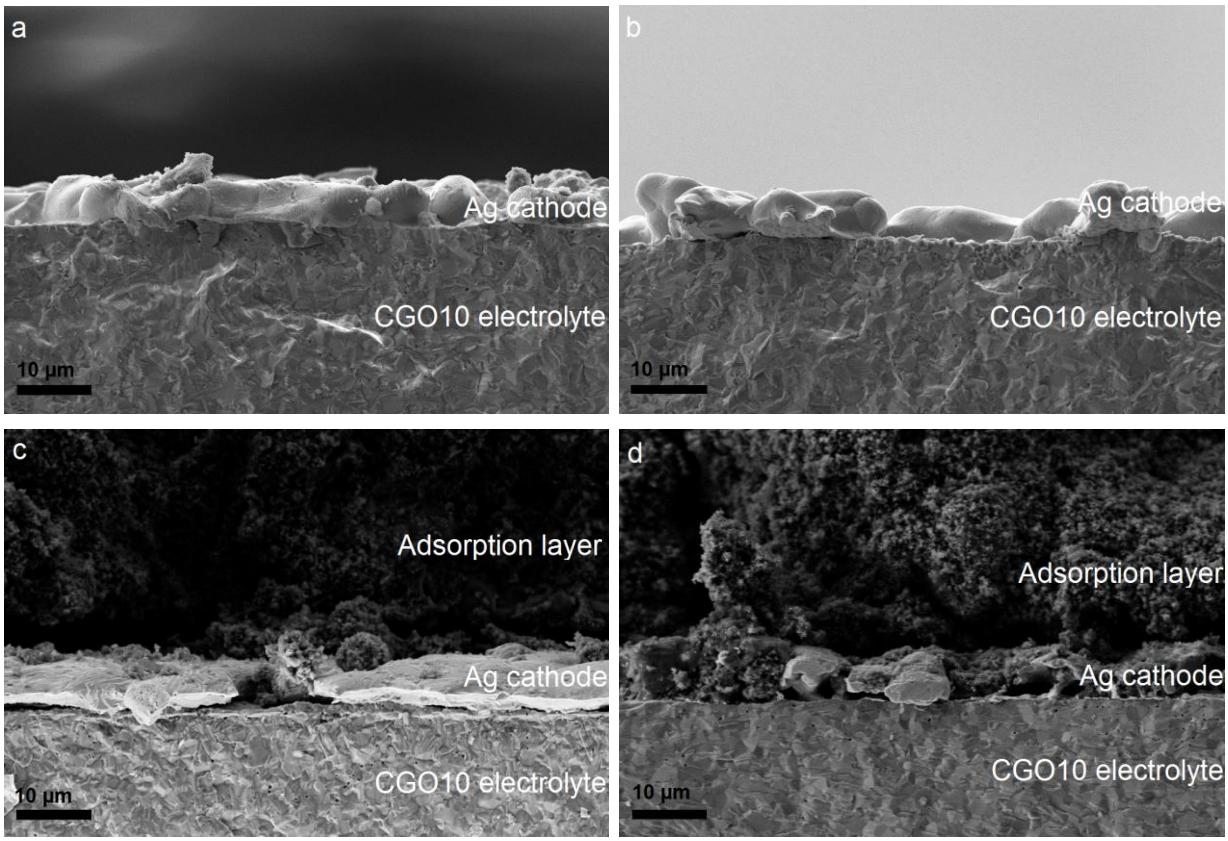

Figure 4.10 Microstructure images for the cathodes of the blank cell and the cell with a K-Pt-Al_2O_3 adsorption layer before and after testing. The images include a) the blank cell before testing, b) the blank cell after testing, c) the cell with the adsorption layer before testing, and d) the cell with the adsorption layer after testing.

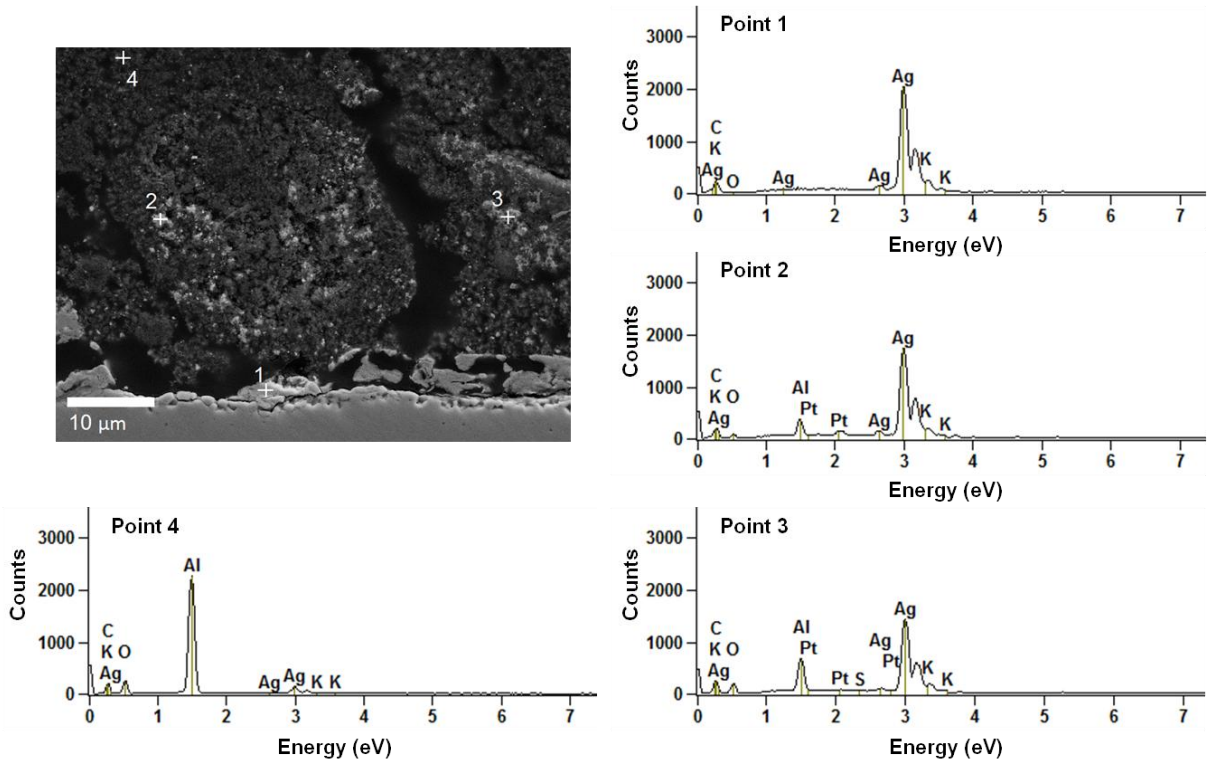

Figure 4.11 Microstructure image and the EDS results for the cathode of the cell with a K-Pt-Al_2O_3 adsorption layer after testing.

4.3.5 Degradation in the NO_x conversion and resistance

The stabilities of the two types of cells were studied by comparing the NO_x conversion and resistances both before and after a 150-hour operational time period (table 4.3). During this operation, the cells experienced two thermo cycles between 300 and 500 °C with frequent switches between the polarization and the OCV. For the blank cell, the NO_x conversion after this long-term operation appeared lower than the values that were previously observed and had been considered to be within the experimental uncertainty. These results suggest that the conversion results were not sufficient to characterize the decrease in performance of the blank cell after the operation. The resistances data obtained from the impedance measurements provided some stability information. The R_s values before and after the operation, which were related to the conductivity of the electrolyte, were almost unchanged for the blank cell. The R_p decreased after the operation, especially at low temperatures, suggesting that the blank cell was actually activated by the operation. For the cell with the adsorption layer, an approximately 50% decrease in NO_x conversion was observed for all the tested temperatures,

with the R_s values remaining almost consistent before and after the operation as also observed with the blank cell. In contrast with the blank cell observations, the R_p increased after the operation for all tested temperatures, indicating that the electrochemical properties of the cell deteriorated. Considering the results from the two types of cells, the degradation was most likely not caused by the cell itself but by the interaction between the adsorption layer and the cell.

Table 4.3 NO_x conversions, serial resistances (R_s), and polarization resistances (R_p) for the blank cell and the cell with a K-Pt-Al_2O_3 adsorption layer before and after a 150-hour operation. The NO_x conversion was measured in 1000 ppm NO with 10% O_2 in Ar at -1.5 V. The resistances were obtained from the impedance spectra recorded in 1000 ppm NO with 10% O_2 in Ar under an open circuit voltage.

Temperature (°C)	Blank						K-Pt-Al_2O_3 adsorption layer					
	NO_x conversion (%)		R_s (Ωcm^2)		R_p (Ωcm^2)		NO_x conversion (%)		R_s (Ωcm^2)		R_p(Ωcm^2)	
	before	after	before	after	before	after	before	after	before	after	before	after
300	0.8	0.7	132	139	$1.04x10^6$	$5.37x10^5$	5.9	3.8	127	130	$1.63x10^5$	$2.52x10^5$
400	1.4	0.5	15.3	16.6	$6.04x10^4$	$4.71x10^4$	39.6	17.0	15.5	16.3	$1.85x10^4$	$2.85x10^4$
500	0.9	0.2	5.4	5.4	3,783	3,714	94.7	52.1	5.4	5.6	1,788	2,753

4.4 Discussion

4.4.1 Identification of the processes for the blank cell

Four arcs were observed in the impedance spectra of the blank cell, table 4.1. Arc 1 appeared in the very high frequency range with a temperature independent C_ω of ~ $5x10^{-7}$ Fcm^{-2} and an E_a of ~ 1 eV. This arc was not affected by the change in the gas atmosphere, which correlated well with the characteristics of the processes related with the transport or transfer of oxygen intermediates between the electrode and the electrolyte.[55, 56, 75, 116] Arc 2, appearing in the middle frequency range, was dependent on the presence of oxygen, indicating that oxygen was participating in this process. The C_ω of this arc varied between $3x10^{-5}$ and $7x10^{-5}$ Fcm^{-2}, which was within the range of the capacitance associated with the adsorption and the dissociation of oxygen on the cathode.[75, 77, 116] Arcs 3 and 4 were observed in the low frequency area of the impedance spectra. For both arcs, the C_ω increased and the resistances decreased with increasing temperatures, suggesting that these two arcs were related with the extension of the three phase boundaries (TPBs) zone. For arc 3, the resistance decreased with increasing the

concentrations of NO and oxygen and was independent of the flow rate. Arc 3 was ascribed to the adsorption, the surface diffusion, and the transfer of the O_2 species and the NO_x species at or near the TPBs, which is in good agreement with previous observations of these processes on composite electrodes.[75, 77] For arc 4, the resistance decreased with decreasing oxygen concentrations, indicating that this low frequency process was dependent on the concentration of the oxygen vacancies.[77] As this arc was also characterized by increasing resistances with either increasing flow rates or decreasing NO concentrations, this arc was ascribed to the conversion of the reaction intermediate NO_2, which was consistent with previous findings in our group.[55, 56, 75, 77]

As a two electrode configuration was used in this study, the response of the Pt counter electrode could also be included in the impedance spectra. The impedance results in this work were compared with the results obtained on the Pt electrodes.[117–119] An arc similar to arc 2 was observed for the Pt electrodes in the temperature range of 400 - 800 °C in the gas atmospheres of O_2 in Ar or N_2, which was identified as the dissociation of oxygen or charge transfer reaction.[117] Therefore, the middle frequency process could also be due to the dissociative adsorption of O_2 and/or charge transfer reactions on the Pt electrode.

4.4.2 Effect of the adsorption layer on the processes

The most obvious effect of the adsorption layer on the electrode processes was an additional arc appearing in the low frequency end in the atmosphere of 1000 ppm NO at temperatures above 400 °C, figure 4.7. The frequency exponent (*n*) of this arc was rather high (~ 0.8) with decreasing resistances with increasing flow rates. These observations were consistent with the characteristics of a typical conversion arc.[120] This arc only appeared in the presence of the adsorption layer, suggesting that it was probably generated by the interaction between the NO and the adsorption layer, which could be the oxidation of the NO on the Pt sites,[121–123] the storage of NO_x into nitrate on the K sites,[96, 124] or the decomposition of the nitrate on the K sites.[125, 126] The first two processes would be impeded with increasing flow rates as the residual time of the necessary intermediates is shortened. The last process would benefit from increasing flow rates, as the product gas species from the nitrate decomposition can be removed. Arc 5 could be identified as a conversion arc associated with the decomposition of the nitrate in the adsorption layer.

For arcs 1 to 4, the characteristics of every individual arc for the cell with the adsorption layer were similar with those for the blank cell, although the values of E_a were lower and the values of f_{max} were larger. These results suggested that the addition of the adsorption layer did not completely alter the reaction mechanism but did increase the activity levels and fastened the reaction speed of each process. The identifications of these four arcs for the cell with the adsorption layer were consistent with those for the blank cell. In addition to the changes in E_a and f_{max}, the decrease in R_p also demonstrated the promotion effect on the electrode processes with the addition of the adsorption layer. According to the resistance changes of the individual processes, the promotion effects were significant on the middle and low frequency processes, which were related to the adsorption and dissociation of oxygen on the electrode, the adsorption, surface diffusion, and transfer of the O_2 species and NO_x species at or near the TPBs, and the conversion of the reaction intermediate NO_2.

The K-Pt-Al_2O_3 adsorption layer, consisting of nano-sized Pt and K_2O distributed over Al_2O_3 nanopowders, was able to effectively oxidize NO to NO_2 by Pt and to trap NO_2 into nitrate by K_2O. The trapped nitrate was decomposed under heating or polarization, releasing NO_x. As reported in the literature, an additional adsorption layer could provide a rich NO_x atmosphere for the reaction zones in the electrode.[72, 110] From the SEM observations (figure 4.10), the adsorption layer contacted directly with the TPBs on the cathode/electrolyte interface through the thin Ag cathode. From the FTIR studies, the adsorbed NO_x is known to be capable of moving from the K-adsorption sites to the CGO-adsorption sites.[127] Therefore, it can be concluded that the presence of a K-Pt-Al_2O_3 adsorption layer improved the adsorption and the surface diffusion of the NO_x species at or near the TPBs of the electrode. For the NO_2 conversion process that was hindered by lack of the reaction intermediate NO_2, the strong oxidation ability of the Pt and the rich NO_x atmosphere brought by the adsorption layer could significantly promote the formation of NO_2. In addition to the effects on the NO_x related processes, the adsorption layer could also facilitate the adsorption, the dissociation, and the surface diffusion of the oxygen species, due to the large surface area and the active components (Pt and K).[25]

4.4.3 Degradation of the cell with the adsorption layer

A comparison of the NO_x conversion and the impedance results for the two types of cells indicated that the degradation of the NO_x removal performance on the cell with an adsorption layer was related to the

interactions between the cell and the adsorption layer rather than the cell itself. A correlation with the microstructure and the composition analysis suggested that the degradation was due to the corrosion of the Ag cathode and the subsequent migration of the Ag into the adsorption layer. For the cathode, the loss of the Ag resulted in a loss of the TPBs region and the electronic conductivity. For the adsorption layer, the loading of the Ag decreased the exposed Pt and K surface area, reducing the NO_x trapping ability.

During the operation, the cells were heated to temperatures ranging from 300 to 500 °C and polarized at negative potentials. At operational temperatures above the melting point of potassium nitrate (334 °C), at least part of the Ag cathode was covered by the nitrate melts. Silver metal is unstable in molten nitrate under negative polarization and will be corroded as shown in equation 4.7.[128, 129]

$$4\mathrm{Ag} + 4\mathrm{KNO_3} + \mathrm{O_2} = 4\mathrm{AgNO_3} + 2\mathrm{K_2O}\ (E^{\circ} = -0.78\ V) \quad (4.7)$$

The formed silver nitrate subsequently evaporated, diffused into the adsorption layer, and decomposed to silver metal, as the boiling and decomposition points of silver nitrate are rather low (440 °C). To overcome these limitations, the use of Ba instead of K in the adsorption layer may avoid a corrosion of the Ag cathode, as the melting point of barium nitrate is increased (592 °C) relative to potassium nitrate and Ba is also commonly used as the NO_x-strorage component in NSR catalysts.[25]

It should be noted that the gas mixtures that only contained NO_x and O_2 were used in this study to simplify the understanding of the underlying electrode processes for the electrochemical NO_x reduction. As real exhaust gases contain significant amounts of CO_2, H_2O, and CO, the effect of these gas species on the deNO_x performance of the cells with the NSR adsorption layers may be important in practical situations. The harmful effects of these gas species on the NO_x trapping ability of the NSR catalysts have been extensively studied.[91, 97–99] The presence of CO_2 and H_2O decreases the rate of NO_x trapping, nitrate formation, or stability on the catalysts. CO competes against NO_x for the sorption sites with a high selectivity. However, it is well established that the NSR catalysts (K-Pt-Al_2O_3) can efficiently remove NO_x species (90% conversion) in real exhaust gases,[28] indicating that the effects of CO_2, H_2O, and CO are not crucial for the NO_x trapping ability of the catalysts.

4.5 Conclusion

In the present work, the electrochemical reduction of NO_x on a blank Ag cell and an Ag cell with a K-Pt-Al_2O_3 adsorption layer was investigated. Detailed impedance characterizations were performed to determine the processes for the electrochemical reduction of NO_x and the effect of the adsorption layer on these processes. The blank Ag cell was incapable of converting NO_x to N_2 under any of the investigated conditions. In contrast, the Ag cell with the adsorption layer had a high NO_x conversion with good N_2 selectivity and current efficiency. An impedance analysis revealed that the addition of the adsorption layer improved the adsorption and the surface diffusion of the NO_x species at or near the TPBs as well as the formation of NO_2. The cell with the adsorption layer degraded severely after a 150-hour operation. An analysis of the SEM observations and the EDS data suggested that the degradation was from a corrosion of the Ag cathode with a subsequent migration of the Ag into the adsorption layer. To avoid to this degradation, the use of Ba instead of K in the adsorption layer may be advantageous.

Acknowledgments

The authors acknowledge the financial support of the Danish Strategic Research Council under contract no. 09-065186. We are grateful to our colleagues at the Department of Energy Conversion and Storage, Technical University of Denmark, for assistance and discussions.

Chapter 5 LSM electrodes with a NO_x adsorption layer

This chapter is the manuscript "Enhancement of NO_x removal performance for $(La_{0.85}Sr_{0.15})_{0.99}MnO_3/Ce_{0.9}Gd_{0.1}O_{1.95}$ electrochemical cells by NO_x storage/reduction adsorption layers" accepted for publication in Electrochimica Acta.

Abstract

This study investigated the effect of adding a NO_x adsorption layer to the cathode of an electrochemical cell on the removal of NO_x from gaseous mixtures. The cathode was a composite of $(La_{0.85}Sr_{0.15})_{0.99}MnO_3$ (LSM15) and $Ce_{0.9}Gd_{0.1}O_{1.95}$ (CGO10). Two different kinds of adsorption layers, K-Pt-Al_2O_3 layer and Ba-Pt-Al_2O_3 layer (known as NO_x storage/reduction (NSR) catalyst), were studied. The effects of the NSR adsorption layers on the electrode processes were characterized by electrochemical impedance spectroscopy (EIS). Both adsorption layers increased the reduction of NO_x to N_2 in an atmosphere that contained only NO. When O_2 was present with NO in the atmosphere, the K-Pt-Al_2O_3 adsorption layer significantly enhanced the conversion of NO_x to N_2, but the Ba-Pt-Al_2O_3 adsorption layer had no effect. The selective removal of NO_x under O_2-rich conditions was achieved by modifying the LSM15/CGO10 cell with a suitable NSR adsorption layer. The improvement for NO_x reduction by the adsorption layers was mainly contributed by the promotion of the adsorption and surface diffusion of NO_x species at/near the triple phase boundary (TPB) regions of the electrode and probably the formation of a short and effective reaction path for NO_x reduction. A stronger capability for oxidizing NO and/or trapping NO_x under the test conditions may have contributed to the superior performance of the K-Pt-Al_2O_3 adsorption layer relative to the Ba-Pt-Al_2O_3 layer.

5.1 Introduction

The use of diesel engines is becoming more widespread because their fuel economy is superior to and their emission levels of carbon monoxide and carbon dioxide are considerably lower than those of gasoline engines.[1] However, the high-temperature combustion in diesel engines generates significant amounts of nitrogen oxides (NO_x), which have harmful effects on the environment[14–16] and human beings,[13] and are limited by increasingly stringent government regulations worldwide.[17] Traditional

three-way catalysts are incapable of reducing NO_x in O_2-rich diesel engine exhaust.[104] Therefore, there is a great demand for new technology to control NO_x emissions in diesel engine exhaust. Research efforts currently focus on two approaches.[25] The first approach uses selective catalytic reduction (SCR) catalysts to selectively reduce NO_x but requires additional reducing agents (ammonia, urea, and so forth), which introduce problems related to storage, spill management, and development of a distribution network. The second approach, represented by NO_x storage/reduction (NSR) catalysts, achieves NO_x reduction by selectively storing NO_x under lean conditions, and subsequently reducing the stored NO_x under rich switch. However, a sophisticated, adaptive control system is needed to implement this approach in mobile applications.

An alternate approach is to reduce NO_x to N_2 on the polarized cathode in a solid state electrochemical cell, figure 5.1.[57] This technology was first introduced by Pancharatnam et al.[32] in 1975 for a zirconia-based cell under O_2-free conditions. Hibino et al.[34, 36, 37] and Cicero[42] subsequently demonstrated that this approach can also work in the presence of O_2. Since then, different studies[41, 52, 58, 60, 65, 77, 130] have identified suitable cathode materials or optimized the cell structure to improve its NO_x removal properties. With this approach, the inherent challenge is to selectively reduce NO_x (rather than O_2) in an O_2-rich environment without consuming large amounts of electrical power.

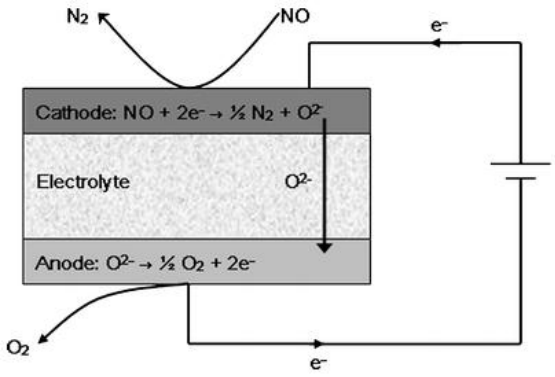

Figure 5.1 Illustration of NO_x reduction on a solid state electrochemical cell. (*reprinted with permission from ref. 56; copyright 2012 springer)*

In this study, $(La_{0.85}Sr_{0.15})_{0.99}MnO_3$ (LSM15)/$Ce_{0.9}Gd_{0.1}O_{1.95}$ (CGO10) cathodes are coated with NO_x adsorption layers made of NSR catalysts. The NO_x removal performance of blank cells (with uncoated cathodes) and cells with cathodes coated with two different kinds of NSR adsorption layers are tested

and compared. The underlying motivation of this study is to solve the selectivity challenge of electrochemical cells by combining it with NSR catalyst and using electrical polarization instead of rich conditions to reduce stored NO_x on an NSR catalyst. With this approach, the engine is operated continuously under lean conditions (to avoid the fuel penalty), and a complicated control system is no longer needed. Furthermore, no additional reducing agents are needed other than electrons. Previous work by Hamamoto et al.[72, 73] and our group[110] showed that NSR adsorption layers improved the performance of electrochemical cells. However, the cathode materials in the current work involve the use of noble metals (Pt, Pd) and a reactive material (Ni). The continuous redox reaction between Ni and NiO during cell operation causes volume expansion that would eventually deteriorate the cell structure.[84] In this work, LSM15 and CGO10 were chosen as the cathode materials. LSM15 has good stability and is widely used as a material for cathodes in solid state fuel cells (SOFC).[85] The ionic conductivity of CGO10 at low temperatures (<600 °C) is superior to that of YSZ.[89] In addition to performance measurements, detailed characterizations by electrochemical impedance spectroscopy (EIS) were also performed to identify the effects of adsorption layers on electrode processes for the electrochemical reduction of NO_x.

5.2 Experimental

5.2.1 Cell fabrication

Three kinds of cells were prepared and tested in this study:

1) Blank cells

2) Cells with K-Pt-Al_2O_3 adsorption layers

3) Cells with Ba-Pt-Al_2O_3 adsorption layers

The last two types of cells were prepared by coating an adsorption layer on the cathode side of the blank cell. The blank cell was supported on a 200 µm thick CGO10 tape (Kerafol, Germany). The cathodes were prepared by screen printing a composite slurry on one side of the tape and sintering at 1150 °C for 2 hours. The slurries contained equal amount of LSM15 (Haldor Topsøe, Denmark) and

CGO10 (Rhodia, France) powders. The anodes were prepared by painting Pt paste (Ferro) on the other side of the tape and sintering at 900 °C for 1 hour. The active area of the cathode was 1.54 cm^2, the same as that of the anode. The thicknesses of the cathode and anode layers were both approximately 10 µm. A mesh-patterned Au layer was painted over the cathode, sintered at 700 °C for 1 hour, and used to collect the current. An Au wire was connected to the Au layer when the cell was coated with an adsorption layer.

The adsorption layer was applied by dripping several drops of adsorbent solution on top of the cathode, drying at 110 °C for 12 hours, and heating at 550 °C for 1 hour. The amount of the adsorption layer coated on the cathode was approximately 8 mg cm^{-2} with a thickness of approximately 50 µm. The adsorbent solution was prepared by dispersing the adsorbents in distilled water with some surfactants. The adsorbents consisted of 10 wt% K with 3 wt% Pt supported on Al_2O_3 nanopowders for the K-Pt-Al_2O_3 system, and 20 wt% Ba with 1 wt% Pt for the Ba-Pt-Al_2O_3 system. These two compositions were chosen because they are commonly used as NSR catalysts. The adsorbents were prepared from Al_2O_3 powders (Alfa Aesar, Germany, metal basis) that were dissolved in distilled water with vigorous stirring. The Al_2O_3 suspensions were mixed with a solution of KNO_3 (Alfa Aesar, Germany, 99%) or $Ba(NO_3)_2$ (E. Merck Dam., Germany, 99+%) and a solution of $Pt(NH_3)_4(NO_3)_2$ (Aldrich, Germany, 99.995%). Each mixture was stirred and heated until a thick paste remained. Each paste was stored at 120 °C overnight and then at 200 °C for 2 hours to completely dry the powder. Then, the powders were milled and sintered at 600 °C for 1 hour.

5.2.2 Performance measurement of NO_x removal

The three kinds of cells were examined under the same conditions. The cells were installed in a glass tube apparatus, figure 5.2. Two pieces of Au mesh were placed on both sides of each cell as current collectors. The apparatus was placed inside a furnace and connected to a Gamry Reference 600 potentiostat. Before the conversion measurements, all the samples were pretreated in 1000 ppm NO with 8% O_2 in Ar at 350 °C for 2 to 4 h in order to remove the carbonates and hydroxides of potassium or barium that potentially co-existed in the adsorption layers with the oxide. The cells were polarized from -1 to -2.5 V for 10 - 15 minutes in the temperature range between 300 and 500 °C. The gases used to test the cells consisted of 1000 ppm NO and 1000 ppm NO with 8% O_2 in Ar with a flow rate of 2 L/h that

was maintained by Brooks mass flow controllers. The outlet gas composition was monitored throughout the test by chemiluminescence (Model 42i HL, Thermo Scientific, USA) for NO, NO_2 and NO_x and mass spectrometry (Omnistar GSD 301, Pfeiffer Vacuum, Germany) for N_2, N_2O, and O_2. A small leak (250-300 ppm N_2 and 70 -100 ppm O_2) in the gas lines was detected by mass spectrometry. Two replicates of each kind of cell were tested and gave results with good reproducibility.

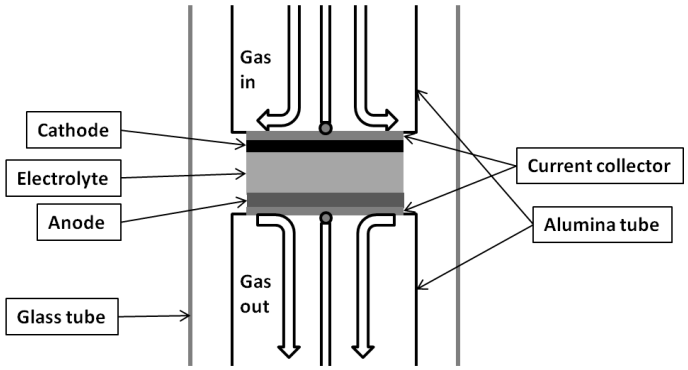

Figure 5.2 Sketch of the test setup for electrochemical cells.

5.2.3 Impedance characterization of electrode performance

Impedance spectra were recorded with a Gamry Reference 600 potentiostat over a frequency range from $1x10^6$ to 0.001 Hz with 6 data points per decade and 36 mV rms amplitude. To study the characteristics of the impedance spectra, a series of variations in the experimental conditions were made, including temperature, gas composition, and polarization. The temperature was varied in the 300-500 °C range. Three different atmospheres were supplied during the test, 1000 ppm NO (5000 ppm NO only in the case of the blank cell), 8% O_2, and 1000 ppm NO + 8% O_2. The majority of the impedance spectra were recorded at open circuit voltage (OCV). However, to study the effect of polarization, a DC voltage of -500 mV was applied at 500 °C in the presence of O_2 for comparison.

5.2.4 Microstructure observation

The microstructure of the cells was investigated by scanning electron microscopy (SEM, Zeiss Supra 35). The cells were cracked manually and used directly for the SEM observations. The SEM images were recorded with a secondary electron detector with a 10 KeV acceleration voltage.

5.3 Results

5.3.1 Microstructure of the cathodes

The SEM images of the as-prepared cathodes in the blank cell and the cells with two types of adsorption layers are shown in figure 5.3. The adsorption layers were rather porous, consisting of nano-sized particles covering the whole surface area of the cathode. The morphologies of the two types of adsorption layer were similar.

5.3.2 Performance results for NO_x removal

Simplified gas mixtures that only contained NO_x and O_2 were used in this study. As real exhaust gases contain significant amounts of CO_2, H_2O, and CO, the effect of these gas species on the deNO_x performance of the cells with the NSR adsorption layers may be important in practical situations. The harmful effects of these gas species on the NOx trapping ability of the NSR catalysts have been extensively studied.[25, 91, 97–99] The presence of CO_2 and H_2O decreases the rate of NO_x trapping, nitrate formation, or stability on the catalysts. CO competes against NO_x for the sorption sites with a high selectivity. However, it is well established that the NSR catalysts (both K-Pt-Al_2O_3 and Ba-Pt-Al_2O_3) can efficiently remove NO_x species (90% conversion) in real exhaust gases,[25, 28] which indicated that the effects of CO_2, H_2O, and CO are not crucial for the NO_x trapping ability of the catalysts. Therefore, it is reasonable to use the simplified gas mixtures as to facilitate the understanding of the underlying electrode processes for the electrochemical NO_x reduction.

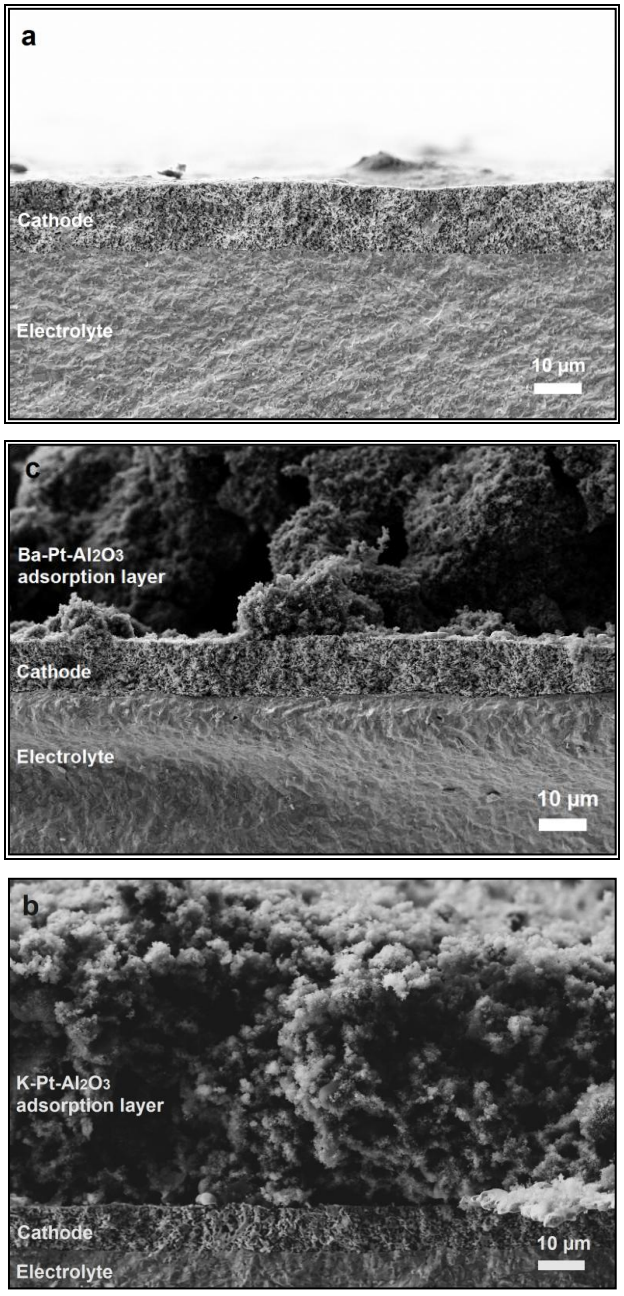

Figure 5.3 SEM images of the cathodes in a) the blank cell, b) the cell with a K-Pt-Al_2O_3 adsorption layer, and c) the cell with a Ba-Pt-Al_2O_3 adsorption layer.

The activity of an electrochemical cell with respect to removal of NO_x is usually evaluated by the NO_x conversion parameter, which is the percentage of NO_x decomposed relative to the total NO_x content. The selectivity of an electrochemical cell is represented by its current efficiency (CE), which is the ratio

of the current consumed by NO_x reduction (I_{NO}) to the total current (I_{tot}) flowing through the cell. Faraday's Law is used to calculate I_{NO}, as shown in equation 5.1.

$$I_{\mathrm{NO}} = z \times v \times \Delta \mathrm{NO_x} \times F \tag{5.1}$$

where ΔNO_x is the amount of NO_x decomposition; z is the charge change of N when it is reduced from NO_x to N_2 (for NO, z = 2; for NO_2, z = 4); v is the total flow rate; and F is Faraday's constant. Another important parameter is N_2 selectivity (η), which shows how much of the decomposed NO_x is converted to N_2. The calculation of η shown in equation 5.2 corresponds to the reaction for the decomposition of NO_x to N_2 shown in equation 5.3.

$$\eta = 2 \times \Delta \mathrm{N_2} / \Delta \mathrm{NO_x} \tag{5.2}$$

$$2\mathrm{NO_x} \rightarrow \mathrm{N_2} + \mathrm{xO_2} \tag{5.3}$$

In an atmosphere of 1000 ppm NO without O_2, the NO_x removal properties of the electrochemical cell are improved by both types of adsorption layers, although the improvement was more pronounced with the K-Pt-Al_2O_3 adsorption layer than with the Ba-Pt-Al_2O_3 adsorption layer. Figure 5.4 shows the results for NO_x reduction in 1000 ppm NO at 500 °C during polarization in the blank cell and in the cells with different adsorption layers.

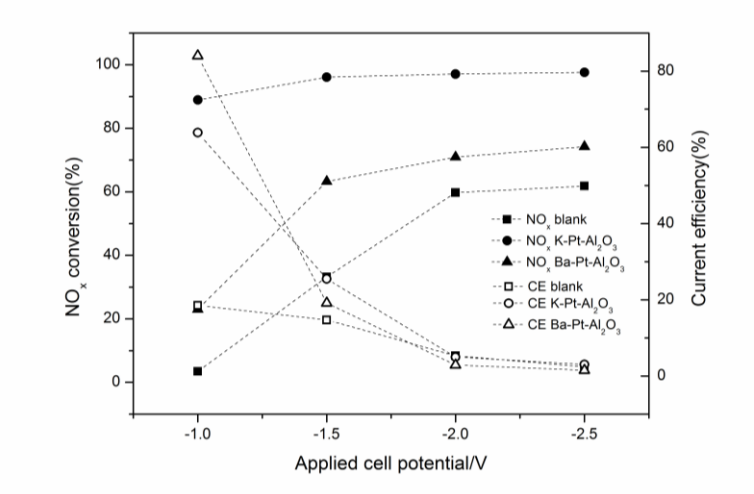

Figure 5.4 NO_x conversion and current efficiency (CE) for the blank cell, the cell with a K-Pt-Al_2O_3 adsorption layer, and the cell with a Ba-Pt-Al_2O_3 adsorption layer under different applied cell potentials in 1000 ppm NO at 500 °C

Table 5.1 NO_x conversion, current efficiency, and N_2 selectivity at different temperatures in 1000 ppm NO under polarization of -2 V on the blank cell, the cell with a K-Pt-Al_2O_3 adsorption layer, and the cell with a Ba-Pt-Al_2O_3 adsorption layer.

Temperature (°C)	NO_x conversion (%)			Current efficiency (%)			N_2 selectivity (%)		
	Blank	K-Pt-Al_2O_3	Ba-Pt-Al_2O_3	Blank	K-Pt-Al_2O_3	Ba-Pt-Al_2O_3	Blank	K-Pt-Al_2O_3	Ba-Pt-Al_2O_3
300	0.2	9.6	5.8	2.4	61	48	67	77	11
400	14	80	49	34	49	24	60	94	53
500	60	97	71	5.3	5.0	2.9	95	100	86

When O_2 was present in the atmosphere with NO, no significant conversion of NO_x to N_2 was detected for the blank cell and the cell with a Ba-Pt-Al_2O_3 adsorption layer, figure 5.5 and table 5.2. However, a significant improvement in NO_x removal was observed for the cell with a K-Pt-Al_2O_3 adsorption layer. An 85% NO_x conversion with 4% CE and 74% N_2 selectivity was achieved at -2 V and 500 °C. For the cell with a K-Pt-Al_2O_3 adsorption layer, the NO_x conversion started at a rather low voltage of -1 V and gradually increased to 90% with increasing voltage (figure 5.5). This cell's CE reached a maximum value of 6% and then decreased to approximately 3% as the voltage increased. Below 500 °C, the activity and selectivity for NO_x reduction decreased in the cell with a K-Pt-Al_2O_3 adsorption layer, but a small conversion of NO_x (3%) was observed, even at 300 °C, in the presence of 8% O_2. Both N_2 and N_2O were detected during the cell operation. The selectivity towards N_2 formation was approximately 30% at 300 and 400 °C, but it increased to more than 70% when the temperature rose to 500 °C. The high selectivity at 500 °C was expected because the stability of N_2O decreased at high temperatures.

Table 5.2 NO_x conversion, current efficiency, and N_2 selectivity at different temperatures in 1000 ppm NO with 8% O_2 under polarization of -2 V on the blank cell, the cell with a K-Pt-Al_2O_3 adsorption layer, and the cell with a Ba-Pt-Al_2O_3 adsorption layer.

Temperature (°C)	NO_x conversion (%)			Current efficiency (%)			N_2 selectivity (%)		
	Blank	K-Pt-Al_2O_3	Ba-Pt-Al_2O_3	Blank	K-Pt-Al_2O_3	Ba-Pt-Al_2O_3	Blank	K-Pt-Al_2O_3	Ba-Pt-Al_2O_3
300	0	3	0	0	26	0	-	35	-
400	-0.7[a]	42	-0.9[a]	-0.1[a]	13	-0.2[a]	-30[a]	26	-120[a]
500	1.1	85	-0.7[a]	0	4	0	50	74	-166[a]

[a] Because the variation of NO_x and N_2 concentration was less than 10 ppm under these conditions, the negative values stated for the blank cell and the cell with a Ba-Pt-Al_2O_3 adsorption layer are considered to be within the general uncertainty of the experiments.

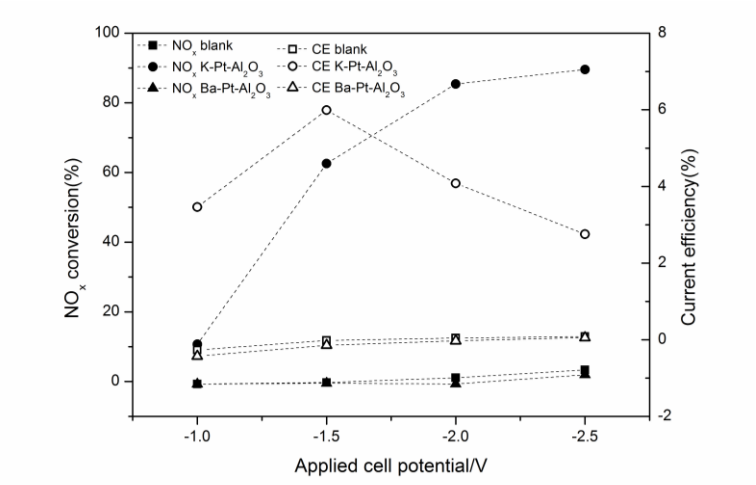

Figure 5.5 NO_x conversion and current efficiency (CE) for the blank cell, the cell with a K-Pt-Al_2O_3 adsorption layer, and the cell with a Ba-Pt-Al_2O_3 adsorption layer under different applied cell potentials in 1000 ppm NO with 8% O_2 at 500 °C.

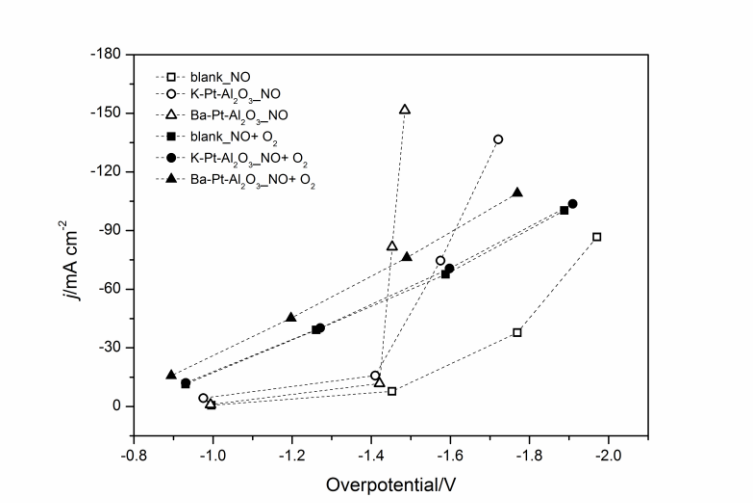

Figure 5.6 Total current density vs. overpotential curves for the blank cell, the cell with a K-Pt-Al_2O_3 adsorption layer, and the cell with a Ba-Pt-Al_2O_3 adsorption layer in atmospheres of 1000 ppm NO in Ar and 1000 ppm NO + 8% O_2 in Ar at 500 °C.

Figure 5.6 shows the total current (I_{tot}) vs. electrode overpotential curves for the three types of cells in atmospheres of 1000 ppm NO in Ar and 1000 ppm + 8% O_2 in Ar at 500 °C. The overpotentials were calculated by subtracting ohmic losses from the applied voltages. In the presence of oxygen, the values of I_{tot} increased rather linearly with increasing overpotential, showing no electronic behavior of CGO. In the absence of oxygen, the values of I_{tot} rose sharply when overpotential exceeded approximately -1.4 V, which was most likely due to a significant electronic conductivity arising from the partial reduction of

CGO. This could also explain the drastic drop in CE with increasing voltages in 1000 ppm NO in the absence of oxygen. It should be noted that under OCV conditions, the electronic conductivity of CGO is negligible even under the most extreme experiment conditions in this study (oxygen partial pressure of ~10^{-4} atm in 1000 ppm NO in Ar with a 70 - 100 ppm O_2 leak at 500 °C), as these conditions are still below the boundary conditions for the ionic domain of doped ceria (oxygen partial pressure of 10^{-13} atm at 600 °C).[90]

5.3.3 Fitting the EIS spectra

An equivalent circuit, which contained an inductance (*L)*, a serial resistance (R_s*)*, and a number of sub-circuits (*RQ,* where the resistance (*R*) and constant phase element (*Q*) were connected in parallel) that were all connected in series, was used to fit the impedance spectra. The constant phase element was used to replace the capacitance, in order to characterize the non-ideal behavior of the electrochemical system under realistic conditions. The impedance of the constant phase element can be written as[114]

$$Z = \frac{1}{Y_0(j\omega)^n} \tag{5.4}$$

where Y_0 is a constant, *j* is an imaginary number, ω is the angular frequency, and *n* is the frequency exponent.

The equivalent capacitance (C_ω) of the constant phase element can be calculated according to the formula.[115]

$$C_\omega = \frac{(RY_0)^{1/n}}{R} \tag{5.5}$$

The summit frequency of the arc was calculated as follows.

$$f_{max} = (\frac{1}{2\pi})(RY_0)^{1/n} \tag{5.6}$$

The inductance of the experimental apparatus was measured and held fixed during the fitting procedure. All of the impedance spectra were fitted with between 2 and 4 sub-circuits. In every case, the smallest number of *RQ* elements was used to obtain a reasonable and satisfactory fit (*chi-squared* < 5x10^{-4}) because an additional arc, which usually improves the fit, does not necessarily correlate with the

physical processes. In addition, trying to fit more unknown parameters from the same amount of data will increase the uncertainty of their values. Representative examples of impedance spectra and their deconvolution for the blank cell, the cell with a K-Pt-Al_2O_3 adsorption layer, and the cell with a Ba-Pt-Al_2O_3 adsorption layer are shown in figure 5.7.

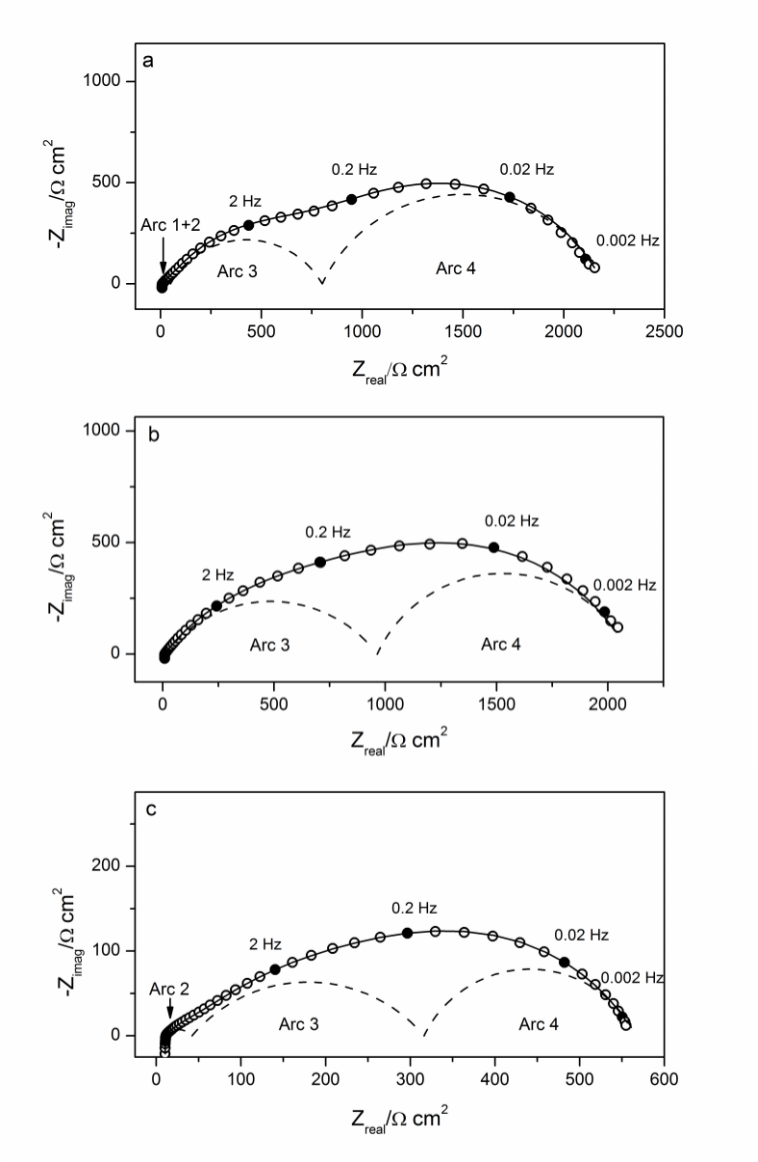

Figure 5.7 Impedance spectra for the different cells in 1000 ppm NO + 8% O_2 in Ar at 500 °C under OCV. Note the different axis scales. The solid lines represent the fitting of the entire spectrum and the dashed lines represent the deconvolution of the individual processes. The frequency is shown for the data points identified with solid circles. The spectra are: a) the blank cell; b) the cell with a K-Pt-Al_2O_3 adsorption layer; and c) the cell with a Ba-Pt-Al_2O_3 adsorption layer.

5.3.4 Characteristics of processes

During the collection of the impedance spectra, the experimental conditions (temperature, gas composition, and polarization) were varied to identify the processes that occurred in the systems. Temperatures were changed from 300 to 500 °C. Three atmospheres were supplied: 1000 ppm NO (5000 ppm NO in the blank cell), 8% O_2, and 1000 ppm NO + 8% O_2. Impedance spectra were recorded both under polarization and OCV. The characteristics of the impedance response on the three types of cells are summarized in tables 5.3 to 5.5.

Table 5.3 Characteristics of processes contributing to the impedance of the blank cell in an atmosphere of 1000 ppm NO, 5000 ppm NO, 8% O_2, and 1000 ppm NO + 8% O_2 in Ar in the temperature range of 300-500 °C. (HF-high frequency, MF-middle frequency, LF-low frequency)

Processes	Arcs	f_{max} (Hz)	C_ω (Fcm^{-2})	R (Ωcm^2)	Characteristics
HF	1	10^3 - 10^4	~ $2x10^{-7}$ Temperature independent	Decreases with increasing temperature	Independent of gas atmosphere Dependent on temperature Ea= 1.01 eV (R^2=0.991)
MF	2	2 - 330	$1x10^{-5}$ - $1x10^{-4}$ Increases with increasing temperature Depends on presence of O_2	Decreases with increasing temperature depends on presence of O_2	Dependent on temperature and presence of O_2 Ea= 1.44 eV (R^2=0.955)
LF	3, 4	0.01- 3	Increases with increasing temperature Increases under polarization decreases with increasing pNO Dependent on gas composition	Decreases with increasing temperature Decreases with increasing pNO Dependent on gas composition Magnitude decreases under polarization	One or two arcs depending on test conditions Dependent on temperature, gas composition, and polarization

Table 5.4 Characteristics of processes that contributed to the impedance of the cell with a K-Pt-Al_2O_3 adsorption layer in atmosphere of 1000 ppm NO, 8% O_2, and 1000 ppm NO+ 8% O_2 in Ar in the temperature range of 300-500 °C. (HF-high frequency, MF-middle frequency, LF-low frequency)

Processes	Arcs	f_{max} (Hz)	C_ω (F cm^{-2})	R (Ω cm^2)	Characteristics
HF	1	10^3 - 10^4	~ $2x10^{-7}$ Independent of temperature from 300 to 400 °C	Decreases with increasing temperature from 300 to 400 °C	Dependent on temperature disappears at 500 °C
MF	2	120 - 160	~ $2x10^{-4}$		Only appears in 1000 ppm NO + 8% O_2 under polarization
LF	3, 4	0.03 - 8	Increases with increasing temperature Increases under polarization Dependent on gas composition	Decreases with increasing temperature Dependent on gas composition Magnitude decreases under polarization	One or two arcs depending on test conditions Dependent on temperature, gas composition, and polarization
LF-*I*	5	0.004	~ 0.24	~ 180	Only appears in 1000 ppm NO

Table 5.5 Characteristics of processes contributing to the impedance of the cell with a Ba-Pt-Al_2O_3 adsorption layer in an atmosphere of 1000 ppm NO, 8% O_2, and 1000 ppm NO+ 8% O_2 in Ar in the temperature range of 300-500 °C. (HF-high frequency, MF-middle frequency, LF-low frequency)

Processes	Arcs	f_{max} (Hz)	C_ω (F cm^{-2})	R (Ω cm^2)	Characteristics
HF	1	500-10^4	~ $3x10^{-7}$ Independent of temperature from 300 to 400 °C	Decreases with increasing temperature from 300 to 400 °C	Dependent on temperature arc 1 disappears at 500 °C
MF	2	100 - 500	$2x10^{-5}$ - $1x10^{-4}$		Occasionally appears at 500 °C
LF	3, 4	0.01-6	Increases with increasing temperature Increases under polarization Dependent on gas composition	Decreases with increasing temperature Dependent on gas composition Magnitude decreases under polarization	One or two arcs depending on test conditions Dependent on temperature, gas composition, and polarization
LF-*I*	5	0.002	~ 0.13	~ 640	Only appears in 1000 ppm NO

5.3.5 Effects of adsorption layers on impedance spectra

The serial resistances and polarization resistances corresponding to the blank cell and cells with adsorption layers were compared (table 5.6). Due to the occasional appearance of the middle frequency arc and strong overlap of the low frequency arcs, the corresponding resistances were calculated together. The serial resistances of the cells with adsorption layers were similar to those of the blank cell, taking into account the variation between replicates. For the high-frequency process, the resistances were lower in the cells with adsorption layers than in the blank cell at 300 °C and 400 °C. When the temperature increased to 500 °C, the HF arc disappeared from the cells with adsorption layers (or became too small to be separated with sufficient accuracy). For the middle- and low-frequency processes, the decrease in the resistance for the cell with a Ba-Pt-Al_2O_3 adsorption layer was significantly greater than that for the blank cell at all temperatures. In the case of the cell with a K-Pt-Al_2O_3 adsorption layer, the resistances differed the most from the blank cell at 300 °C but decreased as the temperature increased. Overall, the introduction of an adsorption layer decreased the polarization resistance of the electrochemical cell at all of the test temperatures for 1000 ppm NO with 8% O_2. This trend was mainly caused by the decrease of the LF resistances because the LF arcs dominated the impedance spectra.

Table 5.6 The serial resistance (R_s), the high-frequency process resistance (*R1*), and the sum of the middle-and low-frequency process resistances (*R2+R3+R4*) for the blank cell, the cell with a K-Pt-Al_2O_3 adsorption layer, and the cell with a Ba-Pt-Al_2O_3 adsorption layer. The percentage change of the resistances between the blank cell and the cells with adsorption layers is also shown. The impedance spectra were recorded in an atmosphere of 1000 ppm NO + 8% O_2 in Ar under OCV.

Temperature (°C)	R_s (Ω cm^2)			*R1* (Ω cm^2)			*R2+R3+R4* (Ω cm^2)		
	Blank	K-Pt-Al_2O_3	Ba-Pt-Al_2O_3	Blank	K-Pt-Al_2O_3	Ba-Pt-Al_2O_3	Blank	K-Pt-Al_2O_3	Ba-Pt-Al_2O_3
300	145	151 (4.1%)	152 (4.8%)	956	668 (-30%)	746 (-22%)	4.35E6	7.75E4 (-98%)	1.04E6 (-76%)
400	18	17 (-5.5%)	20 (11%)	34	17 (-50%)	15 (-55%)	9.36E4	23,708 (-74%)	2.77E4 (-70%)
500	6.1	5.7 (-6.5%)	6.7 (9.8%)	4.9	-	-	2,182	2085 (-4.4%)	555 (-69%)

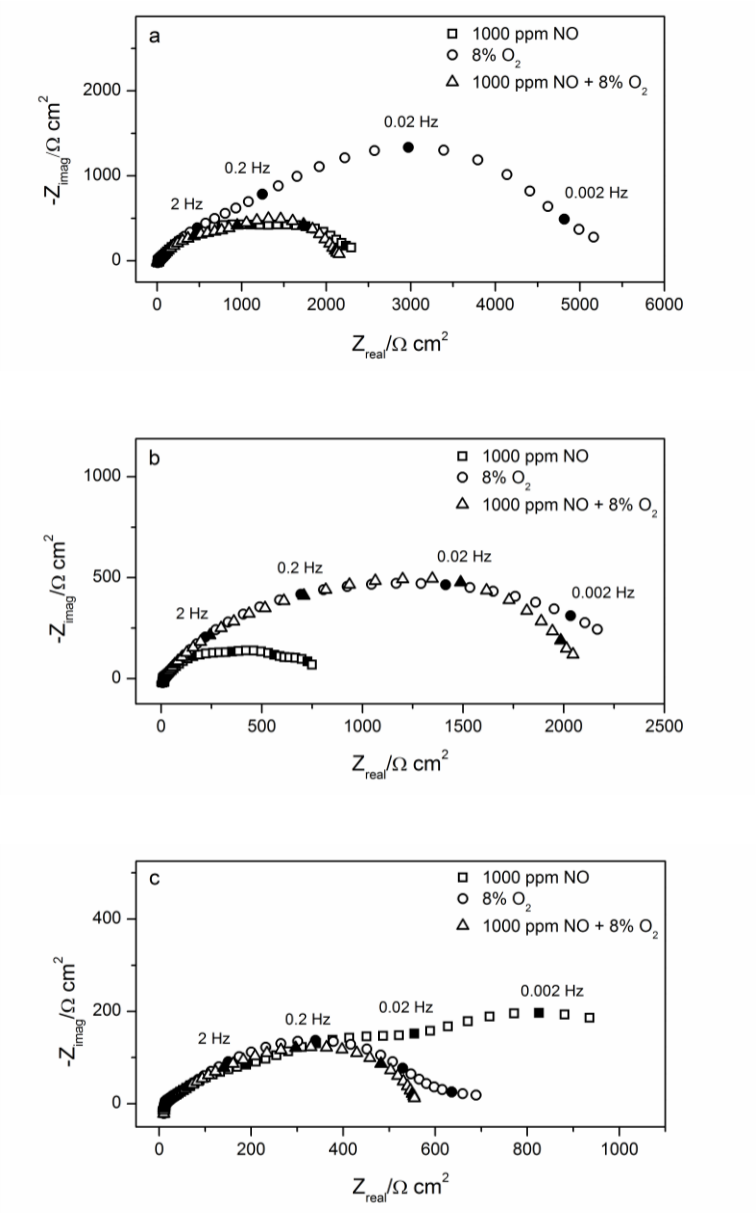

Figure 5.8 Impedance spectra for different cells in 1000 ppm NO, 8% O_2, and 1000 ppm NO + 8% O_2 in Ar at 500 °C under OCV. Note the different axis scales. The frequency is shown for the data points marked with solid circles. The spectra are: a) the blank cell; b) the cell with a K-Pt-Al_2O_3 adsorption layer; and c) the cell with a Ba-Pt-Al_2O_3 adsorption layer.

The effect of the adsorption layers on the electrochemical properties of the cells in different atmospheres was also investigated. The impedance spectra of the three kinds of cells were recorded in 1000 ppm NO, 8% O_2, and 1000 ppm NO + 8% O_2 (figure 5.8). In the blank cell, R_p was minimal in 1000 ppm NO with 8% O_2, slightly larger in 1000 ppm NO, and approximately twice as large in 8% O_2. After

adding the adsorption layers, the resistances in all three atmospheres were lower, and the relative sizes of the resistances in the different atmospheres were altered. In the case of the cell with a K-Pt-Al_2O_3 adsorption layer, the decrease of R_p in 1000 ppm NO was the most pronounced among all the atmospheres. Consequently, the R_p in 1000 ppm NO was the lowest for this case, which was approximately 50% smaller than in O_2-containing atmospheres. In the cell with a Ba-Pt-Al_2O_3 adsorption layer, the decrease of R_p in O_2-containing atmospheres was more significant that in 1000 ppm NO. As a result, the R_p in 1000 ppm NO was the largest, approximately twice as large as that in O_2-containing atmospheres.

For spectra collected in the 1000 ppm NO atmosphere, an additional arc (denoted arc 5) appeared in the lowest frequency range (< 0.02 Hz). This arc was observed only in the presence of the adsorption layers. The resistance of arc 5 was notably larger for the cell with a Ba-Pt-Al_2O_3 adsorption layer than for the cell with a K-Pt-Al_2O_3 adsorption layer (figure 5.8; tables 5.4 and 5.5).

5.4 Discussion

5.4.1 Identification of processes

In the high-frequency range, arc 1 was observed in all the impedance plots for the blank cell both under OCV and under polarization (-0.5 V) and the impedance plots from 300 to 400 °C for the cells with adsorption layers. For the blank cell, this arc was not affected by changes in the gaseous atmosphere and had an activation energy of 1.01 eV under OCV conditions. The equivalent capacitances of this arc for all three cells were approximately 10^{-7} Fcm^{-2} and independent of temperature. These characteristics are consistent with those for the process related to the transfer of oxygen ions across the interface between the electrode and electrolyte and through the electrolyte frame of the composite electrode, as reported for LSM/YSZ[116] and LSM/CGO[55, 75, 77] electrodes. The resistances of the high-frequency process were consistently lower in the cells with adsorption layers than in the blank cell from 300 to 400 °C. At 500 °C, the resistance for the cells with adsorption layers could not be estimated, probably because this arc was so small that it could not be separated from the impedance plot.

A middle-frequency arc, arc 2, in most of the impedance spectra for the blank cell both under OCV and polarization (-0.5 V) conditions, was only found in very few impedance spectra for the cells with

adsorption layers. For this reason, arc 2 will be discussed only for the blank cell. In the case of the blank cell, arc 2 was dependent on the presence of O_2 in the atmosphere. While the C_ω and resistance of this arc were almost identical in O_2-containing atmospheres (1000 ppm NO + 8% O_2 and 8% O_2), their values varied considerably in 1000 ppm NO without O_2. The C_ω of arc 2 increased with temperature in the range of $1x10^{-5}$ to $1x10^{-4}$ Fcm^{-2} and agreed fairly well with the capacitance associated with the adsorption and dissociation of O_2 and/or charge transfer reaction on the composite cathode[56, 77, 116] or in the platinum/zirconia system.[117] The activation energy of the middle-frequency process in the blank cell was calculated to be 1.44 eV, which was lower than the activation energy reported for dissociative adsorption of O_2 in the platinum/zirconia system (2-2.5 eV),[117] but in good agreement with values observed on perovskite/CGO composite electrodes (1.2-1.5 eV).[56] As a two electrode configuration was used in this study, the response of the Pt counter electrode could also be included in the impedance spectra. For the blank cell, the middle-frequency arc was attributed to the dissociative adsorption of O_2 and/or charge transfer reactions on the LSM/CGO10 electrode and/or the Pt electrode.

In the low-frequency area of the impedance spectra, one or two arcs (arcs 3 and 4) were identified under certain test conditions. Due to their strong overlap and similar dependence on the test conditions, these two arcs were combined and denoted as the low-frequency process. No new or missing processes were observed in the spectra recorded under polarization (-0.5 V) when compared with those under OCV. The characteristics of the low-frequency process were similar for the blank cell and the cells with adsorption layers. The increase of C_ω and decrease of the resistance with increasing temperature or applied polarization showed that this process was related to the extension or broadening of the triple phase boundary (TPB) zone. The dependence of this arc on the NO and O_2 concentrations indicated that O_2-related species and NO_x-related species participated in the low-frequency process. As a result, the low-frequency process was ascribed to adsorption, surface diffusion, and transfer of O_2 species and/or NO_x species at or near TPBs, which was in good agreement with previous findings on perovskite/CGO electrodes in our group.[75, 77] However, a profound decrease in the resistance of the low-frequency process was observed for almost every temperature and gas composition in the cells with adsorption layers relative to that in the blank cell, except for the cell with the K-Pt-Al_2O_3 adsorption layer in 1000 ppm NO + 8% O_2 at 500 °C, where the resistance was slightly (4.4%) lower than that in the blank cell.

The fourth process, arc 5, located in the lowest frequency range of the impedance plots, was observed in 1000 ppm NO only when the adsorption layers were present under OCV. The equivalent capacitances

and resistances of this arc, although of the same magnitude, clearly differed from the two adsorption layers. An arc present in a very low frequency range in NO-containing atmosphere could be related with the formation of NO_2 from NO which was catalyzed by LSM, as identified by Werchmeister on an LSM/CGO electrode.[55, 57] However, the absence of arc 5 from the LSM/CGO blank cell made it unlikely that the arc observed in this study was caused by the same process. The dependence of arc 5 on the presence and type of adsorption layers indicated that this arc arose from a process related to the interaction between NO and the adsorption layer, which could be oxidation of NO on Pt sites,[121–123] trapping of NO_x (mainly in the form of a nitrate) on K or Ba sites,[96, 124] or decomposition of nitrate on the trapping sites,[125, 126] as shown in the following equations.

NO oxidation:

$$\mathrm{NO} + \mathrm{O}^* \rightarrow \mathrm{NO_2} \tag{5.7}$$

NO_x trapping:

$$\mathrm{BaO} + 2\mathrm{NO} + 3\mathrm{O}^* \rightarrow \mathrm{Ba(NO_3)_2} \tag{5.8}$$

$$\mathrm{BaO} + 2\mathrm{NO_2} + \mathrm{O}^* \rightarrow \mathrm{Ba(NO_3)_2} \tag{5.9}$$

Nitrate decomposition:

$$\mathrm{Ba(NO_3)_2} \rightarrow \mathrm{BaO} + 2\mathrm{NO} + 3\mathrm{O}^* \tag{5.10}$$

$$\mathrm{Ba(NO_3)_2} \rightarrow \mathrm{BaO} + 2\mathrm{NO_2} + \mathrm{O}^* \tag{5.11}$$

where O^* represents a dissociated oxygen atom. The reactions on K sites are similar to those on Ba sites and have been omitted.

In addition, the absence of arc 5 from the impedance recorded in NO with O_2 suggested that it must be related to a process that was somehow limited by the lack of oxygen. Among the processes inside the adsorption layers (mentioned above), the first two, NO oxidation and NO_x trapping, are hindered by the shortage of oxygen species; whereas the last one, nitrate decomposition, is facilitated by low partial pressure of oxygen because the equilibrium stability of nitrate species is dramatically lower.[25]

Therefore, it is reasonable to attribute arc 5 to a process related to the oxidation of NO on Pt sites and/or the trapping of NO_x on K or Ba sites in the adsorption layers.

5.4.2 Enhancement of activity by adding the adsorption layers

The impedance spectra were obtained by measuring the AC current response of an electrochemical system under a small alternating voltage signal. The impedance of an electrode reveals the degree to which it resists polarization. In other words, the impedance corresponds to the activity of the electrode. Therefore, the impedance of the three cells under different experimental conditions provided information about how the activity of the cell was affected by the adsorption layer. In figure 5.8, the resistance of the blank cell in NO with O_2 was the lowest among the three atmospheres, while the resistance in an atmosphere only containing O_2 was quite large. The significant decrease in resistance due to the addition of NO to the atmosphere was probably due to the improvement in the activity of the electrode for reducing O_2 by means of the formation of more reactive oxygen surface species from the interaction between NO and O_2, as suggested by Reinhardt et al.[131]. After adding adsorption layers, the resistance in an atmosphere containing only NO and in an atmosphere containing only O_2 decreased significantly relative to the blank cell, indicating a general increase in activity towards reduction of both NO and O_2. However, the resistance in O_2 with NO and the resistance in O_2 without NO were similar, indicating that the activity increase for O_2 reduction with the addition of NO was negligible after it was enhanced by the adsorption layer.

Although there was a general increase in activity for both NO and O_2 reduction by the adsorption layers, the extent of enhancement for NO and O_2 reductions differed for each type of adsorption layer. For NO reduction, the resistance in an atmosphere that contained only NO was lowered more significantly by the K-Pt-Al_2O_3 adsorption layer than by the Ba-Pt-Al_2O_3 adsorption layer, indicating that the former enhanced NO reduction to a greater extent than the latter. This finding provided an explanation for the observations that both adsorption layers improved the NO_x removal performance in 1000 ppm NO without O_2, while the performance with the former was even better. For O_2 reduction, the resistance in the O_2-containing atmosphere was decreased dramatically in the cell with a Ba-Pt-Al_2O_3 adsorption layer compared to the blank cell; whereas in the cell with a K-Pt-Al_2O_3 adsorption layer, the decrease was relatively small. Combined with the effect on NO reduction, applying a K-Pt-Al_2O_3 adsorption layer led to

a large enhancement of NO reduction and a relatively small improvement in O_2 reduction, therefore, the selectivity for NO reduction increased. While using a Ba-Pt-Al_2O_3 adsorption layer significantly improved the O_2 reduction, but with a less pronounced enhancement of NO reduction, as a result, the selectivity deteriorated. This statement also explains the experimental results that when excess O_2 was supplied to the atmosphere together with NO, no improvement was observed in the cell with a Ba-Pt-Al_2O_3 adsorption layer compared to the blank cell, whereas a significant enhancement of NO_x removal was observed for the cell with a K-Pt-Al_2O_3 adsorption layer.

5.4.3 Reasons for activity enhancement

It is of great interest to understand how the electrode processes are affected by the adsorption layers, and especially whether any processes are generated by the interactions between the adsorption layers and the NO_x. This understanding could help to reveal the mechanism behind the activity enhancement by adsorption layers. Therefore, the different processes that were recognized in the impedance spectra of the three cells were carefully identified, and their characteristics were compared between the blank cell and the cells with adsorption layers. To summarize, four processes were identified in the impedance spectra of the blank cell: one high-frequency process, one middle-frequency process, and two low-frequency processes. All of the processes were affected by adding the adsorption layers, and an additional process was observed in an atmosphere of NO without O_2. However, the changes in the low-frequency processes were primarily responsible for the overall variations in the impedance spectra, which were dominated by the low-frequency arcs (figures 5.7 and 5.8). Accordingly, the decreases in the resistances of the low-frequency processes were mainly responsible for the activity enhancement by the adsorption layers. The low-frequency processes were identified as adsorption, surface diffusion, and transfer of O_2 species and/or NO_x species at or near the TPB region and oxidation of NO and/or trapping of NO_x in the adsorption layer, for the additional process that appeared only in the presence of the adsorption layers in NO without O_2. The NSR catalyst has a strong NO_x-trapping ability, which is realized by oxidizing NO to NO_2 on Pt sites and subsequently storing NO and NO_2 in the form of nitrates on K or Ba sites. The trapped NO_x species need to be released via the decomposition of the nitrates before the final reduction step can happen. This decomposition is driven by a switch from lean to rich gas conditions under the normal operation mode of the NSR catalyst. In the case of this work, it is induced by applying a negative polarization to the cell. Afterwards, the NO_x species on the trapping sites can

reach the TPBs in the electrode by two pathways, surface diffusion and desorption, and then gas diffusion. The FTRI research by Traulsen et al. verified that adsorbed NO_x is capable of moving between CGO-adsorption sites and K- or Ba-adsorption sites[127]. Therefore, the presence of an NSR adsorption layer could promote the adsorption and surface diffusion of NO_x species at/near TPB regions of the electrode in this work, especially in the interfacial area between the electrode and adsorption layers. Moreover, there is a possibility that the trapped nitrate was reduced directly to N_2 under polarization over the trapping sites adjacent to TPBs (equations 12 and 13). This may provide a short and efficient reaction path for reduction of NO_x.

$$2\mathrm{KNO_3} + 10\mathrm{e^-} \rightarrow \mathrm{K_2O} + \mathrm{N_2} + 5\mathrm{O_O^{2-}}(\mathrm{YSZ}) \quad (5.12)$$

$$\mathrm{Ba(NO_3)_2} + 10\mathrm{e^-} \rightarrow \mathrm{BaO} + \mathrm{N_2} + 5\mathrm{O_O^{2-}}(\mathrm{YSZ}) \quad (5.13)$$

Comparing the impedance spectra of the cells with the two adsorption layers in 1000 ppm NO (figure 5.8), the difference in the impedance resulted from the additional process in the low-frequency end, which was ascribed to the oxidation of NO on Pt sites and/or the trapping of NO_x on K or Ba sites in the adsorption layers. The resistance associated with this process was significantly lower for the cell with a K-Pt-Al_2O_3 layer compared to the cell with a Ba-Pt-Al_2O_3 layer. This result indicated that the capability of the K-Pt-Al_2O_3 layer for oxidizing NO and/or trapping NO_x might be stronger than that of the Ba-Pt-Al_2O_3 layer under this circumstance, which could be one of the reasons that adding a K-Pt-Al_2O_3 adsorption layer gave rise to a more pronounced enhancement for NO_x reduction. The differences in the capability of these two adsorption layers with respect to NO oxidation and NO_x trapping could be caused by a number of factors, such as the loading of the individual components, the interactions between Pt and K or Ba, the basicity of K or Ba, and the stability and mobility of the nitrates of K or Ba, which have been intensively investigated for the NSR catalyst[25] and will not be discussed in detail here.

With respect to the impedance spectra recorded in 8% O_2, the resistances of the low-frequency processes were also lowered by adding the adsorption layers. One possible explanation is that the adsorption layers, which consisted of nano-sized (50-100 nm) Al_2O_3 infiltrated with Pt and K_2O or BaO, promoted O_2 reduction of the electrode due to its large surface area and active components (Pt, K, Ba) that facilitated the adsorption and dissociation of oxygen molecules[25] at the TPBs, at least near the interfacial region. However, the exact cause of the activity enhancement for O_2 reduction by the

adsorption layers is not well understood at this time. Additional experiments are needed to clarify the role of the adsorption layers in O_2 reduction.

5.5 Conclusions

The NO_x removal performance by the blank LSM15/CGO10 cell, the LSM15/CGO10 cell with a K-Pt-Al_2O_3 adsorption layer, and the LSM15/CGO10 cell with a Ba-Pt-Al_2O_3 adsorption layer were investigated. The impedance spectra were analyzed in detail to identify the effects of the adsorption layers. In an atmosphere of only NO in Ar, both types of adsorption layers noticeably increased the activity of reducing NO_x to N_2, but the enhancement by the K-Pt-Al_2O_3 adsorption layer was greater. When O_2 was present in the atmosphere with NO, almost no conversion of NO_x to N_2 was observed in the blank cell and the cell with a Ba-Pt-Al_2O_3 adsorption layer, whereas a significant increase was observed for the cell with a K-Pt-Al_2O_3 adsorption layer. Performance of 85% NO_x conversion with 4% CE and 74% N_2 selectivity was achieved by the cell with a K-Pt-Al_2O_3 adsorption layer and polarized at -2 V at 500 °C in 1000 ppm NO with 8% O_2. This selective NO_x removal under O_2-rich conditions was achieved for the LSM15/CGO10 cell by combining it with a suitable NSR adsorption layer.

The impedance analysis revealed that the absorption layers increased the general activity of the electrochemical cell towards both NO_x and O_2 reduction. In the case of the K-Pt-Al_2O_3 adsorption layer, the enhancement of NO_x reduction was more pronounced than the O_2 reduction. The improvement of NO_x reduction by the adsorption layers was mainly caused by the promotion of adsorption and surface diffusion of NO_x species at/near TPB regions of the electrode and, possibly, by a short and effective reaction path for NO_x reduction generated at the interface between the electrode and adsorption layer. The better NO_x removal performance observed for the cell with a K-Pt-Al_2O_3 adsorption layer compared to that for a cell with a Ba-Pt-Al_2O_3 adsorption layer could be due to a stronger capability for oxidizing NO and/or trapping NO_x under the experimental conditions. The presence of an adsorption layer on the bare surface of the electrode might also facilitate the adsorption and dissociation of oxygen molecules at TPBs of the electrode to enhance the activity for O_2 reduction, but the exact cause of this behavior must be investigated further.

Acknowledgments

The authors acknowledge the financial support of the Danish Strategic Research Council under contract no. 09-065186. We are grateful to our colleagues at the Department of Energy Conversion and Storage, Technical University of Denmark, especially Dr. Johan Hjelm for many fruitful discussions.

Chapter 6 Comparison of the approaches for modifying an LSM/CGO cell with NO_x adsorbents

This chapter is the manuscript "Electrochemical NO_x reduction on an LSM/CGO symmetric cell modified by NO_x adsorbents" accepted for publication in the Journal of Materials Chemistry A.

Abstract

This study investigated the effect of modifying a $(La_{0.85}Sr_{0.15})_{0.99}MnO_3$ (LSM)/$Ce_{0.9}Gd_{0.1}O_{1.95}$ (CGO) symmetric cell by NO_x adsorbents on the electrochemical reduction of NO_x under O_2-rich conditions. The modification was based on a full ceramic cell structure without any noble metals. Three cells were prepared and tested: a blank cell, a cell impregnated with BaO, and a cell coated with a BaO/Pt/Al_2O_3 layer. The electrochemical reduction of NO_x on the three cells was studied by conversion measurement, degradation testing, and microstructure characterization. The modification, either by impregnating the BaO into the electrode or by coating the Ba/Pt/Al_2O_3 layer on the surface of the electrode, significantly increased the activity and selectivity of the NO_x reduction on the LSM/CGO symmetric cell by enhancing the adsorption and storage of the NO_x species or providing reaction sites for direct nitrate reduction. The cell with the BaO/Pt/Al_2O_3 layer exhibited a preferable performance at low temperatures (350 and 400 °C) and low voltages (1.5 to 2 V) due to the NO oxidation ability of the Pt catalyst, although it performance was relatively poor at elevated temperatures and voltages due to the impedance of the diffusion of NO_x to the reaction sites by the adsorption layer. For lowering the operation temperature and minimizing the power consumption, adding an adsorption layer was shown to be the optimum approach for modifying the electrochemical cell by NO_x adsorbents. The square-wave (SV) polarization can balance the trapping and reduction rates of NO_x species on the electrochemical cells as to further improve the NO_x reduction relative to the direct current (DC) polarization.

6.1 Introduction

Due to the harmful effects of NO_x (NO and NO_2) gases on the environment [14–16] and human health,[13] governmental regulations concerning NO_x emissions are becoming increasingly stringent

worldwide.[17] The emission control technology for NO_x is therefore in high demand, especially in the case of diesel engine exhaust, where the O_2-rich environment deactivates the traditional three-way catalysts that work effectively in gasoline engine exhaust. The most extensively researched technologies in this area are currently selective catalytic reduction with ammonia (NH_3-SCR) and NO_x reduction and storage catalysts (NSR), both of which require a reducing agent, either from a secondary supply system or by switching the operation state of the engine between lean and rich conditions.[25] One attractive alternative to these approaches is electrochemical NO_x reduction, as schematically illustrated in figure 6.1. Using this approach, NO_x is reduced to nitrogen at the polarized cathode, thereby eliminating the need for the addition of reducing agents or changes in the operational state of the engine. The main obstacle to the practical application of this technology is the achievement of high selectivity for NO_x reduction in the presence of excess O_2.[41]

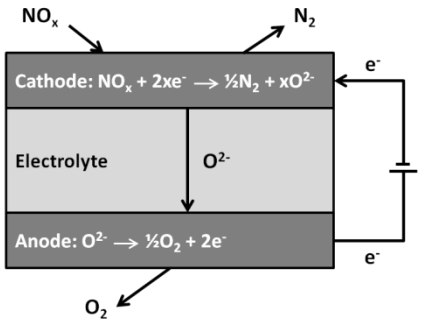

Figure 6.1 Schematic of the principle for the electrochemical reduction of NO_x.

Recent studies on electrochemical NO_x reduction show that modifying the electrochemical cell by NO_x adsorbents can significantly increase the selectivity for NO_x reduction in an O_2-rich atmosphere.[72, 73, 77, 110, 132, 133] This modification is achieved by two different approaches: adding an NO_x adsorption layer comprised of NSR catalysts on top of the electrode[72, 110, 132, 133] or impregnating the active component for NO_x adsorption (K_2O or BaO) into the electrode.[73, 77] It would be of interest to know which approach is preferable for the NO_x reduction properties and the mechanism behind the difference in performance between the approaches. However, the results of previous studies do not facilitate a meaningful comparison because they are based on various electrode materials (NiO/Pt[72, 73, 110], Ag[133], and $La_{1-x}Sr_xMnO_3$[77, 132]), various cell designs (planate cells[72, 110, 132, 133], tubular cells[73], and multilayered cell stacks[77]), and various NO_x adsorbents ($K/Pt/Al_2O_3$[72, 110, 132, 133], K_2O[73], and BaO[77]).

To investigate the NO_x reduction properties of the cells modified with the NO_x adsorbents by different approaches, three types of cells were fabricated in this study: a symmetric $(La_{0.85}Sr_{0.15})_{0.99}MnO_3$ (LSM) /$Ce_{0.9}Gd_{0.1}O_{1.95}$ (CGO) cell, an LSM/CGO cell impregnated with BaO, and an LSM/CGO cell coated with a BaO/Pt/Al_2O_3 layer. LSM was chosen as the electrode material because of its good stability and wide use as a material for cathodes in solid-state fuel cells (SOFCs).[85] CGO was chosen as the electrolyte and component of the electrode because the ionic conductivity of CGO at low temperatures (<600 °C) is superior to that of yttria-stabilized zirconia (YSZ).[89] The backbone of the electrochemical cells used in this study is therefore of an entirely ceramic structure, free of any expensive noble metals such as Pt or Pd. The effect of the impregnation and the adsorption layer on the cell performance was studied by measurements of the NO_x reduction as function of temperature, polarization voltage, and polarization frequency. The stability of the cells was studied in a degradation test. The microstructure of the cells was also investigated by scanning electron microscopy before and after testing.

6.2 Experimental

6.2.1 Cell fabrication

Three cells were prepared and tested in this study:

(1) Blank cells

(2) Cells impregnated with BaO

(3) Cells with BaO/Pt/Al_2O_3 layers

The blank cell was supported on a 300-µm-thick dense CGO tape (Kerafol, Germany). The electrodes were prepared by screen printing a composite slurry on both sides of the tape and sintering at 1150 °C for 2 h. The slurries contained equal amounts of LSM (Haldor Topsøe, Denmark) and CGO (Rhodia, France) powders. The electrodes were identical on both sides of the electrolyte, with an active area of 1.54 cm^2. The electrode layer was approximately 60 µm thick. A Au paste (ESL Electro-Science, UK) mixed with 20 wt% graphite (Graphit Kropfmühl AG, Germany) was painted over the electrodes and sintered at 700 °C for 1 h to create porous Au current collectors.

For the impregnation of the cell with BaO, a 0.32 M $Ba(NO_3)_2$ (Merck, UK) aqueous solution with 10 wt% P123 (BASF, USA) was prepared. The cell was soaked in the $Ba(NO_3)_2$ solution and placed under vacuum for approximately 10 s. Excess impregnation solution was wiped of the surface. The cell was then heated at 700 °C for 1 h to decompose the $Ba(NO_3)_2$ to BaO.

The BaO/Pt/Al_2O_3 layer was applied by dripping several drops of adsorbent solution on top of the electrodes, drying at 110 °C for 12 h, and heating at 600 °C for 1 h. Approximately 20 $mgcm^{-2}$ of the adsorption layer was coated on the electrode, with a thickness of approximately 80 µm. The adsorption layer consisted of 10 wt% Ba with 2 wt% Pt supported on Al_2O_3 nanopowders. The composition was identical to that of a normal NSR catalyst.[25] The adsorbent solution was prepared by dispersing the adsorbents in distilled water with some surfactants. The adsorbents were prepared from Al_2O_3 powders (Alfa Aesar, Germany, metal basis) that were dissolved in distilled water with vigorous stirring. The Al_2O_3 suspensions were then mixed with a solution of $Ba(NO_3)_2$ (E. Merck Dam., Germany, 99+%) and a solution of $Pt(NH_3)_4(NO_3)_2$ (Aldrich, Germany, 99.995%). The mixture was stirred and heated until a thick paste remained. The paste was stored at 120 °C overnight and then at 200 °C for 2 hours to completely dry the powder. Then, the powders were milled and sintered at 600 °C for 1 hour. An Au wire was connected to the Au current collector as the electrode was coated with the BaO/Pt/Al_2O_3 layer.

6.2.2 Electrochemical test

The cells were installed in a glass tube apparatus that was placed inside a furnace and connected to a Gamry Reference 600 potentiostat.[132] Before the conversion measurements, the samples were pretreated in 1000 ppm NO with 10% O_2 in Ar at 350 °C for 2 to 4 h to remove the barium carbonates and hydroxides that potentially existed in the cells with the NO_x adsorbents. The measurements were carried out in the temperature range of 250-450 °C, close to that of the exhaust gas from diesel engines (100-400 °C). The gas used to test the cells consisted of 1000 ppm NO with 10% O_2 in Ar maintained by Brooks mass flow controllers. The flow rate was fixed at 2 L/h. The concentrations of NO and O_2 were chosen to resemble the concentrations of the relative gas species in the diesel engine exhaust. With the co-existence of O_2, a certain amount of NO will convert to NO_2 due to the equilibrium:

$$2NO + O_2 \leftrightarrow NO_2 \quad (6.1)$$

The cells were polarized under two different modes: direct current (DC) mode and square wave (SV) mode. Under the DC mode, the voltage was applied in the negative (cathodic) direction and the positive (anodic) direction relative to the up-side electrode. The absolute value of the voltage was varied in the range of 1.5 to 2.5 V in 0.25 V intervals. Under the SV mode, the direction of the voltage was switched continuously at a certain time interval (τ), as illustrated in figure 6.2. The frequency of the SV polarization is calculated as in equation 6.2. For the frequency variation, the amplitude of the voltage was fixed at 2.25 V, with a frequency varying between 0.0083 and 1 Hz. For the amplitude variation, the absolute value was varied between 1.5 and 2.5 V in 0.25 V intervals at a fixed frequency of 0.5 Hz.

$$f = \frac{1}{2\tau} \tag{6.2}$$

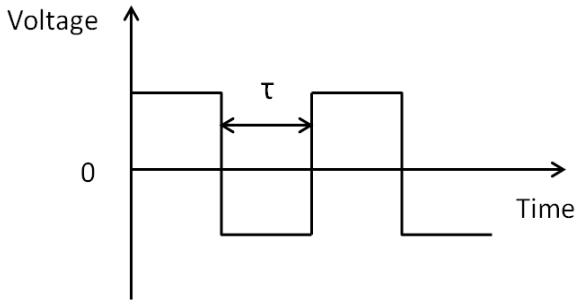

Figure 6.2 Illustration of the square wave polarization.

The outlet gas composition was monitored and recorded throughout the test using chemiluminescence (Model 42i HL, Thermo Scientific, USA) for NO, NO_2, and NO_x and mass spectrometry (Omnistar GSD 301, Pfeiffer Vacuum, Germany) for N_2, N_2O, and O_2. The three types of cells were examined under the same conditions. Two replicates for the blank cells and three replicates for the BaO-impregnated cells and the cells with the BaO/Pt/Al_2O_3 layer were tested.

Simplified gas mixtures that only contained NO_x and O_2 were used in this study. As real exhaust gases contain significant amounts of CO_2, H_2O, and CO, the effect of these gas species on the deNO_x performance of the cells with the NSR adsorption layers may be important in practical situations. The harmful effects of these gas species on the NOx trapping ability of the NSR catalysts have been extensively studied.[25, 28, 91, 97–99] The presence of CO_2 and H_2O decreases the rate of NO_x trapping, nitrate formation, or stability on the catalysts. CO competes against NO_x for the sorption sites with a high selectivity. However, it is well established that the NSR catalysts (Ba-Pt-Al_2O_3) can efficiently

remove NO_x species (90% conversion) in real exhaust gases,[25, 28] which indicated that the effects of CO_2, H_2O, and CO are not crucial for the NO_x trapping ability of the catalysts. Therefore, it is reasonable to use the simplified gas mixtures to facilitate the understanding of the underlying electrode processes for the electrochemical NO_x reduction.

6.2.3 SEM observation

The microstructure of the cells was investigated by scanning electron microscopy (SEM) (Zeiss Supra 35). The cells were cracked manually and used directly for the SEM observations. The SEM images were recorded using two types of detectors. To obtain high-magnification images of the electrode microstructure, an in-lens detector was used with a 3 keV acceleration voltage. To investigate the electrode structure on a slightly larger scale, a secondary electron detector was used with a 15 keV acceleration voltage.

6.3 Results

6.3.1 NO_x removal properties

The NO_x removal properties are usually evaluated by the NO_x conversion, current efficiency (CE), and N_2 selectivity. The NO_x conversion represents the activity of NO_x reduction, which is defined as the percentage of NO_x decomposed relative to the total NO_x content. The CE is used to evaluate the selectivity of the NO_x reduction, which is the ratio of the current consumed by NO_x reduction (I_{NO}) to the total current flowing through the cell (I_{tot}) (Eq. 6.3). The I_{tot} is the sum of the current for NO_x reduction and the current for O_2 reduction (I_{O2}) (Eq. 6.4). The value of CE depends not only on the activity of NO_x reduction but also on that of O_2 reduction.

$$CE = I_{\mathrm{NO}}/I_{\mathrm{tot}} \tag{6.3}$$

$$I_{\mathrm{tot}} = I_{\mathrm{NO}} + I_{\mathrm{O_2}} \tag{6.4}$$

The N_2 selectivity (η) indicates the extent of the decomposed NO_x converted to N_2, which is calculated as in equation 6.5, according to the decomposition reaction of NO_x to N_2 as showing in equation 6.6:

$$\eta = 2 \times \Delta N_2 / \Delta NO_x \quad (6.5)$$

$$2NO_x \rightarrow N_2 + xO_2 \quad (6.6)$$

In the case of a complete conversion of NO_x to N_2, η is equal to 100%. Due to the formation of side products (eg. N_2O), η is usually below 100%. The value of η relies only on the thoroughness of NO_x reduction.

6.3.2 Dependence on temperature

The dependence of the cell performance on temperature was studied by testing the cells at a specific voltage (square wave polarization of ±2.25 V with frequency of 0.5 Hz) in the temperatures range of 250 to 450 °C. Figures 6.3 to 6.5 show the average values and standard deviation of the NO_x conversion, CE, and N_2 selectivity of the three types of cells as a function of temperature. On the blank cell, the NO_x conversion increased slowly with increasing temperature, being less than 10% at 450 °C. On the cells with the NO_x adsorbents, significant increases in NO_x conversion were observed (from less than 20% to at least 60%) when the temperature increased from 350 to 450 °C. Below 350 °C, the NO_x conversion was equal to or less than 2% for all three types of cells, which could be considered to be within the experimental uncertainty. Therefore, the error values of the CE and N_2 selectivity were quite large at these temperatures. With respect to the CE (figure 6.4), the value decreased with increasing temperature on the blank cell above 300 °C. On the cells with the NO_x adsorbents, the effect of temperature on the CE was comparatively weak. For the N_2 selectivity (figure 6.5), the values were significantly higher on the cells with NO_x adsorbents compared to the blank cell from 300 to 450 °C, whereas increases with increasing temperature were only observed on the cell with the $BaO/Pt/Al_2O_3$ layer. Between the two types of cells modified with the NO_x adsorbents, the cells with the $BaO/Pt/Al_2O_3$ layer showed a higher NO_x conversion and CE at 350 and 400 °C. When temperature increased to 450 °C, the NO_x conversion and CE on the BaO-impregnated cell were higher.

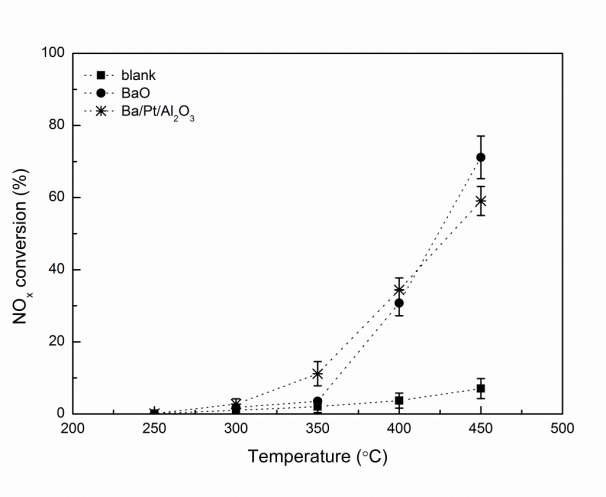

Figure 6.3 NO_x conversions on the blank LSM/CGO cell, the BaO-impregnated LSM/CGO cell, and the LSM/CGO cell with the $BaO/Pt/Al_2O_3$ layer as a function of temperature in 1000 ppm NO with 10% O_2 under a square wave polarization of 2.25 V and 0.5 Hz.

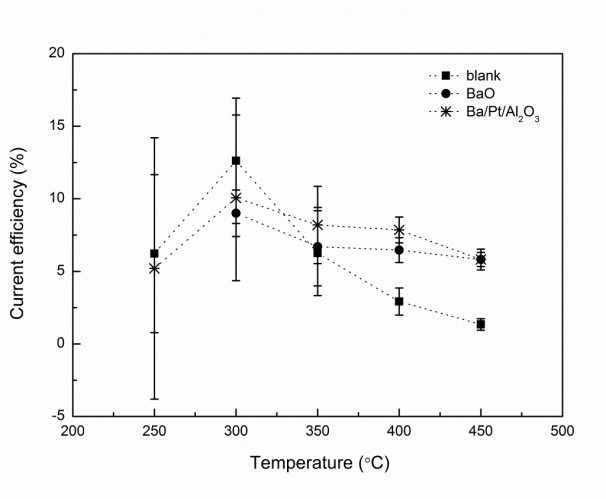

Figure 6.4 Current efficiencies on the blank LSM/CGO cell, the BaO-impregnated LSM/CGO cell, and the LSM/CGO cell with the $BaO/Pt/Al_2O_3$ layer as a function of temperature in 1000 ppm NO with 10% O_2 under a square wave polarization of 2.25 V and 0.5 Hz.

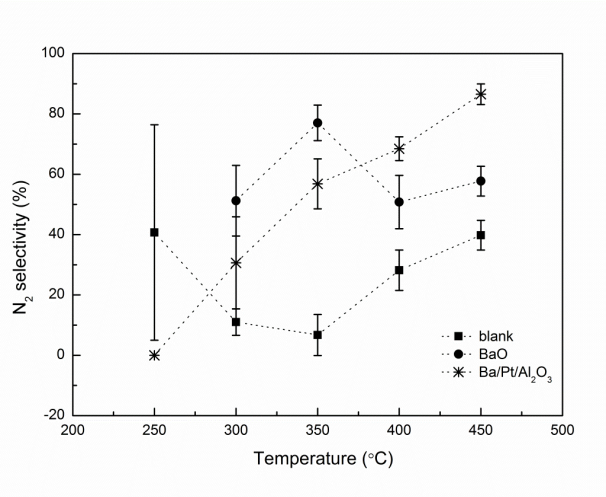

Figure 6.5 N_2 selectivities on the blank LSM/CGO cell, the BaO-impregnated LSM/CGO cell, and the LSM/CGO cell with the $BaO/Pt/Al_2O_3$ layer as a function of temperature in 1000 ppm NO with 10% O_2 under a square wave polarization of 2.25 V and 0.5 Hz.

6.3.3 Dependence on polarization mode

The influence of the polarization mode on the NO_x reduction was investigated by applying the voltage in two different ways: DC mode and SV mode. Under the DC mode, the cell was polarized by a negative (cathodic) voltage and a positive (anodic) voltage. Under the SV mode, the frequency of the polarization was fixed at 0.5 Hz. In each mode, the measurement was first made as the voltage increased from 1.5 to 2.5 V and then repeated as the voltage decreased from 2.5 to 1.5 V. The results recorded under the DC and SV modes are compared in figures 6.6 to 6.8. No evident activation or degradation effect was observed in either mode. For the blank cell, varying the voltage had no effect on the NO_x reduction under the DC mode, as almost no NO_x conversion was found under these conditions. Under the SV mode, the NO_x conversion and CE on the blank cell increased with increasing voltage, but only to a small extent (< 10%). For the cells modified with NO_x adsorbents, increases in the NO_x conversion and CE were clearly observed relative to the blank cell for both polarization modes, with the improvement being much more significant under the SV mode, especially from 2 to 2.5 V. Under the DC mode, the NO_x conversion and CE measured under the positive voltages were higher than those under the negative voltages. Comparing the two types of cells modified with NO_x adsorbents, the cell with the $BaO/Pt/Al_2O_3$ layer

showed a higher NO_x conversion from 1.5 to 2 V (except at the negative DC voltage) but exhibited diffusion-limited behavior above 2 V.

With respect to the N_2 selectivity (figure 6.8), a superior performance was observed on the cell with the $BaO/Pt/Al_2O_3$ layer at all the tested voltages. The values recorded under the DC mode on the cells with the NO_x adsorbents remained almost stable as the voltage was varied. In the case of the blank cell, the values recorded under the DC mode were thought to be within the experimental error, as the NO_x conversion under this condition was below 1%. Under the square wave mode, the N_2 selectivity increased as the voltage increased from 2 to 2.5 V for all three types of cells.

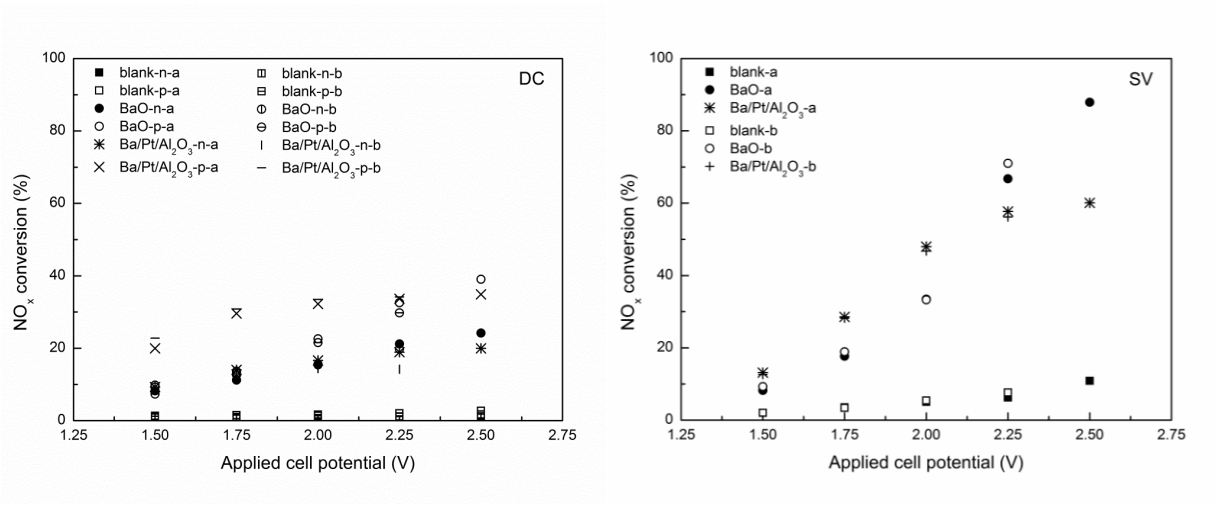

Figure 6.6 NO_x conversions on the blank LSM/CGO cell, the BaO-impregnated LSM/CGO cell, and the LSM/CGO cell with the $BaO/Pt/Al_2O_3$ layer as a function of voltage under the DC mode (left figure) and the SV mode (right figure) in 1000 ppm NO with 10% O_2 at 450 °C. The symbols labeled "n" were measured under negative DC voltages, and those labeled "p" were measured under positive DC voltages. The symbols labeled "a" were recorded during the voltage increase from 1.5 to 2.5 V, whereas those labeled "b" were recorded during the voltage decrease from 2.5 to 1.5 V.

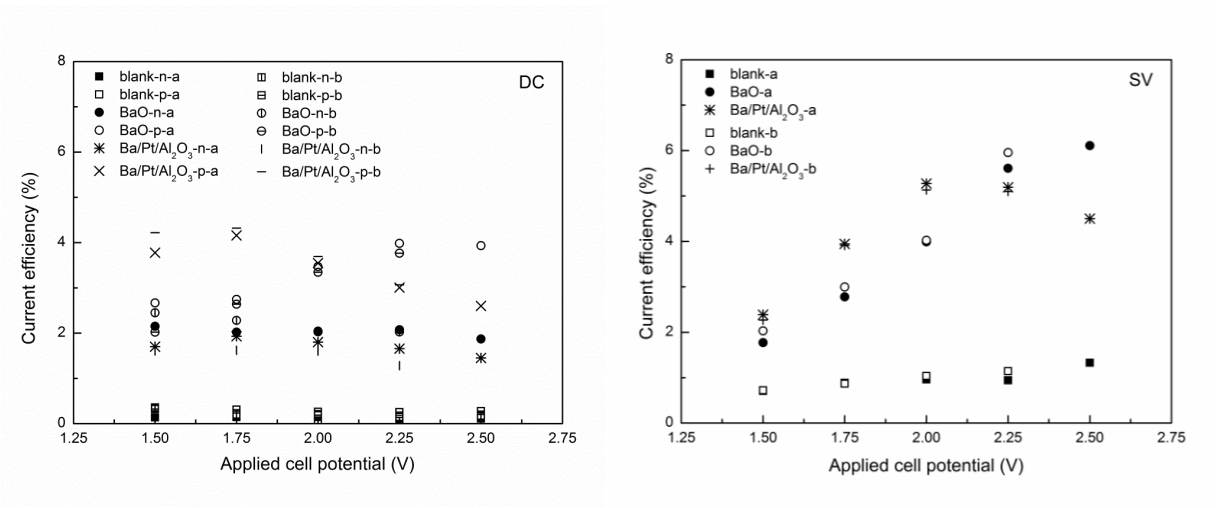

Figure 6.7 Current efficiencies on the blank LSM/CGO cell, the BaO-impregnated LSM/CGO cell, and the LSM/CGO cell with the $BaO/Pt/Al_2O_3$ layer as a function of voltage under the DC mode (left figure) and the SV mode (right figure) in 1000 ppm NO with 10% O_2 at 450 °C. The symbols labeled "n" were measured under negative DC voltages, and those labeled "p" were measured under positive DC voltages. The symbols labeled "a" were recorded during the voltage increase from 1.5 to 2.5 V, whereas those labeled "b" were recorded during the voltage decrease from 2.5 to 1.5 V.

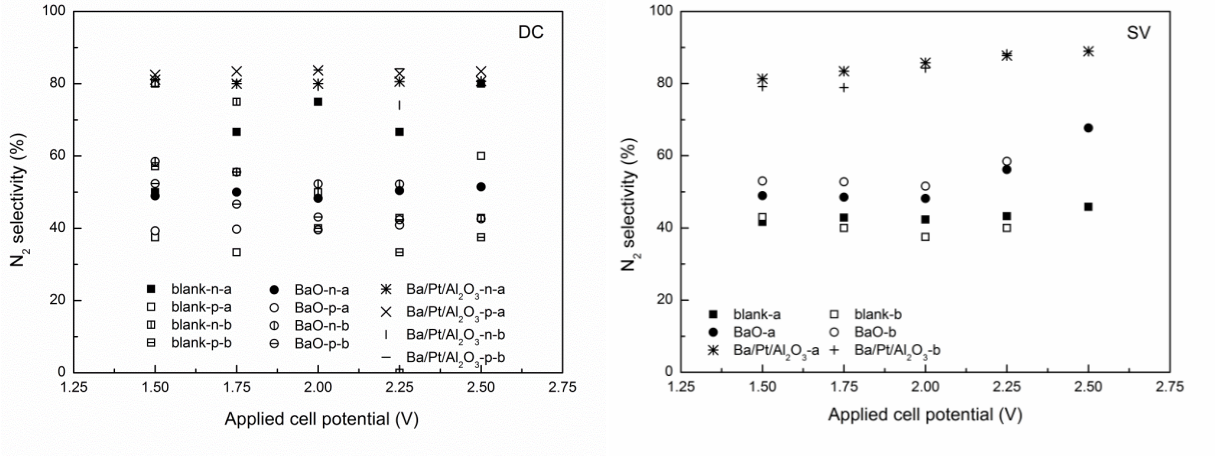

Figure 6.8 N_2 selectivities on the blank LSM/CGO cell, the BaO-impregnated LSM/CGO cell, and the LSM/CGO cell with the $BaO/Pt/Al_2O_3$ layer as a function of voltage under the DC mode (left figure) and the SV mode (right figure) in 1000 ppm NO with 10% O_2 at 450 °C. The symbols labeled "n" were measured under negative DC voltages, and those labeled "p" were measured under positive DC voltages. The symbols labeled "a" were recorded during the voltage increase from 1.5 to 2.5 V, whereas those labeled "b" were recorded during the voltage decrease from 2.5 to 1.5 V.

6.3.4 Dependence on polarization frequency

As a greater increase in NO_x conversion and CE was observed for the square wave voltage than the DC voltage for all three cells, it is of interest to determine how the frequency of the square wave polarization affects the NO_x reduction. Figures 6.9 to 6.11 show the results for the three types of cells measured at various frequencies in 1000 ppm NO with 10% O_2 at 450 °C. The amplitude of the square wave polarization was fixed at 2.25 V. The data were recorded as the frequency increased from 0.0083 and 1 Hz and then as the frequency decreased from 1 to 0.0083 Hz. As in the case of the voltage variation, similar results were obtained during both halves of the measurement. With respect to the blank cell, a monotonic increase in the NO_x conversion and CE with increasing frequency was observed in the tested frequency range. Unlike the blank cell, "turning points" for the increase of the NO_x conversion and CE with increasing the frequency were observed on the cells with the NO_x adsorbents, where the NO_x conversion and CE began to decrease with increasing frequency beyond certain values. The maximum NO_x conversion and CE were achieved at 0.1 Hz for the cell with the $BaO/Pt/Al_2O_3$ layer and 0.5 Hz for the BaO-impregnated cell. For the N_2 selectivity, the effect of frequency appeared to be negligible. Regarding the reproducibility of the frequency test, similar trends were observed with the replicates of the cells with the NO_x adsorbents, with only slight shifts in the optimum frequencies (to 0.06 Hz for the cell with the $BaO/Pt/Al_2O_3$ layer and 0.2 Hz for the BaO-impregnated cell).

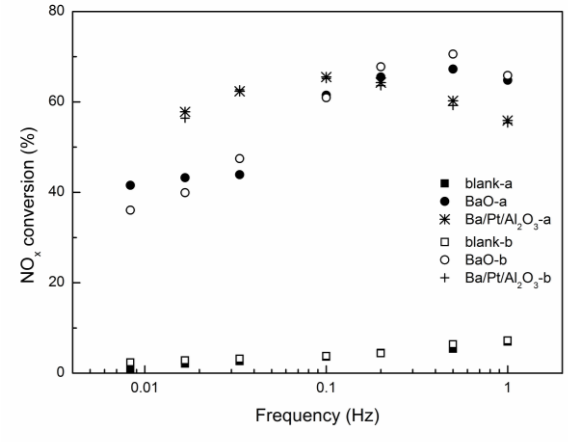

Figure 6.9 NO_x conversions on the blank LSM/CGO cell, the BaO-impregnated LSM/CGO cell, and the LSM/CGO cell with the $BaO/Pt/Al_2O_3$ layer as a function of frequency under the SV mode in 1000 ppm NO with 10% O_2 at 450 °C. The symbols labeled

"a" were recorded during the frequency increase from 0.0083 to 1 Hz, whereas those labeled "b" were recorded during the frequency decrease from 1 to 0.0083 Hz.

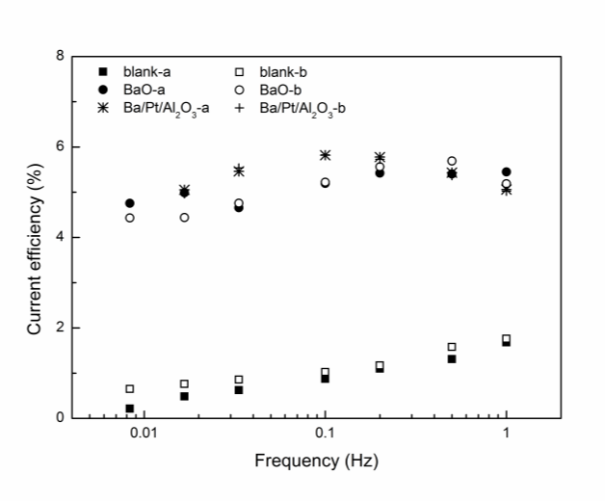

Figure 6.10 Current efficiencies on the blank LSM/CGO cell, the BaO-impregnated LSM/CGO cell, and the LSM/CGO cell with the $BaO/Pt/Al_2O_3$ layer as a function of frequency under the SV mode in 1000 ppm NO with 10% O_2 at 450 °C. The symbols labeled "a" were recorded during the frequency increase from 0.0083 to 1 Hz, whereas those labeled "b" were recorded during the frequency decrease from 1 to 0.0083 Hz.

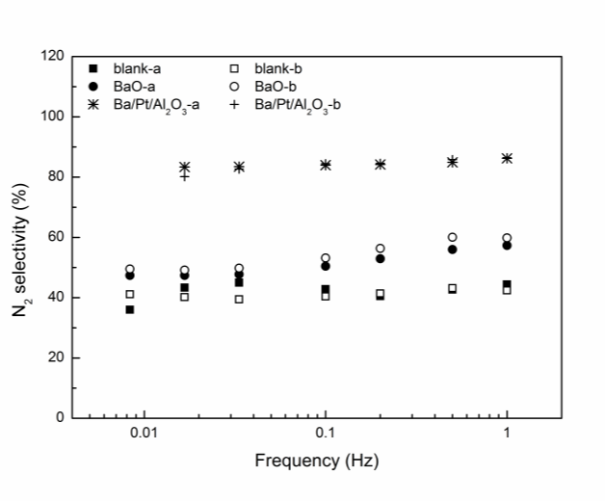

Figure 6.11 N_2 selectivities on the blank LSM/CGO cell, the BaO-impregnated LSM/CGO cell, and the LSM/CGO cell with the $BaO/Pt/Al_2O_3$ layer as a function of frequency under the SV mode in 1000 ppm NO with 10% O_2 at 450 °C. The symbols labeled "a" were recorded during the frequency increase from 0.0083 to 1 Hz, while those labeled "b" were recorded during the frequency decrease from 1 to 0.0083 Hz.

6.3.5 Degradation test

The stability of the cells for NO_x reduction was studied by running a degradation test after the temperature, voltage, and frequency tests. The degradation test was performed on one of the replicates for the three types of cells by operating the cells at 450 °C for approximately 100 h. During this period, the cells experienced frequent switches between the polarization and the open circuit states as well as variations in the gas concentration (0-5000 ppm NO with 0-20% O_2). The results of NO_x reduction on the cells before and after the degradation test are listed in table 6.1. For the blank cell, the variation in the NO_x conversion and CE was negligible considering the deviation caused by the experimental uncertainty. In contrast, a 30-40% decrease in NO_x conversion and an approximately 10% decrease in CE were observed for the cells with the NO_x adsorbents, indicating that the NO_x reduction performance deteriorated after 100 h of operation. With respect to the N_2 selectivity, the values generally remained constant throughout the long-term operation.

Table 6.1 NO_x conversions, current efficiencies, and N_2 selectivities on the blank LSM/CGO cell, the BaO-impregnated LSM/CGO cell, and the LSM/CGO cell with the $BaO/Pt/Al_2O_3$ layer measured at a square wave polarization of 2.25 V with a frequency of 0.5 Hz in 1000 ppm NO with 10% O_2 in Ar at 450 °C before and after 100 h of operation.

	Before (%)			After (%)		
	NO_X conversion	Current efficiency	N_2 selectivity	NO_X conversion	Current efficiency	N_2 selectivity
Blank	8.11	1.42	38.3	7.64	1.22	40.0
BaO	70.6	5.86	58.3	40.8	5.17	62.2
$BaO/Pt/Al_2O_3$	65.1	5.85	86.3	45.8	5.05	84.9

6.3.6 Microstructure of the electrodes

Figure 6.12 shows the microstructure of the electrodes on the three types of cells before and after the electrochemical test. Before the testing, the blank cell showed well-defined electrode grains with a smooth surface (figure 6.12 a). The BaO formed distinct nano-grains distributed over the surface of electrode on the BaO-impregnated cell (figure 6.12 c). The BaO/Pt/Al_2O_3 layer was porous, consisting of nano-sized particles covering the electrode. The Pt and BaO were recognized as ultra-fine particles dispersed over the surface of the Al_2O_3 support (figure 6.12 e). The electrode of the cell with the BaO/Pt/Al_2O_3 layer appeared similar to that of the blank cell before testing (figure 6.12 g). After testing, no evident change was observed on the electrode of the blank cell or the BaO/Pt/Al_2O_3 layer (figure 6.12 b and f). A profound change in the microstructure was observed on both the electrode of the BaO-impregnated cell and that of the cell with the BaO/Pt/Al_2O_3 layer (figure 6.12 d and h). The surface of the two electrodes became “fluffy”, being covered by small grains. Moreover, most of the distinct particles introduced by the impregnation disappeared on the BaO-impregnated cells after testing.

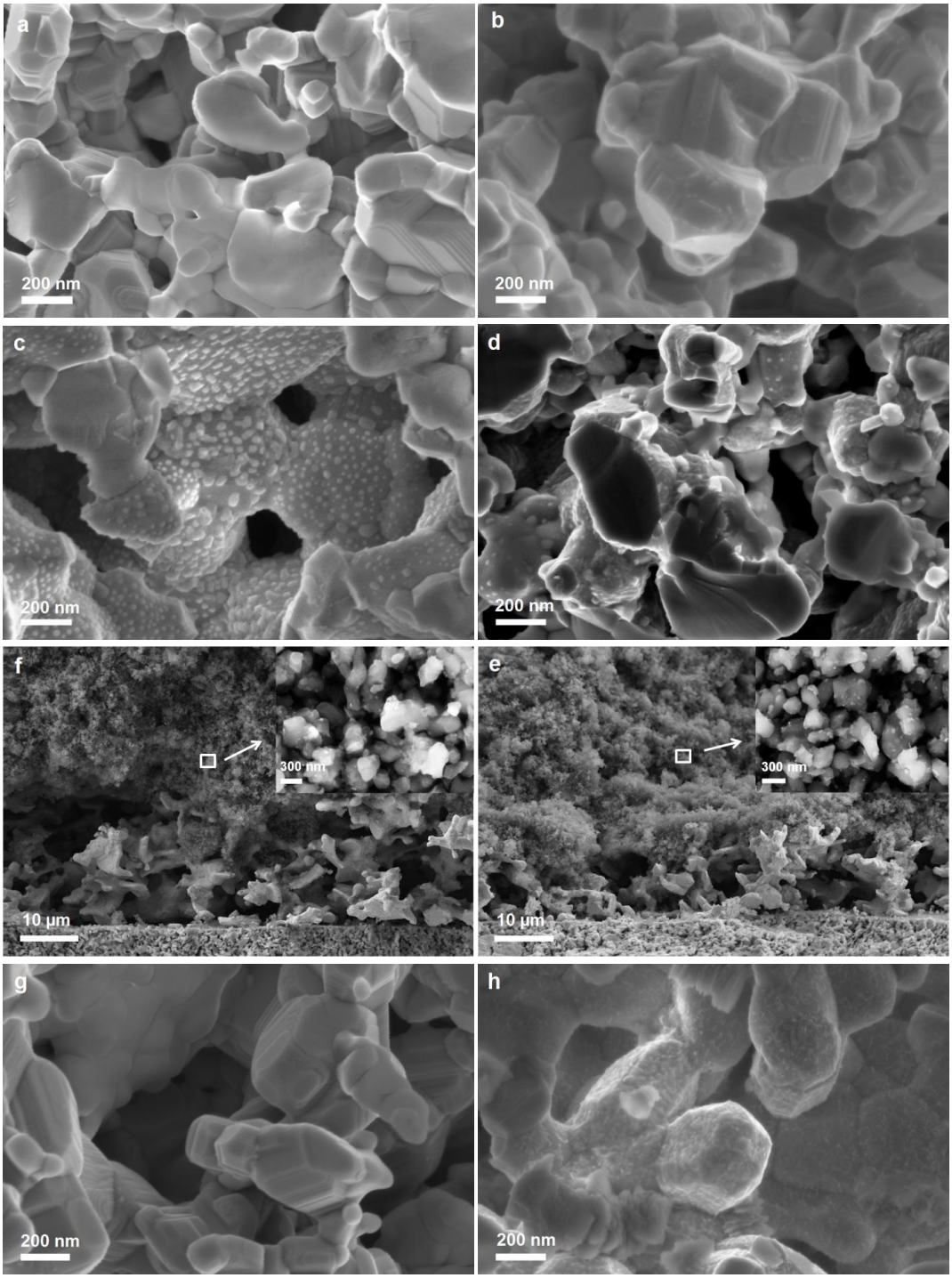

Figure 6.12 Microstructure images for the electrodes of the blank LSM/CGO cell, the BaO-impregnated LSM/CGO cell, and the LSM/CGO cell with the BaO/Pt/Al_2O_3 layer before and after testing. The images include a) the blank electrode before testing, b)

the blank electrode after testing, c) the BaO-impregnated electrode before testing, d) the BaO-impregnated electrode after testing, e) the BaO/Pt/Al_2O_3 layer before testing , f) the BaO/Pt/Al_2O_3 layer after testing, g) the electrode with the BaO/Pt/Al_2O_3 layer before testing, and g) the electrode with the BaO/Pt/Al_2O_3 layer after testing.

6.4 Discussion

6.4.1 Effect of the impregnation and the adsorption layer

For the practical application of the electrochemical NO_x reduction, the major barrier is the low selectivity of the NO_x reduction in the O_2-rich atmosphere. The experimental results showed that not only the NO_x conversion but also the CE and N_2 selectivity were significantly increased by introducing the NO_x adsorbents to the blank LSM/CGO cell, either by adding an adsorption layer on top of the electrodes or by impregnating the adsorbent into the electrodes. This finding indicated that the presence of the NO_x adsorbents was able to effectively improve the selectivity of the NO_x reduction over O_2 reduction and enhance the thoroughness of reducing NO_x to N_2.

For the LSM/CGO electrode, Werchmeister et al.[55] proposed NO_2 as an intermediate for the electrochemical reduction of NO_x based on a study of model electrodes. Later studies on LSM/CGO cell stacks[77] and single cells[132] also supported this assumption. Therefore, NO_2 was suggested as the intermediate for the NO_x reduction in this study. Moreover, NO_2 has been found to be the sorption precursor or a required intermediate in the NO_x storage process (Eq. 6.10).[25] The formation of NO_2 is spontaneous in the O_2-rich atmosphere due to the thermodynamic equilibrium between NO and NO_2 (Eq. 6.1), whereas this reaction is kinetically limited within a small fraction, especially at low temperatures.[25] In the case of the electrochemical cell, NO_2 can also been generated from NO oxidation under positive (anodic) polarization, which may be an important factor in the superior performance of NO_x reduction under positive polarization relative to that under negative polarization, as illustrated in figure 6.13.

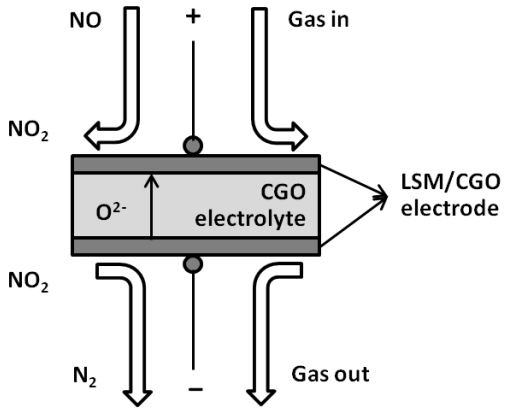

Figure 6.13 Schematic representation of the electrochemical NO_x reduction under the positive DC polarization.

On the blank LSM/CGO cell, the electrochemical reduction of NO_x can be generally described as proceeding according to the following steps: (1) gas-phase diffusion and adsorption of NO_2 on the surface of the electrodes (Eq.6. 7), (2) surface diffusion from the adsorption sites to the reaction sites at the triple-phase boundaries (TPBs) (Eq. 6.8), and (3) the electrochemical reduction of NO_2 to N_2 on the TPBs under the negative polarization (Eq. 6.9). However, as the concentration ratio of O_2 : NO_x was as high as 100 : 1 in the atmosphere, most of the adsorption and reaction sites will be dominated by O_2. The NO_x reduction is therefore negligible on the blank cell.

$$\mathrm{NO_2(g) + Site(LSM/CGO) \rightarrow\ NO_2(LSM/CGO)} \tag{6.7}$$

$$\mathrm{NO_2(LSM/CGO) \rightarrow NO_2(TPB)} \tag{6.8}$$

$$\mathrm{2NO_2(TPB) + 4V_O^{\cdot\cdot} + 8e^- \rightarrow N_2 + 4O_O^{2-}} \tag{6.9}$$

On the BaO-impregnated cell, the adsorption of NO_2 was significantly enhanced because BaO is capable of selectively absorbing and storing NO_2 in the form of nitrates (Eq. 6.10).[25, 124] The stored NO_2 must be released via the decomposition of the nitrates before the final reduction step can occur. The decomposition of nitrates is induced by applying a negative polarization to the cell.[110] Afterwards, the NO_2 species on the trapping sites can reach the TPBs by two pathways, surface diffusion (Eq. 6.11)[127] and desorption, followed by gas diffusion. Moreover, the trapped nitrate may be reduced directly to N_2 under negative polarization over the trapping sites, as they are adjacent to the TPBs (Eq. 6.12). This process may provide a short and efficient reaction path for the reduction of NO_x.

$$2NO_2(g) + O_2(g) + BaO \rightarrow Ba(NO_3)_2 \quad (6.10)$$

$$NO_2(BaO) \rightarrow NO_2(TPB) \quad (6.11)$$

$$Ba(NO_3)_2(TPB) + 5V_O^{\cdot\cdot} + 10e^- \rightarrow N_2(g) + 5O_O^{2-} + BaO\ (TPB) \quad (6.12)$$

On the cell with the BaO/Pt/Al_2O_3 layer, the adsorption and storage of NO_x can also be promoted as on the BaO-impregnated cell. However, unlike the impregnated cell, the storage sites are distant from the reaction sites; thus, the direct reduction of the nitrates seems impossible. Another difference is the Pt particles in the adsorption layer, which are absent in the case of the impregnated cell. As an efficient NO oxidation catalyst, Pt is able to increase the NO_2 fraction[25, 121, 122], which in turn improves the NO_x storage and reduction. This factor may explain why the NO_x conversion on the cell with the BaO/Pt/Al_2O_3 layer was superior to that on the BaO-impregnated cell at low temperatures and low voltages, where the formation of NO_2 from the NO/NO_2 equilibrium and the electrochemical oxidation were insufficient. However, with increasing temperature and voltage, the NO_x conversion on the BaO-impregnated cells increased distinctly, whereas the conversion on the cell with the BaO/Pt/Al_2O_3 layer increased slowly or showed a diffusion-limited behavior, indicating that the additional layer inhibited the gas diffusion of the NO_x species to the reaction sites in the electrode.

In summary, introducing the NO_x adsorbents to the LSM/CGO electrochemical cell selectively promoted NO_x reduction by enhancing the adsorption and storage of the NO_x species or providing reaction sites for direct nitrate reduction (the impregnated cell). The cell with the BaO/Pt/Al_2O_3 layer performed better than the impregnated cell at low temperatures (350 and 400 °C) and low voltages (1.5 to 2 V) due to the NO oxidation ability of the Pt catalyst, whereas the additional layer impeded the diffusion of the NO_x species to the reaction sites, resulting a worse performance than the impregnated cell at elevated temperatures and voltages.

6.4.2 NO_x storage and reduction

When polarized under SV mode instead of DC mode, an increase in the NO_x conversion and CE was clearly observed from 2 to 2.5 V for all three cells. During the SV polarization, the direction of the voltage was switched continuously. The instantaneous voltage at the moment of the switch should be twice that of the steady state, which was verified by the “spark” of the current recorded simultaneously.

From this viewpoint, it seems that the improvement in the NO_x reduction by the SV mode was partially due to the effect of magnifying the voltage. Thus, the higher the frequency of the SV polarization, the larger the effect should be. However, the experimental results showed that the NO_x conversion did not increase monotonically with frequency, instead decreasing with frequency after reaching peak values on the cells with the NO_x adsorbents. Moreover, based on the results that the CE decreased with increasing DC voltage above 2.25 V, the value of CE was expected to be lower under the SV mode than the DC mode. Therefore, the effect of magnifying the instant voltage cannot be the primary reason for the improvement of NO_x reduction by the SV polarization.

Based on the analysis of the reaction mechanism provided in the previous section, the process of the NO_x conversion on the electrochemical cell with the NO_x adsorbents can be divided into two steps: the NO_x trapping step, including the gas phase diffusion, the adsorption, and the storage of NO_x as nitrate on the storage sites (BaO), followed by the reducing step, including the decomposition of nitrate, the surface diffusion or gas diffusion of the released NO_x species, and the electrochemical reduction of NO_x to N_2 under polarization on the reaction sites (TPBs). If the overall reaction was limited by the second step, the difference in the activities of NO_x reduction between the DC mode and the SV mode would not be significant. If the first step is the rate-limiting step, under the DC mode, the NO_x stored at the BaO sites will soon be depleted by the following reduction step and the slow NO_x trapping rate will subsequently impede the overall reaction. Using the SV mode, the reduction step can be switched to the other electrode after the stored NO_x has been exhausted on the current electrode, consequently improving the overall NO_x reduction. Therefore, the improvement of NO_x reduction by the SV mode was most likely due to the balance of the trapping and reduction rates of NO_x species on the electrochemical cells, which is also suggested as the cause of the better NO_x removal properties at the SV voltages than the DC voltages on a NiO/YSZ cell with a NO_x adsorption layer by Hamamoto et al.[72]. Accordingly, the optimum frequency of the SV polarization is dependent on the rate of NO_x trapping and reduction on the electrochemical cells. On the BaO-impregnated cell, the storage sites was adjacent to the reaction sites, which may benefit the surface diffusion and gas diffusion of the released NO_x species to the reaction sites, in turn promoting the decomposition of nitrate on the storage sites and potentially enabling the direct reduction of nitrate to N_2 under polarization. Moreover, the impregnated cell avoided the limitation of gas diffusion by the additional layer compared with the cell with the $BaO/Pt/Al_2O_3$ layer. These factors could accelerate the storage and/or reduction rate of the NO_x species

on the BaO-impregnated cell, thus leading to a higher optimum frequency on the impregnated cell. In the case of the blank cell, as the NO_x conversion and CE increased with increasing frequency in the tested range, no optimum frequency was observed. One possible reason is that the optimum frequency is above the test limit because the adsorption and reduction rate of NO_x on the blank cell might be comparatively fast due to the absence of nitrate formation and decomposition. However, omitting the NO_x storage step also resulted in a poor activity of the NO_x reduction in the O_2-rich atmosphere.

6.4.3 Degradation related with the microstructure change

The correlation of the degradation test with the microstructure observations indicates that the degradation of the NO_x removal performance on the BaO-impregnated cell and the cell with the $BaO/Pt/Al_2O_3$ layer may be due to the profound change in the microstructure. Between these two types of cells, the microstructure appears fairly similar after testing despite being quite different before testing. One possible explanation of this observation is that the microstructure change could be caused by the same type of reaction on the two different cells, such as the reaction between the electrode materials with the Ba compounds (BaO and or $Ba(NO_3)_2$) either dispersing over the surface of the electrode or diffusing from the $BaO/Pt/Al_2O_3$ layer to the electrode. With respect to the reactivity between LSM/CGO and Ba compounds under heating, no significant reaction between CGO and the Ba-containing materials has been found below 1000 °C in the literature.[134–138] Most of the studies on LSM indicate that LSM does not react with the Ba-containing materials.[139–141] However, considering the polarization effect, especially the strong corrosivity of nitrate under polarization and heating,[108, 129, 142] the reaction between the electrode materials and the Ba compounds is possible. Traulsen et al.[77] reported a distinct change in the microstructure on the LSM/CGO cell stacks infiltrated with BaO after the electrochemical test and attributed it to the reaction between BaO and LSM/CGO under the test conditions. Our study on the NiO/YSZ/Pt electrode[110] shows that the electrodes can be corroded by potassium nitrate under polarization, which changed the microstructure of the electrodes after testing. Nevertheless, further microstructure and elemental analysis is needed to investigate the exact cause of the microstructure change, whether new phases are formed, and what the compositions of the phases are on the cells with the NO_x adsorbents.

With respect to the degradation of the BaO/Pt/Al_2O_3 layer, it is reported that Pt agglomeration begins at 600 °C when exposed to an oxidizing atmosphere[100] and the BaO will react with the Al_2O_3 support at temperatures exceeding 600 °C.[101] The sintering of Pt is not definitively detrimental to all the catalyst functions, but the formation of Ba- and Al- containing compounds is directly related to the loss in NO_x trapping ability.[25, 100, 101] As all the measurements were performed at temperatures far below 600 °C in this study, no significant degradation is expected in the adsorption layer. The microstructure observation that the morphology of the adsorption layer remained almost identical before and after the tests also confirms this assumption.

6.5 Conclusions

The electrochemical reduction of NO_x on a blank symmetric LSM/CGO cell, an LSM/CGO cell impregnated with BaO, and an LSM/CGO cell with a BaO/Pt/Al_2O_3 layer has been investigated to evaluate the two main approaches for modifying the electrochemical cells by NO_x adsorbents based on a full ceramic cell structure. The NO_x conversion on the blank LSM/CGO cell was negligible at the DC voltages and was less than 10% at the SV voltages in 1000 ppm NO with 10% O_2. For the BaO-impregnated cell and the cell with the BaO/Pt/Al_2O_3 layer, the activity and selectivity of the NO_x reduction were significantly increased under DC and SV voltages due to the enhancement of the adsorption and storage of the NO_x species or the availability of reaction sites for direct nitrate reduction (the impregnated cell). The cell with the BaO/Pt/Al_2O_3 layer showed a preferable performance at low temperatures (350 and 400 °C) and low voltages (1.5 to 2 V) relative to the impregnated cell due to the NO oxidation ability of the Pt catalyst, but the adsorption layer impeded the diffusion of the NO_x species to the reaction sites, which resulted in a worse performance at elevated temperatures and voltages than the impregnated cell. From the aspect of lowering the operation temperature and minimizing the electrical consumption, the approach of adding a NO_x adsorption layer appeared to be more favorable than that of the impregnation. Moreover, the electrochemical cells were suggested to be operated under SV mode instead of DC mode because the SV polarization can balance the trapping and reduction rates of the NO_x species on the cells as to further improve the NO_x conversion and CE relative to the DC polarization. The optimum frequencies for the SV polarization were recorded on the BaO-impregnated cell (0.06-0.1 Hz) and the cell with the BaO/Pt/Al_2O_3 layer (0.2-0.5 Hz). The higher optimum frequency on the impregnated cell was most likely due to the storage sites' being close to the reaction sites,

accelerating the trapping and/or reduction rate of the NO_x species with respect to the cell with the $BaO/Pt/Al_2O_3$ layer. A 30-40% decrease in NO_x conversion and approximately 10% decrease in CE were observed on the BaO-impregnated cell and the cell with the $BaO/Pt/Al_2O_3$ layer after 100 h of operation, which may have been associated with the profound microstructure change after testing. The exact cause of the microstructure change requires further investigation.

Acknowledgments

This work was supported by the Danish Strategic Research Council under contract no. 09-065186. The authors would like to thank colleagues at the Department of Energy Conversion and Storage, Technical University of Denmark, for their assistance and discussions.

Chapter 7 Impedance characterization of LSM/CGO cells modified with NO_x adsorbents

This chapter is the manuscript "Characterization of LSM/CGO symmetric cells modified by NO_x adsorbents for electrochemical NO_x removal with impedance spectroscopy" accepted for publication in the Journal of the Electrochemical Society.

Abstract

This study uses electrochemical impedance spectroscopy (EIS) to characterize an LSM/CGO symmetric cell modified by NO_x adsorbents for the application of electrochemical NO_x reduction. Three cells were prepared and tested: a blank cell, a cell impregnated with BaO, and a cell coated with a BaO-Pt-Al_2O_3 layer. The impedance analysis revealed that modification with the NO_x adsorbents, either by impregnating the BaO into the electrode or by adding a BaO-Pt-Al_2O_3 layer on top of the electrode significantly enhanced the electrode activity. This activity enhancement was mainly due to the decrease in the resistance of the low-frequency processes, which were ascribed to adsorption, diffusion, and transfer of O_2 species and NO_x species at or near the triple phase boundary (TPB) region and the formation of the reaction intermediate NO_2. The BaO impregnation improved the adsorption of NO_x on the LSM/CGO electrode by selectively trapping NO_2 in the form of nitrate over the BaO sites and provided availability for a direct reduction of the stored nitrate. The BaO-Pt-Al_2O_3 layer enhanced the NO_x adsorption and promoted the formation of NO_2 due to the NO oxidation ability of the Pt catalyst, but hindered the gas diffusion to the reaction sites.

7.1 Introduction

The fuel consumption of transportation vehicles must be lowered to decrease greenhouse gas emissions and dependence on fossil fuels. Diesel engines offer superior fuel economy and reduced emissions of CO and CO_2 relative to gasoline engines.[1] However, the oxygen-rich exhaust produced by diesel engines prevents the reduction of nitrogen oxides (NO_x) via the traditional three-way catalyst commonly used for gasoline engines.[25] NO_x is dangerous for both human beings and the environment, causing heath

problems,[13] acid rain,[14] photochemical smog,[15] and depletion of the protective ozone layer.[16] The emission of NO_x is limited by increasingly stringent government regulations worldwide.[17] Therefore, an effective method to reduce NO_x emissions from diesel engine exhaust is needed. The most extensively researched technologies at present are selective catalytic reduction (SCR) catalysts and NO_x storage/reduction (NSR) catalysts.[25] The implementation of these two technologies for automotive applications requires either a secondary fluid system for the reducing agents such as ammonia or a sophisticated control system to switch the mode of operation of the engine.

One attractive alternative is electrochemical NO_x reduction,[32, 33, 37] which reduces NO_x to N_2 on the polarized cathode in a solid state electrochemical cell, as illustrated in Figure 7.1.

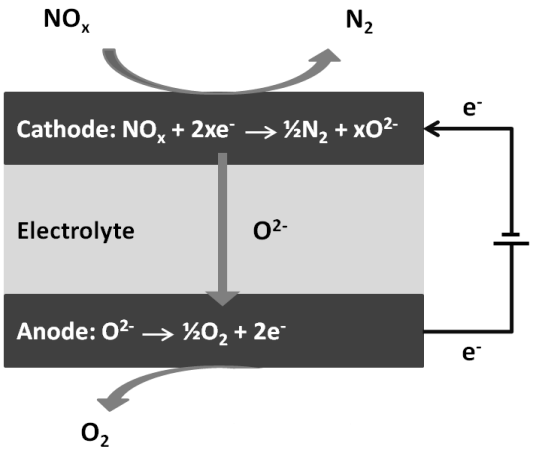

Figure 7.1 Illustration of the principle of the NO_x reduction on a solid state electrochemical cell.

This approach requires no additional reducing agents other than electrons and no variations in the state of operation of the engine. The main challenge of this technology is to achieve selective reduction of NO_x in the presence of excess O_2. Modification of the electrochemical cell by the NO_x adsorbents has been proven to significantly increase the selectivity for NO_x reduction in the oxygen-rich environment.[72, 73, 77, 110, 132, 133] This modification is mainly achieved by two different approaches: adding an NO_x adsorption layer comprised of NSR catalysts on top of the electrode[72, 110, 132, 133] or impregnating the adsorbents (K_2O or BaO) into the electrode.[73, 77] One topic of interest is to understand the reaction mechanism behind the activity enhancement achieved by the modification and the difference in performance between these two approaches. However, it is difficult to meaningfully compare how the electrode processes are affected by the two different approaches base

on the results from previous studies as these were based on various electrode materials (NiO/Pt[72, 73, 110], Ag[133], and $La_{1-x}Sr_xMnO_3$ [77, 132]), various cell designs (planate cells[72, 110, 132, 133], tubular cells [73], and multilayered cell stacks [77]), and various NO_x adsorbents (K-Pt-Al_2O_3[72, 110, 132, 133], K_2O [73], and BaO[77]).

Three cells were prepared in this study: a symmetric $(La_{0.85}Sr_{0.15})_{0.99}MnO_3$ (LSM) /$Ce_{0.9}Gd_{0.1}O_{1.95}$ (CGO) cell, an LSM/CGO cell impregnated with BaO, and an LSM/CGO cell coated with a BaO-Pt-Al_2O_3 layer. The modification was based on the backbone of a fully ceramic structure. The impedance of the three cells were systematically tested to identify the electrode processes for electrochemical reduction of NO_x and to determine the effects of the two approaches to electrochemical cell modification on these processes. The stability of the cells was studied in a degradation test. The microstructure of the cells was also investigated by scanning electron microscopy before and after testing.

7.2 Experimental

7.2.1 Cell fabrication

Three cells were prepared and tested in this study:

(1) Blank cells

(2) Cells impregnated with BaO

(3) Cells with BaO-Pt-Al_2O_3 layers

The blank cell was supported on a 300 µm thick dense CGO tape (Kerafol, Germany). The electrodes were prepared by screen printing a composite slurry on both sides of the tape and sintering at 1150 °C for 2 h. The slurries contained equal amounts of LSM (Haldor Topsøe, Denmark) and CGO (Rhodia, France) powders. The electrodes were identical on both sides of the electrolyte, with an active area of 1.54 cm^2. The electrode layer was approximately 60 µm thick. An Au paste (ESL Electro-Science, UK) mixed with 20 wt% graphite (Graphit Kropfmühl AG, Germany) was painted over the electrodes and sintered at 700 °C for 1 h to create porous Au current collectors.

For the impregnation of the cell with BaO, a 0.32 M $Ba(NO_3)_2$ (Merck, UK) aqueous solution with 10 wt% P123 (BASF, USA) was prepared. The cell was soaked in the $Ba(NO_3)_2$ solution and placed under vacuum for approximately 10 s. The cell was then heated at 700 °C for 1 h to decompose the $Ba(NO_3)_2$ to BaO.

The BaO-Pt-Al_2O_3 layer was applied by dripping several drops of adsorbent solution on top of the electrodes, drying at 110 °C for 12 h, and heating at 600 °C for 1 h. Approximately 20 $mgcm^{-2}$ of the adsorption layer was coated on the electrode, with a thickness of approximately 80 μm. The adsorption layer consisted of 10 wt% Ba with 2 wt% Pt supported on Al_2O_3 nanopowders. The composition was identical to that of a normal NSR catalyst.[25] The detailed procedure used to prepare the adsorption layer can be found elsewhere.[110] An Au wire was connected to the Au current collector as the electrode was coated with the BaO-Pt-Al_2O_3 layer.

7.2.2 Impedance characterization

The cells were installed in a glass tube apparatus that was placed inside a furnace.[132] The gas composition and flow rate were maintained by Brooks mass flow controllers. The outlet gas composition was monitored throughout the test by chemiluminescence (Model 42i HL, Thermo Scientific, USA) for NO, NO_2 and NO_x and mass spectrometry (Omnistar GSD 301, Pfeiffer Vacuum, Germany) for N_2, N_2O, and O_2. A small leak (250-300 ppm N_2 and 70 -100 ppm O_2) in the gas lines was detected by mass spectrometry. Before any measurements, the samples were pretreated in 1000 ppm NO with 10% O_2 in Ar at 350 °C for 2 to 4 h to remove any barium carbonates and hydroxides that potentially existed in the cells with the NO_x adsorbents.

The electrochemical impedance was measured using a Gamry Reference 600 potentiostat. The measurement was performed over a frequency range from $1x10^6$ to 2 or 1 mHz with 6 or 12 data points per decade and 36 mV rms amplitude at the open circuit voltage (OCV). To study the characteristics of the impedance spectra, the experimental conditions were varied, including temperature, gas composition, and flow rate. The temperature was varied from 300-500 °C with 50 °C intervals. Three kinds of gas atmosphere were used: NO with O_2 in Ar, NO without O_2 in Ar, and only O_2 in Ar. For the atmosphere of NO with O_2 in Ar, the concentrations of NO and O_2 were varied from 1000-5000 ppm and 1-10%, respectively. For the atmosphere of NO without O_2 in Ar, the flow rate increased from 2 L/h to 6 L/h.

7.2.3 Microstructural observations

The microstructure of the cells was investigated by scanning electron microscopy (SEM) (Zeiss Supra 35). The cells were manually cracked and directly subjected to SEM observation. The SEM images were recorded using two types of detectors. To obtain high-magnification images of the electrode microstructure, an in-lens detector was used with a 3 keV acceleration voltage. To investigate the electrode structure on a slightly larger scale, a secondary electron detector was used with a 15 keV acceleration voltage.

7.3 Results

7.3.1 Data processing

An equivalent circuit that contained an inductance (*L)*, a serial resistance (R_s*)*, and a number of sub-circuits (*RQ*, where the resistance (*R*) and constant phase element (*Q*) were connected in parallel) was used to fit the impedance spectra, as demonstrated in Figure 7.2. The constant phase element was used to replace the capacitance to characterize the non-ideal behavior of the electrochemical system under realistic conditions. The impedance of the constant phase element can be written as[114]

$$Z = \frac{1}{Y_0(j\omega)^n} \tag{7.1}$$

where Y_0 is a constant, *j* is an imaginary number, ω is the angular frequency, and *n* is the frequency exponent.

The equivalent capacitance (C_ω) of the constant phase element can be calculated according to the following formula.[115]

$$C_\omega = \frac{(RY_0)^{1/n}}{R} \tag{7.2}$$

The summit frequency of the arc was calculated as follows.

$$f_{max} = (\frac{1}{2\pi})(RY_0)^{1/n} \tag{7.3}$$

The inductance of the experimental apparatus was measured and held constant during the fitting procedure. Approximately 30 impedance spectra were recorded for one tested cell. Two replicates for the blank cells and the cells with the BaO-Pt-Al_2O_3 layer and three replicates for the BaO-impregnated cells were tested. In total, approximately 210 impedance spectra were obtained. The impedance spectra were fit in the following steps:

First, every set of impedance spectra was fit with an equivalent circuit without restrictions on the values of the parameters (except the inductance) and the number of arcs. In every case, the smallest number of *RQ* elements was used to obtain a reasonable and satisfactory fit (*chi-squared* < $5x10^{-4}$) because an additional arc, which usually improves the fit, does not necessarily correlate with the physical processes. In addition, trying to fit more unknown parameters from the same amount of data will increase the uncertainty of the resulting values.

Second, the resulting equivalent circuits were compared. Arcs sharing similar capacitances, n values, and characteristic frequencies were identified.

Then, the average n values were calculated for the identified arcs.

Finally, all the data were fitted again with the identified number of arcs and a fixed average n value.

All of the impedance spectra were fit with between 3 and 4 sub-circuits. Figure 7.2 shows a representative example in which the fit was obtained for the impedance plot recorded on the blank cell at 400 °C in 1000 ppm NO with 10% O_2 with an equivalent circuit of 4 *RQ* elements.

The serial resistances (R_s) and polarization resistances of the individual arcs (R_1-R_4) were obtained by fitting the impedance spectra. The total polarization resistances (R_p) were the sum of the individual polarization resistances. The apparent activation energy (E_a) of the individual processes was calculated according to the Arrhenius equation,

$$\delta = \delta_o e^{\left(-\frac{E_a}{k_B T}\right)} \tag{7.4}$$

where δ is the electrical conductivity, δ_o is the pre-exponential factor, k_B is the Boltzmann constant, and T is the absolute temperature.

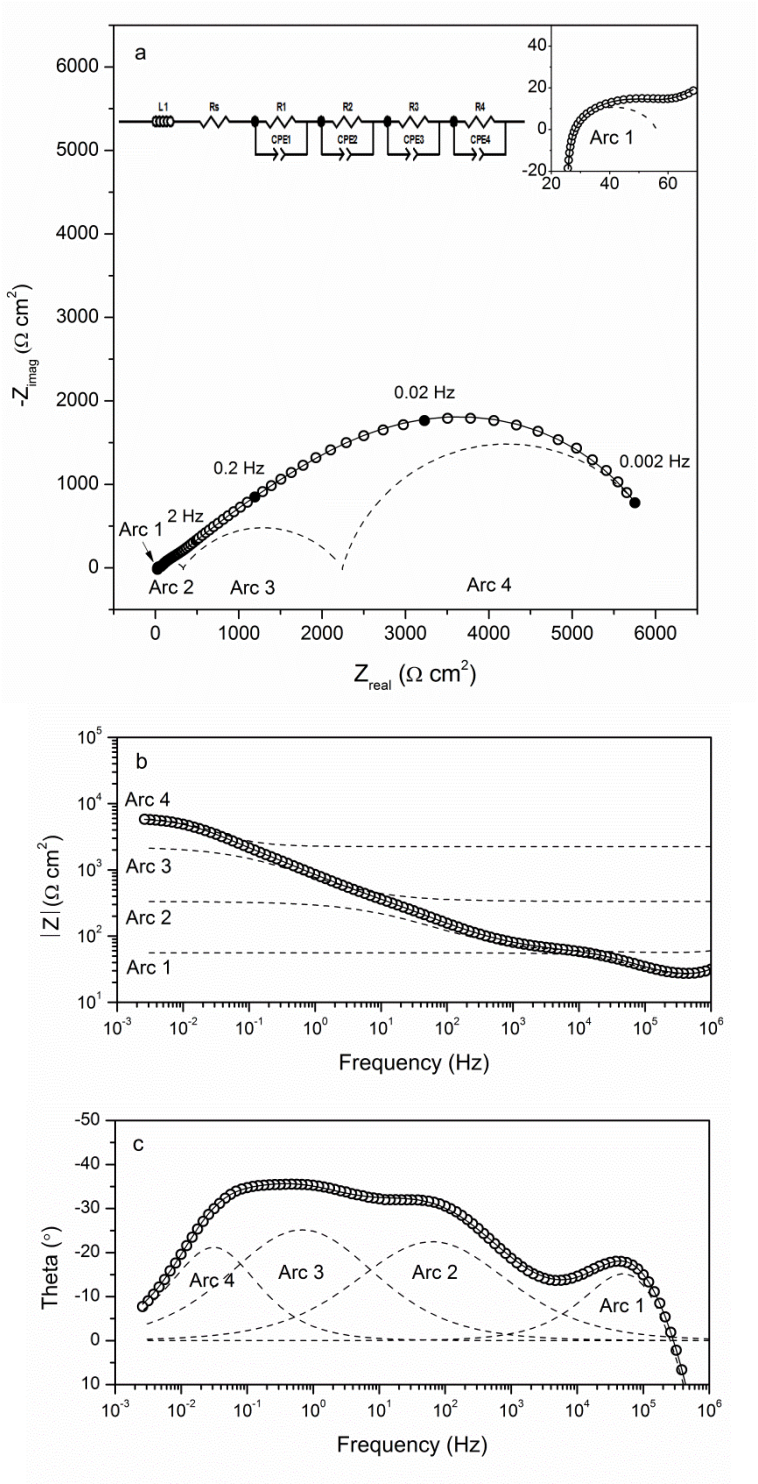

Figure 7.2 Deconvolution of the impedance spectra recorded on the blank cell in 1000 ppm NO with 10% O_2 in Ar at 450 °C as a typical example of fitting the impedance data using the equivalent circuits: a) aNyquist plot with a magnification of the high frequency part and the applied equivalent circuit, b) a Bode plot of magnitude vs. frequency, and c) a Bode plot of phase angle

vs. frequency. The solid lines represent the fitting of the entire spectrum and the dashed lines represent the deconvolution of the individual processes. The frequency is shown for the data points marked with solid circles in the Nyquist plot.

7.3.2 Temperature dependence

The impedance spectra were recorded from 300-500 °C with 50 °C intervals in 1000 ppm NO with 10% O_2 in Ar to investigate the dependence of the electrode processes on temperature. The characteristics of the individual processes (arcs) for the blank cell, the BaO impregnated cell, and the cell with a Ba-Pt-Al_2O_3 layer at various temperatures were listed in Tables 7.1 to 7.3.

Table 7.1 Characteristics of the four arcs (*RQ* elements) used to fit the impedance spectra recorded in 1000 ppm NO with 10% O_2 in Ar for the blank LSM/CGO symmetric cell.

Arcs	n	E_a (eV)	C_ω (F cm^{-2})			f_{max} (Hz)		
			300 °C	400 °C	500 °C	300 °C	400 °C	500 °C
1	0.80	1.03 ± 0.01	1.6E-7	1.3E-7	-	1,432	38,044	-
2	0.56	0.81 ± 0.04	1.4E-5	2.4E-5	4.4E-5	4.8	13	117
3	0.59	1.06 ± 0.04	4.3E-4	6.1E-4	1.4E-3	0.002	0.1	0.5
4	0.82	1.01 ± 0.06	9.2E-4	2.4E-3	2.4E-3	0.001	0.02	0.14

Table 7.2 Characteristics of the four arcs (RQ elements) used to fit the impedance spectra recorded in 1000 ppm NO with 10% O_2 in Ar for the BaO impregnated LSM/CGO cell.

Arcs	n	E_a (eV)	C_ω (F cm^{-2})			f_{max} (Hz)		
			300 °C	400 °C	500 °C	300 °C	400 °C	500 °C
1	0.90	1.11 ± 0.02	1.3E-7	1.4E-7	-	2,341	60,406	-
2	0.56	0.89 ± 0.03	1.7E-5	3.0E-5	5.9E-5	17	80	480
3	0.62	0.90 ± 0.12	7.3E-4	1.1E-4	2.0E-4	0.1	0.9	16
4	0.72	1.16 ± 0.08	9.3E-4	2.5E-3	2.3E-3	0.002	0.02	0.9

Table 7.3 Characteristics of the four arcs (RQ elements) used to fit the impedance spectra recorded in 1000 ppm NO with 10% O_2 in Ar for the LSM/CGO cell with a BaO-Pt-Al_2O_3 layer.

Arcs	n	E_a (eV)	C_ω (F cm^{-2})			f_{max} (Hz)		
			300 °C	400 °C	500 °C	300 °C	400 °C	500 °C
1	0.85	1.10 ± 0.03	1.3E-7	1.1E-7	-	1,980	64,775	-
2	0.59	1.00 ± 0.13	1.5E-5	2.6E-5	6.2E-5	11	48	288
3	0.62	0.48 ± 0.06	8.8E-5	2.1E-4	2.7E-4	0.8	0.6	2.7
4	0.65	1.06 ± 0.10	6.3E-4	2.2E-3	3.6E-3	0.008	0.03	0.3

Four arcs were identified for the majority of the impedance spectra, except at 500 °C, where the arc located at the very high frequency end (arc 1) could not be observed. The capacitance of arc 1 was almost constant at different temperatures, with values ranging from 1E-7 to 2E-7 F cm^{-2} across all the cells. Arc 2 appeared in the frequency range of several Hz to several hundred Hz for all the cells with a capacitance increasing with increasing temperature in the range of 1E-5 to 1E-4 F cm^{-2}. Arcs 3 and 4 were observed in the low-frequency range of 20 Hz to 1 mHz. The capacitance of arc 3 increased with increasing temperature from 1E-4 to 1E-3 F cm^{-2}. In the case of arc 4, the capacitance varied at different temperatures, but did not show a clear monotonic increasing or decreasing trend with increasing temperature. The activation energy values of arc 1, arc 2, and arc 4 were similar across the three cells, whereas the value of arc 3 was significantly lower for the cell with a Ba-Pt-Al_2O_3 layer relative to the other two cells.

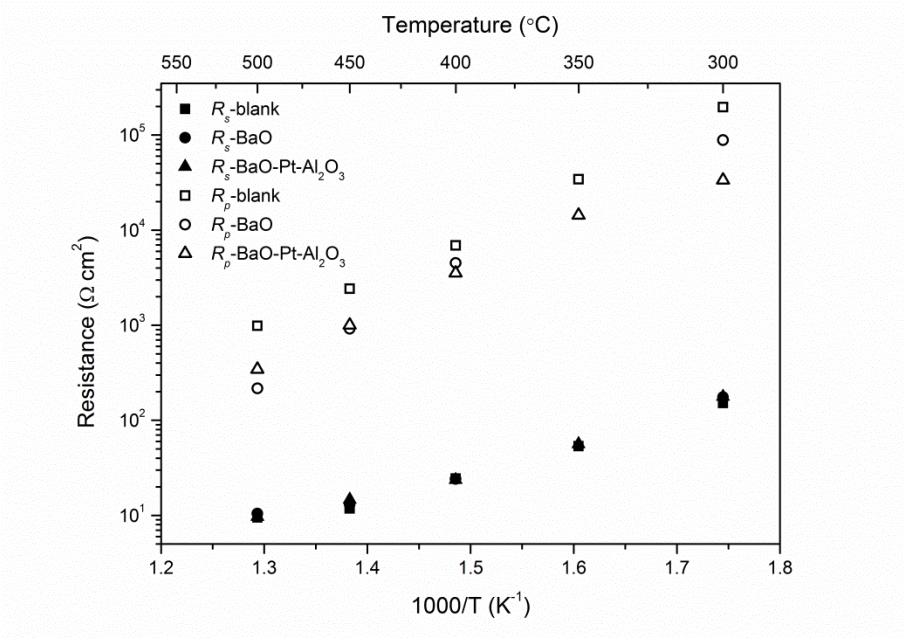

Figure 7.3 Serial resistances (R_s) and polarization resistances (R_p) of the blank cell, the BaO impregnated cell, and the cell with a BaO-Pt-Al_2O_3 adsorption layer in 1000 ppm NO with 10% O_2 in Ar as a function of the inverse temperature. The values reported here are the average values of two or three replicates, and the deviations between replicates were within 9%.

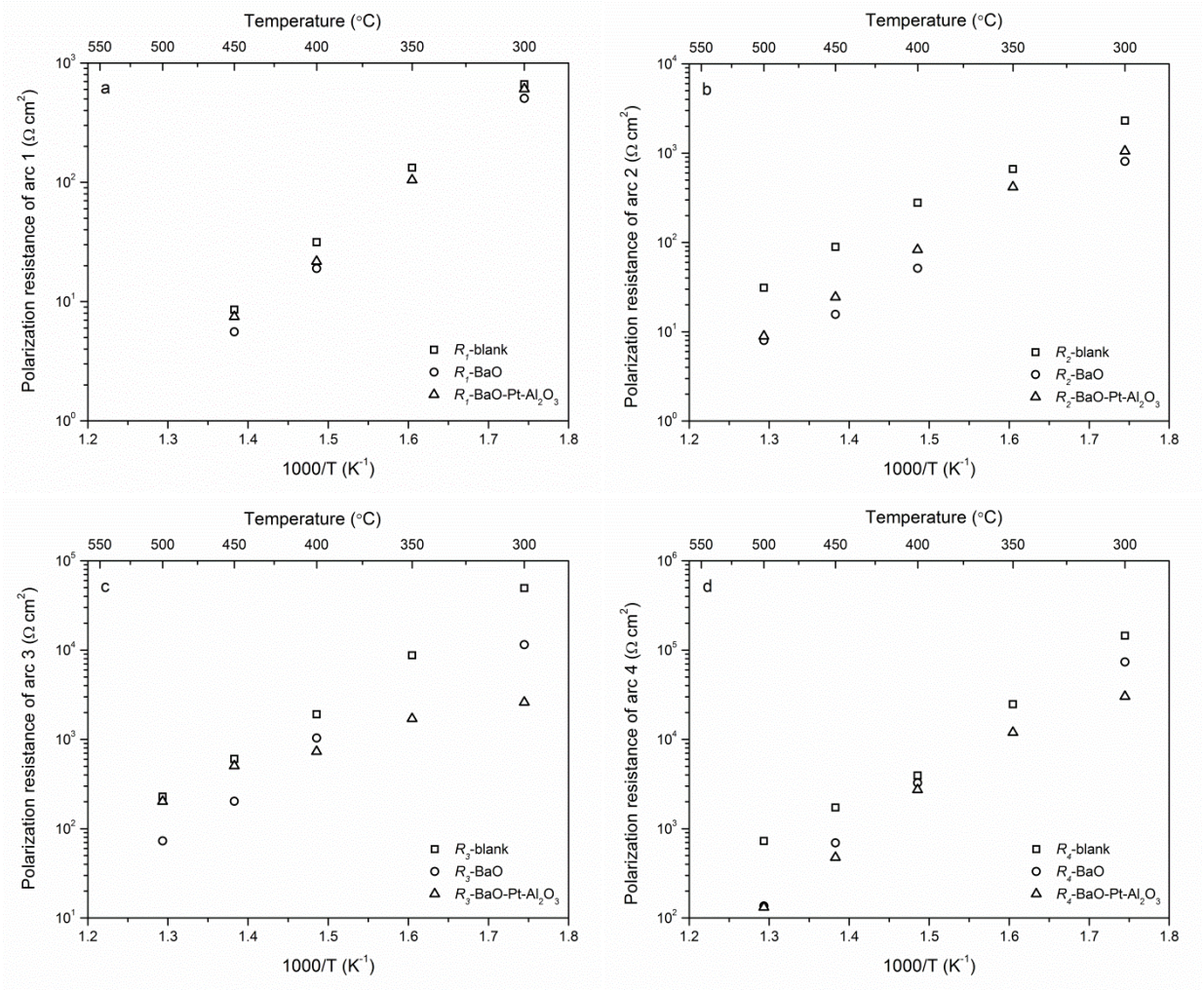

Figure 7.4 Polarization resistances of the individual processes for the blank cell, the BaO impregnated cell, and the cell with a BaO-Pt-Al_2O_3 adsorption layer in 1000 ppm NO with 10% O_2 in Ar as a function of the inverse temperature: a) the resistances of arc 1, b) the resistances of arc 2, c) the resistances of arc 3, and d) the resistances of arc 4. The values reported here represent the average values of two or three replicates, and the deviations between replicates were within 15%. Note the different scale of the vertical axis.

Figure 7.3 shows the serial resistances and the total polarization resistances for the three cells as a function of temperature. The serial resistances were almost the same among the three cells as the electrolytes of the three cells were identical. However, the polarization resistances were consistently lower in the cells modified with the NO_x adsorbents than in the blank cell, indicating an activation effect of adding the NO_x adsorption materials. To estimate which of the processes (arcs) mainly contributed to this activation effect, the resistances of the individual processes were calculated and compared in Figure

7.4. The resistances of arc 1 for the cells with the NO_x adsorbents were close to or slightly lower than those for the blank cell. For arc 2, the resistances for the cells with the NO_x adsorbents were lower than that for the blank cell, with this difference increasing as temperature increased. For arcs 3 and 4, the resistances of the BaO impregnated cell were consistently lower than those of the blank cell. The resistances of the two arcs for the cell with the Ba-Pt-Al_2O_3 layer were the lowest among the three cells from 300 to 400 °C, but the resistance tended to decrease more slowly with increasing temperature than those of the BaO impregnated cell, especially in the case of arc 3. Consequently, the resistances of the cell with the adsorption layer became greater than (for arc 3) or close to (for arc 4) those of the impregnated cell at temperatures above 400 °C. Because the resistances of these two low-frequency process, arc 3 and 4, dominated the polarization resistances at all temperatures tested for the three cells, the activation effect of adding the NO_x adsorbents was primarily contributed by the decrease in the resistances of the low-frequency processes.

7.3.3 Impedance spectra in different gas atmospheres

To investigate the effect of the gas atmospheres on these electrode processes, the impedance spectra were recorded in three different kinds of gas atmospheres at 450 °C for all three cells: 1000 ppm NO with 10% O_2 in Ar, 10% O_2 in Ar, and 1000 ppm NO in Ar, as shown in Figures 7.5 to 7.7. For all three cells, the spectra in 1000 ppm NO with 10% O_2 appeared similar to those in 10% O_2 without NO. However, the polarization resistances were noticeably lower in the atmosphere containing both NO and O_2 than those in the atmosphere containing only O_2. This observation was consistent with those reported by Werchmeister et al. and Reinhardt et al., which were suggested to be due to the formation of NO_2 or more reactive oxygen surface species from the interaction between NO and O_2, increasing the activity of the electrode for O_2 reduction. In contrast with the spectra recorded in the O_2 containing atmospheres, a distinctive low-frequency arc was observed in the spectra recorded in 1000 ppm NO without O_2, as arc 4 moved into even lower frequency range and was well separated from the rest of the arcs.

The R_p was much lower for the cells with the NO_x adsorbents than for the blank cell regardless of the atmosphere. Comparing the two types of cells modified with NO_x adsorbents, the R_p of the BaO impregnated cell was smaller in the O_2 containing atmospheres, whereas in the atmosphere with NO but

without O_2, the R_p of the cell with a Ba-Pt-Al_2O_3 layer became smaller as arc 4 was significantly reduced by adding the adsorption layer.

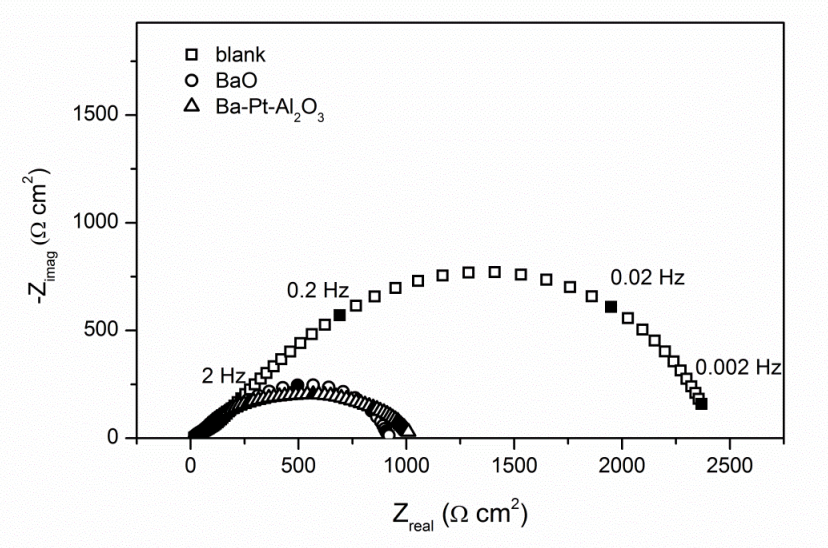

Figure 7.5 Impedance spectra for the blank LSM/CGO cell, the BaO-impregnated LSM/CGO cell, and the LSM/CGO cell with the BaO-Pt-Al_2O_3 layer in 1000 ppm NO with 10% O_2 in Ar at 450 °C.

.

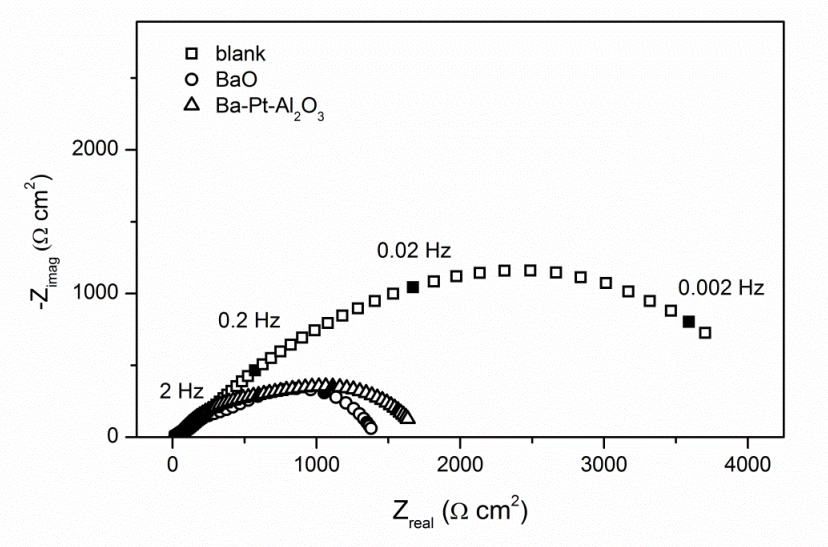

Figure 7.6 Impedance spectra for the blank LSM/CGO cell, the BaO-impregnated LSM/CGO cell, and the LSM/CGO cell with the BaO-Pt-Al_2O_3 layer in 10% O_2 in Ar at 450 °C.

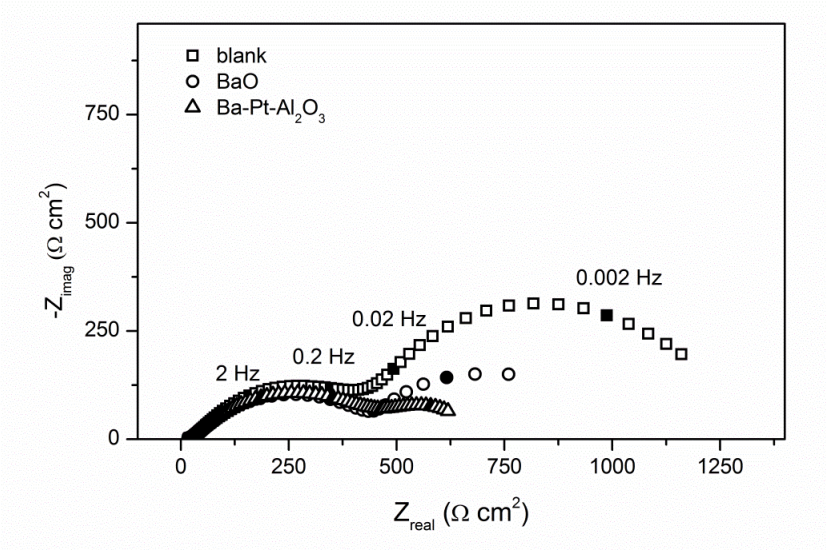

Figure 7.7 Impedance spectra for the blank LSM/CGO cell, the BaO-impregnated LSM/CGO cell, and the LSM/CGO cell with the BaO-Pt-Al_2O_3 layer in 1000 ppm NO in Ar at 450 °C.

7.3.4 Dependence on gas concentration

During the impedance measurements, both the NO and O_2 concentrations were varied at 450 °C. The O_2 content was fixed at 10% while the NO concentration was varied to 1000, 2500, and 5000 ppm. For the variation of O_2 concentration, the NO concentration was kept constant at 1000 ppm and the O_2 concentration was offset to 1, 4, and 10%. Table 7.4 lists the resistances and equivalent capacitances of the three cells at different in NO concentrations, while Table 7.5 presents the results at different O_2 concentrations. The resistances of arc 1 were not affected by the changes in either NO or O_2 concentrations in any of the cells. The resistances of arc 2 were almost constant with varying NO concentration, but decreased with increasing O_2 concentration. The resistances of arc 3 decreased with increasing NO and O_2 concentrations. The resistances of arc 4 decreased with increasing NO concentration, but increased with increasing O_2 concentration. The variations in resistance with gas concentration were much more significant for arc 4 than for arc 3. With respect to the C_ω, variations in the gas concentration almost did not affect the C_ω of arc 1 for any the three cells. The C_ω of arc 2 remained more or less constant when the NO concentration was changed, while it decreased with increasing O_2 concentration. The C_ω of arc 3 changed with the variation in both NO and O_2 concentration,

behaving differently in different cells. For arc 4, the C_ω varied in a similar manner in all three cells, increasing with increasing NO concentration and decreasing with increasing O_2 concentration.

Table 7.4 Resistances and equivalent capacitances for the three cells as various NO concentrations. The data were recorded at 450 °C and the oxygen concentration was constant at 10%.

		R (Ω cm^{-2})			C_ω (F cm^{-2})		
		1000 ppm NO	2500 ppm NO	5000 ppm NO	1000 ppm NO	2500 ppm NO	5000 ppm NO
Blank	Arc 1	8.6	9.0	8.2	1.2E-7	1.2E-7	1.2E-7
	Arc 2	89	88	92	2.9E-5	2.6E-5	3.2E-5
	Arc 3	604	567	431	8.5E-4	8.1E-4	7.4E-4
	Arc 4	1726	1499	862	2.0E-3	2.2E-3	2.5E-3
BaO	Arc 1	5.5	5.7	5.9	2.5E-7	2.1E-7	2.1E-7
	Arc 2	16	16	17	5.2E-5	5.1E-5	5.3E-5
	Arc 3	202	177	141	1.7E-4	3.8E-4	3.4E-4
	Arc 4	693	441	339	1.5E-3	2.7E-3	3.0E-3
BaO-Pt-Al_2O_3	Arc 1	7.4	7.4	7.4	1.5E-7	1.5E-7	1.5E-7
	Arc 2	24	23	23	4.3E-5	4.3E-5	4.3E-5
	Arc 3	505	466	390	2.3E-4	2.0E-4	1.8E-4
	Arc 4	456	234	181	5.0E-3	1.1E-2	1.6E-2

Table 7.5 Resistances and equivalent capacitances for the three cells at various oxygen concentrations. The data were recorded at 450 °C and the NO concentration was constant at 1000 ppm.

		R (Ω cm^{-2})			C_ω (F cm^{-2})		
		1% O_2	4% O_2	10% O_2	1% O_2	4% O_2	10% O_2
Blank	Arc 1	9.0	8.8	8.6	1.4E-7	1.4E-7	1.2E-7
	Arc 2	101	90	89	3.7E-5	3.0E-5	2.9E-5
	Arc 3	763	649	604	7.6E-4	8.0E-5	8.5E-4
	Arc 4	850	1490	1726	4.8E-3	2.7E-3	2.0E-3
BaO	Arc 1	5.6	5.2	5.5	2.1E-7	2.0E-7	2.5E-7
	Arc 2	24	19	16	6.1E-5	5.4E-5	5.2E-5
	Arc 3	264	217	202	3.2E-4	2.0E-4	1.7E-4
	Arc 4	361	441	693	3.2E-3	2.1E-3	1.5E-3
BaO-Pt-Al_2O_3	Arc 1	7.3	7.0	7.4	1.7E-7	1.5E-7	1.5E-7
	Arc 2	30	26	24	5.1E-5	4.4E-5	4.3E-5
	Arc 3	660	536	505	4.2E-4	2.3E-4	2.3E-4
	Arc 4	202	376	456	1.1E-2	5.2E-3	5.0E-3

7.3.5 Dependence on flow rate

The flow rate was varied in 1000 ppm NO in Ar at 450 °C. Table 7.6 compares the resistances and the C_ω of the individual arcs for the blank cell, the BaO impregnated cell, and the cell with a Ba-Pt-Al_2O_3 layer at gas flow rate of 2 L/h and 6 L/h. Increasing the flow rate has almost no influence on arcs 1 and 2 for the three cells. A small increase in the resistance of arc 3 and a large increase in that of arc 4 were observed when the flow rate increased from 2 to 6 L/h. The C_ω of arcs 3 and 4 decreased at an increased flow rate for the three cells, except for that of arc 3 for the blank cell, which increased slightly with increasing the flow rate.

Table 7.6 Resistances and equivalent capacitances for the three cells with different flow rates. The data were recorded in an atmosphere of 1000 ppm NO in Ar without oxygen at 450 °C.

		R (Ω cm^{-2})		C_ω (F cm^{-2})	
		2 L	6 L	2 L	6 L
Blank cell	Arc 1	8.5	8.3	1.3E-7	1.3E-7
	Arc 2	19	20	1.3E-5	1.1E-5
	Arc 3	459	501	5.7E-4	5.9E-4
	Arc 4	759	939	6.0E-2	5.0E-2
BaO	Arc 1	5.8	5.7	2.4E-7	2.2E-7
	Arc 2	38	39	6.7E-5	6.2E-5
	Arc 3	386	408	4.7E-4	3.6E-4
	Arc 4	383	567	2.4E-1	1.6E-1
BaO-Pt-Al_2O_3	Arc 1	7.5	8.0	1.6E-7	1.3E-7
	Arc 2	36	34	9.1E-5	8.7E-5
	Arc 3	434	471	4.5E-4	3.9E-4
	Arc 4	221	254	3.1E-1	2.2E-1

7.3.6 Degradation

The stability of the cells for electrochemical NO_x reduction was studied by performing a degradation test. The test was performed on the cells at 400 to 500 °C for 70 to 200 h. During this period, the cells experienced frequent switches between the polarization and the open circuit states as well as variations in the gas concentration (0-5000 ppm NO with 0-20% O_2). The impedance data recorded before and after the degradation test were compared. Table 7.7 shows the results of the percentage changes in resistances for one of the replicates for the three cells before and after the degradation test at 450 °C

for approximately 100 h. In general, the variation in R_s was negligible for the three cells and the change in R_p depended on the change in R_3 and R_4 due to the dominant effect of the two low-frequency arcs on the impedance spectra. For the blank cell, a small increase in R_1 was observed along with a large decrease in R_2, R_3, and R_4. For the BaO impregnated cell, the increase in R_1 was minor, similar to that for the blank cell; the R_2, R_3, and R_4 increased significantly after the test, indicating severe degradation on the impregnated cell. Less degradation occurred in the cell with a Ba-Pt-Al_2O_3 layer, but the degradation followed a similar trend.

Table 7.7 Percentage changes in resistances of the three cells before and after a degradation test at 450 °C for approximately 100 h. The resistances were obtained by fitting the impedance spectra recorded at 450 °C in 1000 ppm NO with 10% O_2 in Ar. Positive values indicate that the resistance increases, while negative values represent a decrease in resistance.

	R_s	R_p	R_1	R_2	R_3	R_4
Blank cell	3	-36	12	-1	-22	-45
BaO	1	38	9	91	30	38
BaO-Pt-Al_2O_3	4	24	14	81	17	29

7.3.7 Microstructure

The microstructures of the electrodes on the three cells before and after the test were observed by the microscopy as shown in Figure 7.8. No obvious change was observed in the electrode of the blank cell before and after testing. The electrode grains were well defined and the surface was smooth. For the BaO impregnated cell, a profound change was observed in the electrode microstructure (Fig. 7.8 a and b). The surface of the electrode became “fluffy” and was fully covered by tiny particles, which were much smaller than the distinct BaO particle distributed over the surface of the electrode before testing (Fig. 7.8 c and d). With respect to the cell with a Ba-Pt-Al_2O_3 layer, no evident change was observed on the Ba-Pt-Al_2O_3 layer coated on the top of the electrode after testing (Fig. 7.8 e and f), whereas a clear change was observed on the electrode, which was similar with that on the BaO impregnated cell (Fig. 7.8 g and h). Note that the large particles underneath the adsorption layer in Figure 7.8 e and f are part of the Au current collector layer.

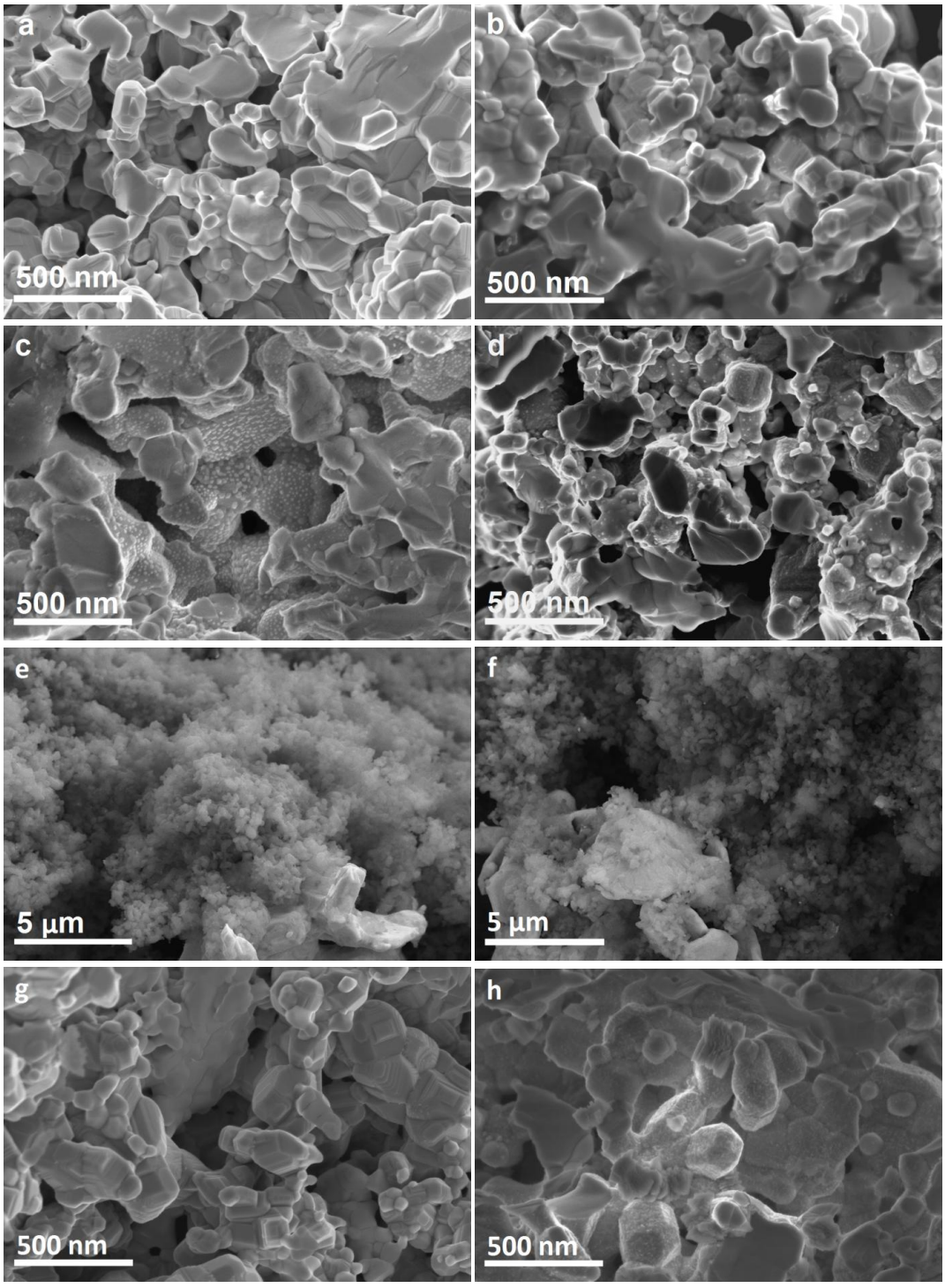

Figure 7.8 Microstructural images for the electrodes of the blank LSM/CGO cell, the BaO-impregnated LSM/CGO cell, and the LSM/CGO cell with the BaO-Pt-Al_2O_3 layer before and after testing. The images include a) the blank electrode before testing, b) the blank electrode after testing, c) the BaO-impregnated electrode before testing, d) the BaO-impregnated electrode after

testing, e) the BaO-Pt-Al_2O_3 layer before testing, f) the BaO-Pt-Al_2O_3 layer after testing, g) the electrode with a BaO-Pt-Al_2O_3 layer before testing, and g) the electrode with the BaO-Pt-Al_2O_3 layer after testing.

7.4 Discussion

7.4.1 Identification of the electrode processes

In general, four arcs were identified on the impedance spectra for the three cells. No new or missing process was observed on the spectra recorded on the cells modified with the NO_x adsorbents compared with the blank cell.

Arc 1 was observed in the very high frequency range on most of the impedance spectra for the three cells with a *n* value of 0.8 to 0.9 and an E_a of approximately 1 eV (1000 ppm NO + 10% O_2). The C_ω of this arc was independent of the temperature and atmosphere with a value of 1E-7 to 2E-7 F cm^{-2}. These characteristics are consistent with those of the process related to the transfer of oxygen ions across the interface between the electrode and electrolyte and through the electrolyte frame of the composite electrode, as reported for the LSM/YSZ[116] and LSM/CGO[55, 75, 77, 132] electrodes. At 500 °C, the high frequency arc could not be estimated, probably because this arc was so small that it could not be separated from the impedance spectra.

Arc 2 was observed in the intermediate frequency range on all the impedance spectra. This arc was fit with an *n* value of 0.59 for the cell with a Ba-Pt-Al_2O_3 layer and 0.56 for the blank cell and the BaO impregnated cell. The E_a of this arc was approximately 0.81 eV for the blank cell, 0.89 eV for the impregnated cell, and 1 eV for the cell with the adsorption layer in the atmosphere of 1000 ppm NO with 10% O_2. This arc showed no dependence on the flow rate or NO concentration but a significant dependence on O_2 concentration. The resistance and C_ω of this arc decreased with increasing O_2 concentration. Moreover, the C_ω increased from 1E-5 to 1E-4 F cm^{-2} with increasing temperature, in fairly good agreement with the capacitance associated with the adsorption and dissociation of O_2 and/or the charge transfer reaction at the triple phase boundaries (TPBs) on the composite cathode. [132, 117]

Arc 3 was fit with the *n* values of 0.59 for the blank cell and 0.62 for the BaO impregnated cell and the cell with the Ba-Pt-Al_2O_3 layer. The increase in C_ω and the decrease in the resistance with increasing

temperature showed that this process was related to the extension or broadening of the TPB zone. For this arc, the dependence on the flow rate was weak but the dependence on the gas atmosphere was strong. The resistance of this arc decreased with increasing NO or O_2 concentration, indicating the participation of O_2-related species and NO_x-related species in this process. According to the previous findings on perovskite/CGO electrodes in our group,[55, 75, 132] a similar process could be ascribed to adsorption, surface diffusion, and transfer of species at or near TPBs. The E_a for this process was reported to be in the range of 0.7-1.2 eV in the NO_x containing atmosphere,[55, 75] overlapping with the values of E_a obtained in this study for the blank cell (1.06 eV) and the impregnated cell (0.9 eV), but higher than the value for the cell with the adsorption layer (0.48 eV). The significant decrease in E_a for the cell with the adsorption layer indicated that the decrease in resistance resulting from increasing temperature was greatly lessened by the addition of the adsorption layer, which was probably due to the limitation of gas diffusion by the additional adsorption layer. Therefore, arc 3 was ascribed to the adsorption, diffusion, and transfer of O_2 species and NO_x species at or near TPBs.

In the lowest frequency range of the impedance spectra, arc 4 was identified with a *n* value of 0.82 for the blank cell, 0.72 for the BaO impregnated cell, and 0.65 for the cell with a Ba-Pt-Al_2O_3 layer. The resistance of this arc decreased with decreasing oxygen concentration, indicating that this low-frequency process depended on the concentration of the oxygen vacancies.[75] As this arc was also characterized by significant increases in resistance with either an increasing flow rate in 1000 ppm NO without O_2 or a decreasing NO concentration in the atmosphere of NO with O_2, this arc could be associated with the formation of the reaction intermediate NO_2 in the NO containing atmospheres.[55, 75, 132, 133] The E_a of this arc was similar among the three cells with a value of approximately 1.1 eV in 1000 ppm NO with 10 % O_2, greater than the value reported by Werchmeister et al. (0.34 eV) for the identical process in 1% NO,[55] but close to the values reported by Traulsen et al. (0.9 eV) in the same atmosphere.[75]

7.4.2 Effect of the modification with the NO_x adsorbents on the electrode processes

A significant decrease in the R_p was observed for the BaO impregnated cell and the cell with the Ba-Pt-Al_2O_3 layer relative to the blank cell, demonstrating that the addition of the NO_x adsorbents activates the electrode processes. Comparing the changes in the individual processes, the resistances of the four

processes were all reduced by the addition of the NO_x adsorbents; however, the changes in the low-frequency processes (arcs 3 and 4) were primarily responsible for the overall variations in the impedance spectra, as the impedance spectra were dominated by these arcs. Accordingly, the decreases in the resistances of the low-frequency processes were mainly responsible for the activity enhancement by the NO_x adsorbents. The low-frequency processes were identified as adsorption, diffusion, the transfer of O_2 species and NO_x species at or near the TPB region and the formation of the reaction intermediate NO_2.

The introduction of nano-particles into the electrode in the BaO impregnated cell could expand the length of the TPB and/or modify the surface chemistry of the electrode, making it more electrochemically active.[58] These factors should affect both the NO_x- and O_2-related processes and lead to a general increase in the activity of the electrode, which could explain the decrease in resistance of the impregnated cell relative to the blank cell in all tested atmospheres. Besides, the BaO particles are capable of selectively absorbing and storing NO_2 in the form of nitrates (Eq. 5) to effectively enhance the adsorption of NO_2 on the LSM/CGO electrode, which in turn may benefit the formation of NO_2 from the NO/NO_2 equilibrium.[25, 124] Over the BaO sites adjacent to the TPBs, the stored nitrate may be reduced directly to N_2 (Eq. 6), a process that provides a short and efficient reaction path to the reduction of NO_x. Therefore, BaO impregnation can greatly improve the electrode activity of the low-frequency processes related with the NO_x and O_2 species at or near the TPB region and the formation of NO_2.

$$2NO_2(g) + O_2(g) + BaO \rightarrow Ba(NO_3)_2 \quad (7.5)$$

$$Ba(NO_3)_2(TPB) + 5V_O^{\cdot\cdot} + 10e^- \rightarrow N_2(g) + 5O_O^{2-} + BaO\ (TPB) \quad (7.6)$$

For the cell with the BaO-Pt-Al_2O_3 layer, the large surface area (~100 nm particles) and active components (Pt and BaO) of the adsorption layer could lead to a general increase in the electrode activity.[25] The adsorption of NO_x can also be selectively promoted as on the BaO-impregnated cell.[25] However, unlike the impregnated cell, the direct reduction of the nitrates seems to be impossible as the storage sites are distant from the reaction sites. Another difference is the Pt particles in the adsorption layer, which are absent in the case of the impregnated cell. The strong NO oxidation ability of Pt catalysts could significantly promote the formation of NO_2, especially under the conditions where the formation of NO_2 from the NO/NO_2 equilibrium was kinetically limited, such as low temperatures.[25],

[121, 122] Therefore, the resistance of the NO_2 formation arc (arc 4) was the lowest for the cell with the BaO-Pt-Al_2O_3 layer among the three cells, and the reduction in the resistance resulting from the adsorption layer was greater at low temperatures (300 and 350 °C). For arc 3, which was ascribed to adsorption, diffusion, and the transfer of O_2 species and NO_x species at or near the TPB region, the large decrease in the resistance below 400 °C relative to the BaO impregnated cell may also be related to the promotion of NO_2 formation because NO_2 was suggested to be the reaction intermediate for the NO_x adsorption and reduction. However, above 400 °C, the resistance of arc 3 significantly increased for the cell with the adsorption layer relative to the BaO impregnated cell, as the resistance decreased slowly with increasing temperature for the cell with the adsorption layer, most likely due to the limitation of gas diffusion by the additional adsorption layer.

7.4.3 Degradation correlated with microstructural changes

As shown in the results section, the activity of the electrodes decreased after long-term operation for the BaO impregnated cell and the cell with the BaO-Pt-Al_2O_3 layer. The degradation was generally similar between the two types of cells modified with the NO_x adsorbents and was mainly caused by the increase in the resistance of the processes related with the TPBs (arc 2 and 3) and the NO_2 formation (arc 4). The SEM images reveal a profound change in the microstructure of the electrode on the BaO impregnated cell and the cell with a BaO-Pt-Al_2O_3 layer after testing, which may correlate with the deterioration in the electrode activity. Between the two types of cells with the NO_x adsorbents, the microstructure appears fairly similar after testing despite being quite different before testing. One possible explanation of this observation is that the microstructural changes could be caused by the same type of reaction on the two different cells, such as the reaction between the electrode materials with the Ba compounds (BaO and or $Ba(NO_3)_2$) either dispersing over the surface of the electrode[77] or diffusing from the BaO-Pt-Al_2O_3 layer to the electrode. The microstructural changes have been discussed in detail elsewhere and thus this discussion will not be repeated here.[143]

7.5 Conclusion

This study investigated the effect of modifying the LSM/CGO cell with the NO_x adsorbents on the electrode processes for the electrochemical reduction of NO_x by characterizing the cells using the

electrochemical impedance spectra. Three types of cells were prepared and tested, including a blank symmetric LSM/CGO cell, an LSM/CGO cell impregnated with BaO, and an LSM/CGO cell coated with a BaO-Pt-Al_2O_3 layer. The impedance analysis revealed that the modification with the NO_x adsorbents, either by impregnation of BaO or by adding a BaO-Pt-Al_2O_3 layer significantly enhanced the activity of the electrode processes. The activity enhancement achieved by the NO_x adsorbents was mainly resulted from the decrease in the resistance of the low-frequency processes (arcs 3 and 4), which were ascribed to the adsorption, diffusion, and transfer of O_2 species and NO_x species at or near the TPB region and the formation of the reaction intermediate NO_2. BaO impregnation increased the overall activity of the electrode and enhanced the adsorption of NO_x by selectively trapping NO_2 in the form of nitrate, which also enabled direct reduction of the stored nitrate to N_2 over the BaO sites adjacent to the TPBs. The BaO-Pt-Al_2O_3 layer also increased the general activity of the electrode and improved NO_x adsorption. Moreover, the adsorption layer was capable of promoting the formation of NO_2 due to the strong NO oxidation ability of the Pt catalyst. However, the additional adsorption layer hindered the gas diffusion to the reaction sites, which resulted in a larger resistance of arc 3 at elevated temperatures relative to the impregnated cell. The activity of the electrodes deteriorated on the cells with the NO_x adsorbents after a long-term operation. The degradation may be related to the profound microstructural changes observed on the electrodes after testing, which could be due to the reaction between the electrodes and the Ba compounds.

Acknowledgements

The authors would like to acknowledge the financial support of the Danish Strategic Research Council under contract no. 09-065186. We are grateful to our colleagues at the Department of Energy Conversion and Storage, Technical University of Denmark for help and discussion.

Chapter 8 Impregnating a LSM/CGO cell with both BaO and Pt

8.1 Introduction

According to the previous studies on the $(La_{0.85}Sr_{0.15})_{0.99}MnO_3$ (LSM) /$Ce_{0.9}Gd_{0.1}O_{1.95}$ (CGO) symmetric cells modified by NO_x adsorbents, it has been indicated that the presence of NO oxidation catalysts is important for the NO_x reduction at low temperatures and low voltages, as under these conditions the NO_x reduction is probably limited by the lack of intermediate NO_2. Thus, by introducing the Pt component into the BaO impregnated electrode, the performance of the electrode at low temperatures and voltages could be improved. This chapter described the preliminary work on preparing and testing a LSM/CGO symmetric cell impregnated with both BaO and Pt for the NO_x reduction in an O_2-rich environment.

8.2 Experimental

The blank LSM/CGO symmetric cells used in this chapter are identical with that used in chapters 6 and 7, and their active electrode area is 1.54 cm^2. Firstly, three blank LSM/CGO cells were impregnated with BaO, following the same procedure as described in the previous two chapters. Next, two of the cells were soaked in a 0.034 M $Pt(NH_3)_4(NO_3)_2$ (Aldrich, Germany) aqueous solution with 3 wt% Triton-45 (Fluka, Belgium) and one was soaked in a 0.068 M $Pt(NH_3)_4(NO_3)_2$ solution (table 8.1).

Table 8.1 Preparation parameters of impregnation with BaO and Pt.

Names	Concentration of Pt precursor solution	No. of impregnation
Ba+Pt-1	0.034M	1
Ba+Pt-2	0.034M	1
Ba+Pt-3	0.068M	2

All the cells were placed under vacuum for approximately 2 min. Excess impregnation solution was wiped of the surface. The cells were then heated at 270 °C for 1 h to decompose the $Pt(NH_3)_4(NO_3)_2$ to Pt. The first two cells were impregnated for one time and the last cell was impregnated twice. The two cells impregnated once in a 0.034 M solution was denoted as Ba+Pt-1 and Ba+Pt-2. The cell impregnated twice in a 0.068 M solution was denoted as Ba+Pt-3. Usually the loading of impregnation components

was determined by measuring the weight increase after impregnation, but in this case the weight increase was too small to be detected. The exact loading of BaO and Pt is thusly unknown.

The cells were installed in a test set up and connected to a Gamry Reference 600 potentiostat. The NO_x conversion were measured from 300 to 450 °C in 1000 ppm NO with 10% O_2 in Ar with a flow rate of 2 L/h maintained by Brooks mass flow controllers. The cells were polarized under square wave (SV) mode from 1.5 to 2.5 V. The outlet gas composition was monitored using chemiluminescence (Model 42i HL, Thermo Scientific, USA) for NO, NO_2, and NO_x and mass spectrometry (Omnistar GSD 301, Pfeiffer Vacuum, Germany) for N_2, N_2O, and O_2.

The electrochemical impedance was measured by the Gamry Reference 600 potentiostat from $1x10^6$ to 2 or 1 mHz with 6 or 12 data points per decade and 36 mV rms amplitude at the open circuit voltage (OCV) in 1000 ppm NO with or without 10% O_2 in Ar from 300 to 450 °C.

The microstructure of the cells was investigated by scanning electron microscopy (SEM) (Zeiss Supra 35). The cells were cracked manually and directly subjected to the SEM observations. The SEM images were recorded using an in-lens detector with a 3 keV acceleration voltage and a secondary electron detector with a 15 keV acceleration voltage.

8.3 Results and discussion

8.3.1 Microstructure observation

Figure 8.1 illustrates the difference in microstructure between the electrodes being impregnated with both BaO and Pt and the ones only with BaO, before and after testing. By comparing the SEM micrographs of the impregnated cells, regardless the different impregnation solutions that they have been immersed into, it is obvious that before testing, many more distinct nano-particles could be observed, evenly distributed throughout the cells microstructure. According to the EDS measurements performed on these particles, it has been indicated to be formed out of BaO, whereas the presence of Pt has not been confirmed. This could be attributed either to the low Pt loading that has been applied or to the fact that the particle size of the Pt is too small to be observed by SEM. If this was due to a negligible Pt loading, by increasing the concentration of the precursor solution and the number of impregnation

cycles, it should result in an increase of the Pt loading. However, no evident difference was observed between the electrodes Ba+Pt-2 and Ba+Pt-3. It seems necessary to further investigate the microstructure and composition of the impregnated electrode by transmission electron microscopy (TEM).

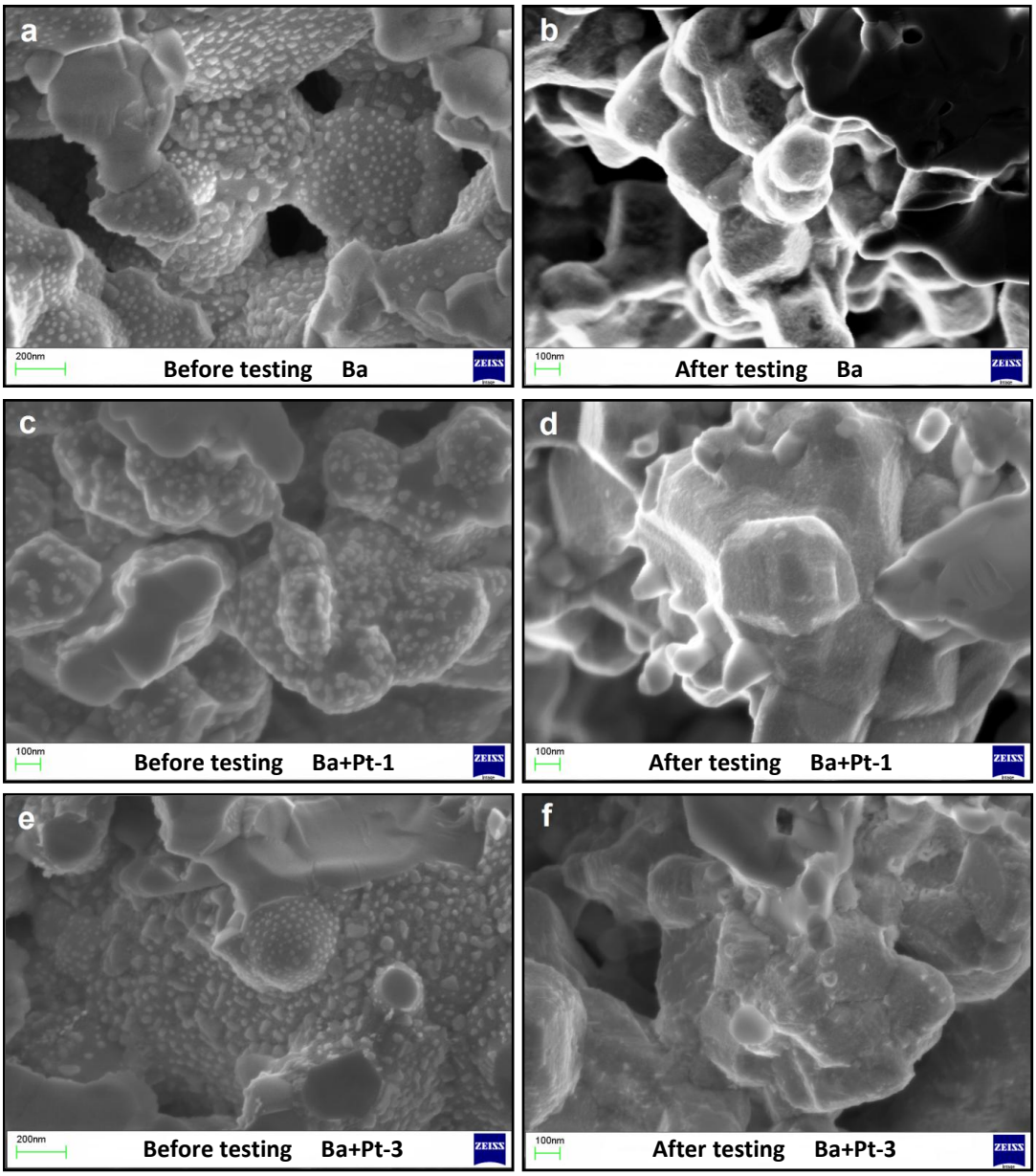

Figure 8.1 SEM images of the LSM/CGO electrodes impregnated with BaO and that impregnated with BaO plus Pt, before and after testing. The images include a) the electrode impregnated with BaO before testing, b) the electrode impregnated with BaO

after testing, c), the electrode of Ba+Pt-1 before testing, d) the electrode of Ba+Pt-1 after testing, e) the electrode of Ba+Pt-3 before testing, and f) the electrode of Ba+Pt-3 after testing.

8.3.2 NO_x conversion measurement

The NO_x removal properties of the LSM/CGO cells impregnated with BaO and Pt in 1000 ppm NO with 10% O_2 at various temperatures are compared with that of the cells impregnated with BaO in figures 8.2-8.4. The values of NO_x conversion and current efficiency for the BaO and Pt impregnated cells were close to the values for the BaO impregnated cells in the tested temperature range especially considering the experimental uncertainty at low temperatures and the deviation between different samples. With respect to the N_2 selectivity, the values measured on the cells of Ba+Pt-1 and Ba+Pt-2 were similar with the values measured on the cells impregnated with only BaO and the values on the cell of Ba-Pt+3 were higher than those on the BaO-impregnated cells. The NO_x removal properties were almost identical between the cells impregnated with BaO and the cells impregnated with both BaO and Pt. By increasing the concentration of Pt precursor and the times of Pt impregnations the N_2 selectivity increased but no profound iimprovement of the NO_x conversion and current efficiency has been dectected.

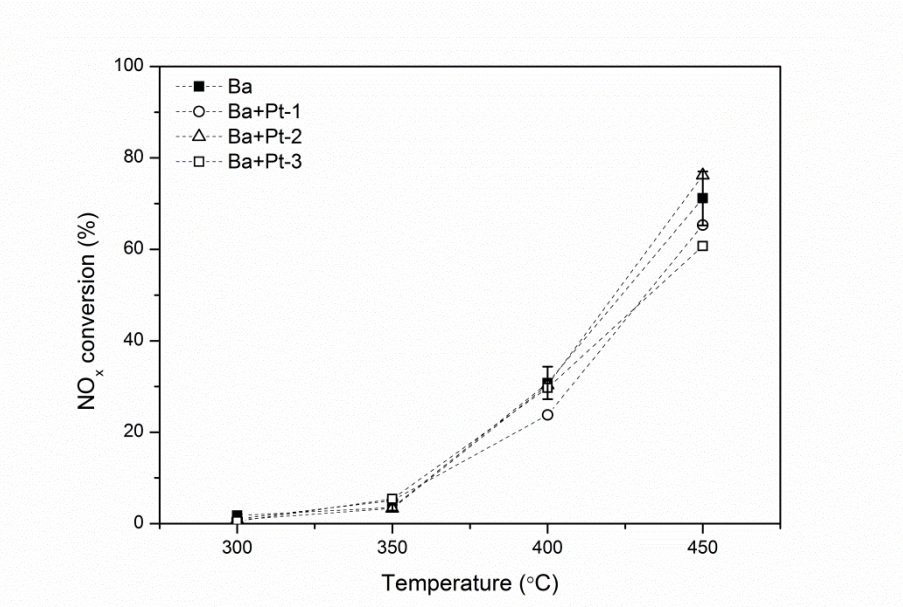

Figure 8.2 NO_x conversions on the LSM/CGO cell impregnated with BaO and the LSM/CGO cell impregnated with BaO and Pt, as a function of temperature in 1000 ppm NO with 10% O_2 under a square wave polarization of 2.25 V and 0.5 Hz.

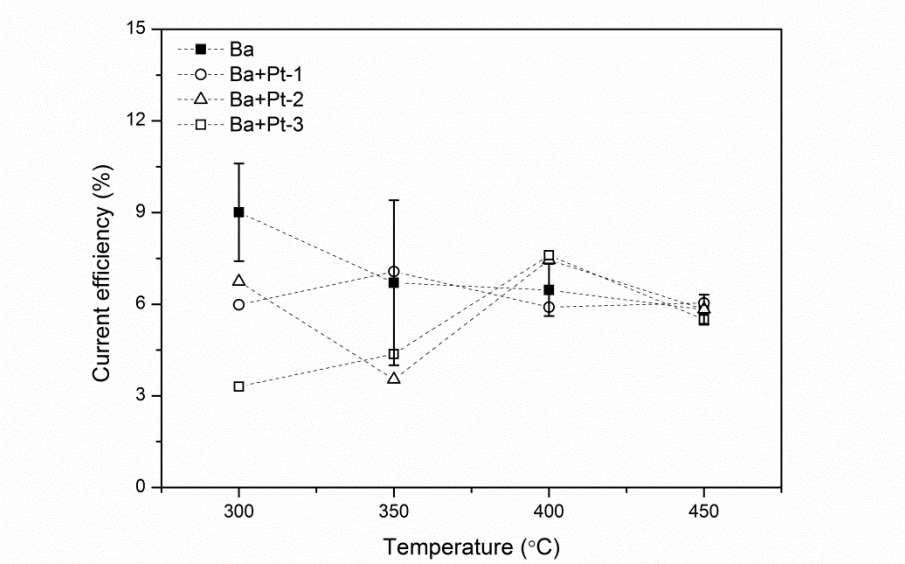

Figure 8.3 Current efficiency on the LSM/CGO cell impregnated with BaO and the LSM/CGO cell impregnated with BaO and Pt as a function of temperature in 1000 ppm NO with 10% O_2 under a square wave polarization of 2.25 V and 0.5 Hz.

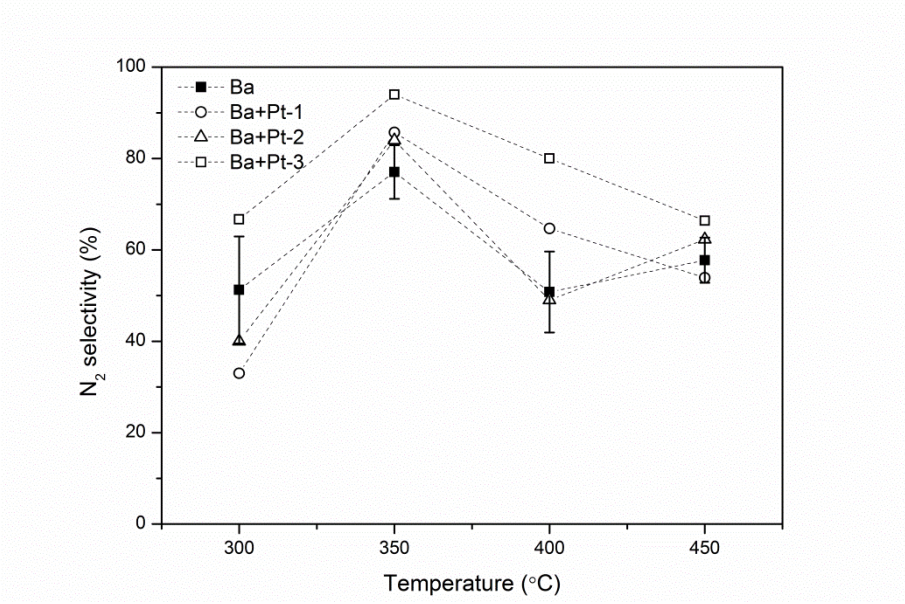

Figure 8.4 N_2 selectivity on the LSM/CGO cell impregnated with BaO and the LSM/CGO cell impregnated with BaO and Pt as a function of temperature in 1000 ppm NO with 10% O_2 under a square wave polarization of 2.25 V and 0.5 Hz.

8.3.3 Impedance characterization

Figure 8.5 shows the impedance spectra for the cell impregnated with BaO and the cell impregnated with BaO and Pt in 1000 ppm NO at 450 °C. While, figure 8.6 lists the polarization resistances of the two different type of cells in 1000 ppm NO and 10 % O_2 from 300 to 450 °C. No significant difference was observed between the impedance data for the two types of cells recorded in the different atmospheres and at various temperatures. The influence of Pt impregnation seemed to be negligible on the impedance spectra. In an attempt to correlate the results coming out of impedance characterization with those of conversion measurements and microstructure observation, it can be concluded that the Pt impregnation is having almost no effect either on the microstructure, nor the NO_x removal properties or the impedance spectra of the electrodes, which was the most likely due to the fact that the amount of Pt impregnated into the electrode was negligible. The SEM images of the electrodes showed that most of the electrode surface was occupied by the BaO particles before being impregnated with Pt, which may be one of the reasons why the Pt cannot be successfully impregnated into the electrode. As a result, the preparation parameters for the Pt impregnation need to be further optimized in order to get a sufficient Pt loading.

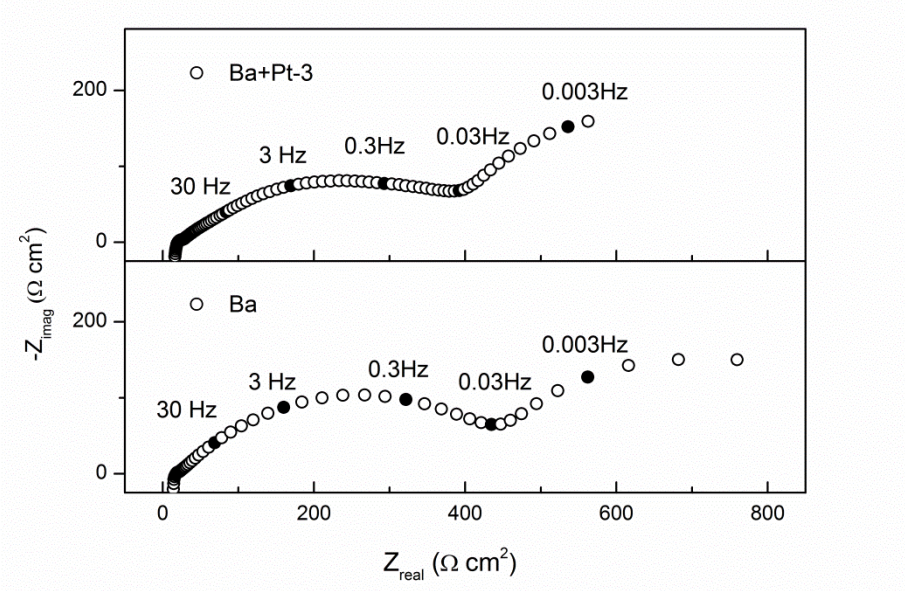

Figure 8.5 Impedance spectra of the LSM/CGO symmetric cells impregnated with BaO and that with BaO and Pt, in 1000 ppm NO at 450 °C.

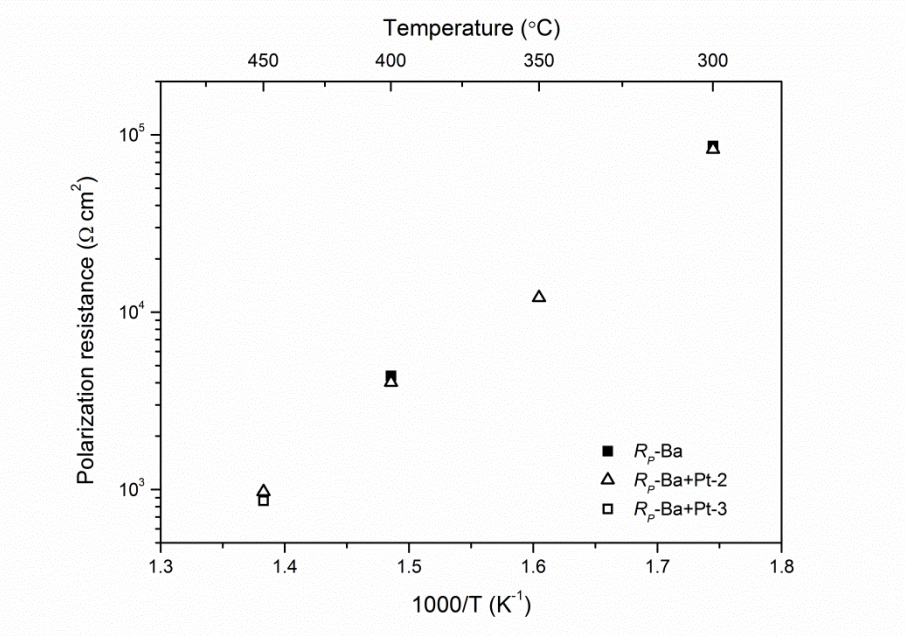

Figure 8.6 Polarization resistances for the LSM/CGO cell impregnated with BaO and the LSM/CGO cell impregnated with BaO and Pt as a function of temperature in 1000 ppm NO with 10% O_2.

8.4 Conclusion

The LSM/CGO symmetric cells impregnated with both BaO and Pt were prepared and tested for the NO_x reduction in O_2-rich environment. The microstructure, the NO_x conversion, and the impedance spectra measured on the cells impregnated both BaO and Pt were compared with those measured on the cells impregnated only with BaO. No significant difference caused by the Pt impregnation was observed under the testing conditions, which was probably due to the low Pt loading in the electrode. As a conclusion, the preparation procedure of impregnating the electrode with both BaO and Pt needs to be optimized further.

Chapter 9 Summary and outlook

9.1 Discussion

9.1.1 Optimization of electrode structure

Before the NO_x adsorbents were introduced to the electrochemical cells, the optimization of electrode structure was primarily focus on inhibiting the competitive reaction of O_2. For this purpose, the electrodes were made to be rather dense or coated with cover layers. After adding the NO_x adsorbents, the benefit of using such structures decreased. It may be necessary to optimize the electrode structure for facilitating the "cooperation" between the cell and the adsorption layer. In this work, the structure of a multilayered electrochemical cell with a NO_x adsorption layer was modified by removing the intervening YSZ layer, which was deposited on the surface of the cathode to inhibit the O_2 decomposition reaction. By removing the YSZ layer, the diffusion of NO_x species from the adsorption layer to the cathode became unobstructed, which in turn improved the NO_x trapping efficiency of the adsorption layer. Moreover, the decomposition of NO_x could be promoted at the interface between the directly connected adsorption layer and the cathode. As a result, both the activity and selectivity for NO_x reduction were significantly enhanced by omitting the YSZ layer in spite of the increase in O_2 reduction. The simplified electrode was more suitable for combining with the adsorption layer relative to the multilayered electrode. This demonstrated the importance of the interaction between the electrode and the adsorption layer on the NO_x removal properties.

9.1.2 Exploration of electrode materials

Structure optimization was based on an electrode consisted of precious metal Pt and reactive material Ni. Although the optimized electrode exhibited quite high activity and selectivity for NO_x reduction, materials with lower cost and higher stability were needed for practical applications. Therefore, Ag and LSM were evaluated as the electrode materials for the electrochemical cell modified with the NO_x adsorbents. The blank Ag and LSM/CGO electrodes were almost incapable of converting NO_x to N_2 in an O_2-rich environment. After adding the NO_x adsorption layer, both the electrodes could effectively reduce NO_x to N_2 in the presence of excess O_2. With the addition of a K-Pt-Al_2O_3 adsorption layer, 82% NO_x

conversion with 7.7% current efficiency and 100% N_2 selectivity were achieved on the Ag electrode and a 85% conversion with 4% current efficiency and 74% N_2 selectivity on the LSM/CGO electrode, both at 500 °C in 1000 ppm NO and 8-10% O_2.

With respect to the stability of the electrodes, significant degradation was observed on the Ag electrode coated with the K-Pt-Al_2O_3 layer after long-term operation, due to the corrosion of the Ag electrode by molten potassium nitrate under negative polarization, a species present as the melting point of potassium nitrate is rather low (334 °C). Therefore, Ba was used instead of K as the storage components for the LSM/CGO electrode as the melting point of barium nitrate is much higher (592 °C). However, a 30-40% decrease in NO_x conversion was observed on the LSM/CGO electrode with Ba-based adsorbent materials after 100 h of operation. The degradation may be associated with the profound change in microstructure after testing. One possible reason for the microstructure change is that the electrode material reacted with the Ba-related compounds, especially the nitrate, under operation conditions, but the exact cause of this microstructure change requires further investigation.

9.1.3 Comparison of modification approaches

The two main approaches for modifying the electrochemical cells using NO_x adsorbents were compared for a symmetric LSM/CGO cell. Both of the approaches, adding a Ba-Pt-Al_2O_3 layer on top of the electrode or impregnating the BaO into the electrode could effectively enhance NO_x reduction on the LSM/CGO cell. The cell with the adsorption layer showed a superior performance relative to the impregnated cell at low temperatures and low voltages due to the NO oxidation ability of the Pt catalyst, whereas the impregnated cell performed better at elevated temperatures and voltages as there was no diffusion limitation of NO_x species caused by the additional adsorption layer. The trapping and reduction rates of the NO_x species on the electrodes could be balanced by applying a square wave (SV) polarization with an optimum frequency. The higher optimum frequency on the impregnated cell indicated that the trapping and/or reduction rates of the NO_x species were faster on the impregnated cell than on the cell with the adsorption layer, which was probably due to the storage sites being close to the reaction sites on the impregnated cell. From the perspective of lowering the operating temperature and minimizing the electrical consumption of the electrochemical NO_x reduction cell, the approach of adding an adsorption layer seems more favorable than that of impregnating, but it may be possible to improve the

performance of the BaO impregnated cell at low temperatures and voltages by introducing Pt into the electrode. The preliminary experimental results showed no significant difference in performance between the cell impregnated with both BaO and Pt and that impregnated with only BaO, which was most likely due to the Pt loading in the electrode being negligible with respect to the BaO loading. The impregnation procedure needs to be adjusted further to obtain sufficient Pt loading.

9.1.4 Identification of reaction mechanism

The impedance spectra of the cells modified with the NO_x adsorbents were measured under various experimental conditions to identify the effect of NO_x adsorbents on the electrode processes related to electrochemical NO_x reduction. The impedance analysis revealed that the modification by NO_x adsorbents did not completely alter the reaction mechanism but did enhance the electrode activity. This activity enhancement was primarily caused by the promotion of adsorption, surface diffusion, and transfer of the NO_x and O_2 species at/near the triple phase boundary region and the formation of NO_2. The contact of the adsorption layer with the electrode or the impregnation of NO_x trapping materials into the electrode may also allow for the direct reduction of the stored nitrate.

9.1.5 Potential for realistic applications

The energy consumption of the cells, with different electrodes and NO_x adsorbents, required to achieve their best deNO_x efficiency under the experimental conditions were calculated and are listed in table 9.1.

Table 9.1 Comparison of the deNO_x efficiency and power consumption of the cells investigated in this study. The conversion of NO_x to N_2 is calculated by multiplying NO_x conversion with N_2 selectivity. The test atmosphere is 1000 ppm NO and 8-10% O_2 in Ar with a flow rate of 2L/h.

Electrodes	NO_x adsorbents	Temperature (°C)	Conversion of NO_x to N_2 (%)	Energy consumption (W)
Ni/Pt/YSZ	K-Pt-Al_2O_3	450	84	0.062
Ag	K-Pt-Al_2O_3	500	58	0.024
LSM/CGO	K-Pt-Al_2O_3	500	63	0.216
LSM/CGO	BaO	450	41	0.146
LSM/CGO	Ba-Pt-Al_2O_3	450	56	0.121

The current EU emission standards (Euro 4) require more than 60% reduction of NO_x in diesel exhaust. The Ag electrode with the K-Pt-Al_2O_3 layer consumed the lowest amount of electrical power to reach approximately 60% NO_x reduction among the electrodes investigated in this work. For a 1.4 L 69 PS diesel engine with an output of around 51.4 kW, the exhaust flow at the maximum speed (4000 rpm) is approximately 42 L/s (20°C, 1 bar). Assuming the concentrations of NO_x and O_2 in the exhaust gases are the same with those used in this study, the energy consumption to clean 60% NO_x at 500 °C by using the Ag electrode is approximately 1.8 kW, equal to a fuel penalty of 3.5%. This result is promising, but still needs to be improved upon to reach commercial levels, as a fuel penalty below 1% and operation temperatures below 300 °C are required for practical applications.

9.2 Conclusion

The structure of a multilayered electrode has been optimized by eliminating the YSZ cover layer to make the electrode structure more compatible with the NO_x adsorption layer. The NO_x removal properties of the electrochemical cell were dramatically enhanced through this optimization, especially under conditions of low voltages, intermediate temperatures, and high O_2 concentrations. The pronounced increase in activity and selectivity for NO_x decomposition after removing the YSZ cover layer was attributed to the extensive opening up of selective reaction sites for NO_x species and a strong promotion for NO_x reduction from the interaction of the directly connected adsorption layer and the electrode. This structural optimization was performed on an electrode consisted of Pt and Ni, which are cost prohibitive or too unstable for practical applications. Later, Ag and LSM were investigated to substitute Pt and Ni as the electrode materials. Selective NO_x reduction in the presence of excess O_2 was achieved for both Ag and LSM electrodes by modifying the electrodes with NO_x adsorbents. Performances of 82% NO_x conversion with 7.7% current efficiency and 100% N_2 selectivity for the Ag electrode, and of 85% conversion with 4% current efficiency and 74% N_2 selectivity for the LSM/CGO electrode were achieved in 1000 ppm NO and 8-10% O_2 at 500 °C with the addition of a K-Pt-Al_2O_3 adsorption layer. The reaction mechanism behind the performance improvement was investigated using electrochemical impedance spectroscopy (EIS). The impedance analysis revealed that the NO_x adsorbents greatly enhanced the electrode activity, which was mainly contributed through the promotion of adsorption, surface diffusion, and transfer of the NO_x and O_2 species at/near the triple phase boundary region, the formation of intermediate NO_2, and possible formation of a short and effective reaction pathway for NO_x reduction. The stability of the Ag electrode and the LSM/CGO electrode in the presence of the NO_x adsorbents was studied using a degradation test. Severe degradation was observed on both the electrodes, which was caused by the corrosion of electrode covered by a nitrate melt for the Ag electrode or associated with a profound change in the microstructure after testing for the LSM/CGO electrode. The exact cause of the microstructure change on the LSM/CGO electrode needs further investigation.

The two main approaches to modifying the electrochemical cells with NO_x adsorbents were compared through systematic investigations of conversion measurements, degradation tests, microstructure observation, and impedance characterization. The modifications were performed on a LSM/CGO symmetric cell, a full ceramic structure without any noble metals. Both of the approaches, adding an

adsorption layer on top of the electrode or impregnating the storage components into the electrode, significantly increased the activity and selectivity of the NO_x reduction of the LSM/CGO symmetric cell by enhancing the adsorption and storage of the NO_x species or providing reaction sites for direct nitrate reduction. The cell with the Ba-Pt-Al_2O_3 layer exhibited a better performance at low temperatures (350 and 400 °C) and low voltages (1.5 to 2 V) relative to the BaO impregnated cell due to the NO oxidation ability of the Pt catalyst, although it performance was relatively poor at elevated temperatures and voltages due to impedance of the diffusion of NO_x to the reaction sites by the adsorption layer. This finding indicated that the presence of an NO oxidation catalyst was important for lowering the operation temperature and minimizing the power consumption of the electrochemical cell. Square-wave (SV) polarization can balance the trapping and reduction rates of NO_x species on the electrochemical cells to further improve the NO_x reduction activity relative to the performance under the direct current (DC) polarization. To the best of the author's knowledge, this is the first time a comprehensive comparison between the two main approaches for modifying the electrochemical cells by NO_x adsorbents was reported. The electrochemical cell with the Ag or LSM/CGO electrodes modified with NO_x adsorbents may provide a promising solution for NO_x emission control under lean-burning engine operation.

9.3 Outlook

To shorten the time to the development of this technology in realistic applications, future work should include decreasing the operating temperature and power consumption, and improving the stability of the Ag or LSM/CGO electrochemical cells in the presence of NO_x adsorbents. According to previous studies, the applied voltage and operation temperature can be reduced by optimizing the structure of the electrode or increasing the ionic conductivity of the electrolyte. The current electrochemical cells were support on a 200-300 µm thick electrolyte. By using an electrode-supported cell structure, it is possible to reduce the thickness of the electrolyte to 10-20 µm, thus decreasing the resistance of the electrolyte by 10 times. For electrode optimization, it is first necessary to perform more detailed studies on the influence of the electrode thickness, porosity, and particle size on the NO_x removal performance for the Ag and LSM/CGO electrodes to determine the optimum backbone structure of these two electrodes. For modification by NO_x adsorbents, as the performance of the BaO impregnated cells appeared to be limited by the lack of a strong NO oxidation ability, it is suggested to focus on co-infiltration of Pt with BaO to promote the NO_x reduction at low temperatures and low voltages. The preparation procedure needs to be modified to get sufficient loading of Pt into the electrode.

With respect to the stability of the electrode, future work should first be focused on clarifying the exact cause of the microstructure change of the LSM/CGO electrode modified with the Ba-related absorbents, whether new phases are formed, and what the compositions of the phases are on the cells with the NO_x adsorbents. Furthermore, it is also important to identify under what conditions (temperatures and voltages) the reaction between the electrode materials and the absorbents will happen on the LSM/CGO electrode and the Ag electrode in order to determine the boundary conditions for operating the cells with the NO_x adsorbents remaining stable.

The majority of the impedance spectra in this work were recorded under OCV conditions, which was dictated by the two electrode configuration used here lacking a reference electrode with constant potentials. In general, the OCV results appeared to correlate well with the conversion measurements, but a dramatic decrease was observed in the resistances of impedance spectra recorded under polarization. The impedance data under current loading may provide more realistic information about the reactions proceeding on the electrode during cell operation. For this reason, it is suggested to use a three electrode configuration setup to better measure the impedance spectra under polarization.

Finally, simplified gas mixtures that only contained NO_x and O_2 were used in this study to facilitate the understanding of the electrode processes. As the electrochemical cell is developed for use in real diesel exhaust ultimately, the effect of other gas components in the exhaust gases, such as CO_2, CO, H_2O, soot, hydrocarbon, and SO_2 on the cell performance need to be investigated in future studies.

References

[1] J. E. Parks, “Less costly catalysts for controlling engine emissions,” *Science*, vol. 327, no. 5973, pp. 1584–1585, 2010.

[2] http://www.acea.be/news/news_detail/diesel_market_highly_developed_in_europe/. Accessed: 02-May-2013.

[3] http://www.forbes.com/sites/joannmuller/2013/02/07/are-americans-ready-to-embrace-diesel-cars-chevy-hopes-so/. Accessed: 02-May-2013.

[4] http://www.businessweek.com/articles/2012-12-20/in-japan-diesel-cars-get-a-second-chance. Accessed: 02-May-2013.

[5] J. Kašpar, P. Fornasiero, and N. Hickey, “Automotive catalytic converters: current status and some perspectives,” *Catalysis Today*, vol. 77, no. 4, pp. 419–449, 2003.

[6] E. L. Merryman and A. Levy, “Nitrogen oxide formation in flames: the roles of NO_2 and fuel nitrogen,” *15th Symposium (International) on Combustion*, vol. 15, no. 1, pp. 1073–1083, 1975.

[7] S. . Hill and L. Douglas Smoot, “Modeling of nitrogen oxides formation and destruction in combustion systems,” *Progress in Energy and Combustion Science*, vol. 26, no. 4–6, pp. 417–458, 2000.

[8] Y. B. Zeldovich, “The oxidation of nitrogen in combustion and explosion,” *Acta Physicochim, U.S.S.R.*, vol. 21, p. 577, 1946.

[9] P. C. Malte and N. M. Marinov, “The effect of low-concentration fuels on the conversion of nitric oxide to nitrogen dioxide,” *24th Symposium (International) in Combustion*, vol. 24, no. 1, pp. 909–916, 1992.

[10] G. M. Johnson, M. Y. Smith, and M. F. R. Mulcahy, “The presence of NO_2 in premixed flames,” *17th Symposium (International) on Combustion*, vol. 17, no. 1, pp. 647–660, 1979.

[11] C. P. Fenimore, “The ratio NO_2/NO in fuel-lean flames,” *Combustion and Flame*, vol. 25, pp. 85–90, 1975.

[12] F. Garin, “Mechanism of NO_x decomposition,” *Applied Catalysis A*, vol. 222, pp. 183–219, 2001.

[13] I. N. Krivoshto, J. R. Richards, T. E. Albertson, and R. W. Derlet, “The toxicity of diesel exhaust: implications for primary care,” *Journal of the American Board of Family Medicine: JABFM*, vol. 21, no. 1, pp. 55–62, 2008.

[14] M. T. Lerdau, J. W. Munger, and J. D. Jacob, “The NO_2 flus conundrum,” *Science*, vol. 289, pp. 2291–2293, 2000.

[15] B. J. Finlayson-Pitts and J. N. Pitts, “Tropospheric air pollution: ozone, airborne toxics, polycyclic aromatic hydrocarbons, and particles,” *Science*, vol. 276, no. 5315, pp. 1045–52, 1997.

[16] T. B. Ryerson, M. Trainer, J. S. Holloway, D. D. Parrish, L. G. Huey, D. T. Sueper, G. J. Frost, S. G. Donnelly, S. Schauffler, E. L. Atlas, W. C. Kuster, P. D. Goldan, G. Hubler, J. F. Meagher, and F. C. Fehsenfeld, “Observations of ozone formation in power plant plumes and implications for ozone control strategies,” *Science*, vol. 292, no. 5517, pp. 719–23, 2001.

[17] http://www.dieselnet.com/standards/. Accessed: 04-Feb-2013.

[18] K. Hallstrom and J. M. Schiavon, “Euro IV and V diesel emission control system review,” *SAE Technical Paper series*, 2007–01–2617.

[19] M. Shelef, “Selective catalytic reduction of NO_x with N-free reductants,” *Chemical Reviews*, vol. 95, no. 1, pp. 209–225, 1995.

[20] T. Johnson, “Vehicular emissions in review,” *SAE Technical Paper series*, 2013–01–0538.

[21] F. J. J. G. Janssen, F. M. G. Van Den Kerkhof, H. Bosch, and J. R. H. Ross, “Mechanism of the reaction of nitric oxide, ammonia, and oxygen over vanadia catalysts. 2. isotopic transient studies with oxygen-18 and nitrogen-15†,” The *Journal of Physical Chemistry*, vol. 91, pp. 6633–6638, 1987.

[22] C. Ciardelli, I. Nova, E. Tronconi, and B. Bandl-konrad, “A ‘Nitrate Route’ for the low temperature ‘Fast SCR’ reaction over a V_2O_5-WO_3/TiO_2 commercial catalsyt,” *Chemical Communications*, vol. 20133, no. 4, pp. 2718–2719, 2004.

[23] G. Busca, L. Lietti, G. Ramis, and F. Berti, “Chemical and mechanistic aspects of the selective catalytic reduction of NO_x by ammonia over oxide catalysts : A review,” *Applied Catalysis B: Environmental*, vol. 18, pp. 1–36, 1998.

[24] http://www.amminex.com/. Accessed: 19-Apr-2013.

[25] W. S. Epling, L. E. Campbell, A. Yezerets, N. W. Currier, and J. E. Parks, “Overview of the fundamental reactions and degradation mechanisms of NO_x storage/reduction catalysts,” *Catalysis Reviews*, vol. 46, no. 2, pp. 163–245, 2004.

[26] S. Brandenberger, O. Kröcher, A. Tissler, and R. Althoff, “The state of the art in selective catalytic reduction of NO_x by ammonia using metal-exchanged zeolite catalysts,” *Catalysis Reviews*, vol. 50, no. 4, pp. 492–531, 2008.

[27] T. V Johnson, “Vehicular emissions in review,” *SAE Technical Paper series*, 2012–01–0368.

[28] N. Takahashi, H. Shinjoh, T. Iijima, T. Suzuki, K. Yamazaki, K. Yokota, H. Suzuki, N. Miyoshi, S. Matsumoto, T. Tanizawa, T. Tanaka, S. Tateishi, and K. Kasahara, "The new concept 3-way catalyst for automotive lean-burn engine: NO_x storage and reduction catalyst," *Catalysis Today*, vol. 27, no. 1–2, pp. 63–69, 1996.

[29] M. Iwamoto and H. Hamada, "Removal of nitrogen monoxide from exhaust gases through novel catalytic processes," *Catalysis Today*, vol. 10, pp. 67–71, 1991.

[30] T. V Johnson, "Diesel emission control in review," *SAE Technical Paper series*, 2006–01–0030.

[31] K. Kammer, "Electrochemical $DeNO_x$ in solid electrolyte cells—an overview," *Applied Catalysis B: Environmental*, vol. 58, no. 1–2, pp. 33–39, 2005.

[32] S. Pancharatnam, R. A. Huggins, and D. M. Mason, "Catalytic decomposition of nitric oxide on zirconia by electrolytic removal of oxygen," *Journal of the Electrochemical Society*, vol. 122, no. 7, pp. 869–875, 1975.

[33] T. M. Gür and R. A. Huggins, "Decomposition of nitric oxide on zirconia in a solid-state electrochemical cell," *Journal of The Electrochemical Society*, vol. 126, no. 6, pp. 1067–1075, 1979.

[34] T. Hibino, "Electrochemical removal NO and CH_4 from oxidizing atmosphere," *Chemistry Letters*, no. 5, pp. 927–930, 1994.

[35] T. Hibino, T. Inoue, and M. Sano, "Electrochemical reduction of NO by alternating current electrolysis using yttria-stabilized zirconia as the solid electrolyte Part I . Characterizations of alternating current electrolysis of NO," *Solid State Ionics*, vol. 130, pp. 19–29, 2000.

[36] T. Hibino, K. Ushiki, and Y. Kuwahara, "Mechanism of NO decomposition in a solid electrolyte reactor by SEP method," *Solid State Ionics*, vol. 98, no. 3–4, pp. 185–190, 1997.

[37] T. Hibino, K. Ushiki, Y. Kuwahara, and M. Mizunob, "Electrochemical removal of NO and CH_4 in the presence of excess O_2, H_2O and CO_2 using Sm_2O_3-doped CeO_2 as a solid electrolyte," *Journal of the Chemical Society Faraday Transactions*, vol. 92, no. 21, pp. 4297–4300, 1996.

[38] K. J. Walsh and P. S. Fedkiw, "Nitric oxide reduction using platinum electrodes on yttria-stabilized zirconia," *Solid State Ionics*, vol. 93, pp. 17–31, 1997.

[39] K. J. Walsh and P. S. Fedkiw, "Nitric oxide reduction using iridium electrodes on yttria-stabilized zirconia," *Solid State Ionics*, vol. 104, no. 1–2, pp. 97–108, 1997.

[40] K. K. Hansen, "Electrochemical reduction of O_2 and NO on Ni, Pt and Au," *Journal of Applied Electrochemistry*, vol. 38, no. 5, pp. 591–595, 2008.

[41] K. K. Hansen, "Solid state electrochemical $DeNO_x$—An overview," *Applied Catalysis B: Environmental*, vol. 100, no. 3–4, pp. 427–432, 2010.

[42] D. C. Cicero and L. A. Jarr, “Application of ceramic membranes in advanced coal-based power generation systems,” *Separation Science and Technology*, vol. 25, no. 13–15, pp. 1455–1472, 1990.

[43] K. K. Hansen, H. Christensen, E. M. Skou, and S. V Skaarup, “Electrochemical reduction of NO and O_2 on C /CuO,” *Journal of Applied Electrochemistry*, vol. 30, pp. 193–200, 2000.

[44] K. K. Hansen, H. Christensenb, and E. M. Skou, “Electrochemical reduction of NO and O_2 on oxide based electrodes,” *Ionics*, vol. 6, pp. 340–345, 2000.

[45] K. Kammer and E. Skou, “LSFM perovskites as cathodes for the electrochemical reduction of NO,” *Solid State Ionics*, vol. 176, no. 9–10, pp. 915–920, 2005.

[46] K. K. Hansen, E. M. Skou, and H. Christensen, “Perovskites as cathodes for nitric oxide reduction,” vol. 147, no. 5, pp. 2007–2012, 2007.

[47] V. L. E. Simonsen, D. Find, M. Lilliedal, R. Petersen, and K. Kammer, “Spinels as cathodes for the electrochemical reduction of O_2 and NO,” *Topics in Catalysis*, vol. 45, no. 1–4, pp. 143–148, 2007.

[48] V. L. E. Simonsen, L. Nørskov, and K. K. Hansen, “Electrochemical reduction of NO and O_2 on $La_{2-x}Sr_xCuO_4$-based electrodes,” *Journal of Solid State Electrochemistry*, vol. 12, no. 12, pp. 1573–1577, 2008.

[49] F. Bræstrup and K. K. Hansen, “The $NiFe_2O_4$ - $MgFe_2O_4$ series as electrode materials for electrochemical reduction of NO_x,” *Journal of Solid State Electrochemistry*, vol. 13, no. 8, pp. 1241–1250, 2008.

[50] F. Bræstrup and K. K. Hansen, “$NiCr_xFe_{2-x}O_4$ as cathode materials for electrochemical reduction of NO_x,” *Journal of Solid State Electrochemistry*, vol. 14, no. 1, pp. 157–166, 2009.

[51] F. Bræstrup and K. K. Hansen, “Characterization of $MgMn_xFe_{2-x}O_4$ as a possible cathode material for electrochemical reduction of NO_x,” *Journal of Applied Electrochemistry*, vol. 39, no. 12, pp. 2369–2374, 2009.

[52] E. D. Wachsman, P. Jayaweera, G. Krishnan, and A. Sanjurjo, “Electrocatalytic reduction of NO_x on $La_{1-x}A_xB_{1-y}B'_yO_{3-\delta}$: evidence of electrically enhanced activity,” *Solid State Ionics*, vol. 137, pp. 775–782, 2000.

[53] H. J. Hwang, J. Moon, and M. Awano, “Microstructure and NO decomposition behavior of sol−gel derived $(La_{0.8}Sr_{0.2})_{0.95}MnO_3$/yttria-stabilized zirconia nanocomposite thin film,” *Materials Research Bulletin*, vol. 38, pp. 311–318, 2003.

[54] H. J. Hwang and M. Awano, “Preparation of $LaCoO_3$ catalytic thin film by the sol–gel process and its NO decomposition characteristics,” *Journal of the European Ceramic Society*, vol. 21, pp. 2103–2107, 2001.

[55] R. M. L. Werchmeister, K. K. Hansen, and M. Mogensen, "Characterization of $(La_{1-x}Sr_x)_sMnO_3$ and doped ceria composite electrodes in NO_x-containing atmosphere with impedance spectroscopy," *Journal of The Electrochemical Society*, vol. 157, no. 5, pp. P35–P42, 2010.

[56] R. M. L. Werchmeister, K. K. Hansen, and M. Mogensen, "EIS Measurements on $La_{1-x}Sr_xCo_{1-y}Fe_yO_{3-\delta}$ based composite electrodes in NO_x containing atmosphere," *Journal of The Electrochemical Society*, vol. 157, no. 12, pp. P107–P112, 2010.

[57] R. M. L. Werchmeister, K. K. Hansen, and M. Mogensen, "Electrochemical testing of composite electrodes of $(La_{1-x}Sr_x)_sMnO_3$ and doped ceria in NO-containing atmosphere," *Journal of Solid State Electrochemistry*, vol. 16, no. 2, pp. 703–714, 2012.

[58] R. M. L. Werchmeister, K. K. Hansen, and M. Mogensen, "Electrochemical removal of NO_x with porous cell stacks," *Materials Research Bulletin*, vol. 45, no. 11, pp. 1554–1561, 2010.

[59] J. Nakatani, Y. Ozeki, K. Sakamoto, and K. Iwayama, "NO decomposition in the presence of excess O_2 using the electrochemical cells with Pd electrodes treated at high temperature and coated with $La_{1-x}Sr_xCoO_3$," *Chemistry Letters*, no. 4, pp. 315–316, 1996.

[60] K. Iwayama and X. Wang, "Selective decomposition of nitrogen monoxide to nitrogen in the presence of oxygen on RuO_2/Ag (cathode)/yttria-stabilized zirconia/Pd (anode)," *Applied Catalysis B: Environmental*, vol. 19, pp. 137–142, 1998.

[61] S. Park, "NO decomposition over the electrochemical cell of lanthanum stannate pyrochlore and YSZ composite electrode," *Solid State Ionics*, vol. 175, no. 1–4, pp. 625–629, 2004.

[62] S. Bredikhin, K. Maeda, and M. Awano, "Electrochemical cell with two layers cathode for NO decomposition," *Ionics*, vol. 7, no. 1–2, pp. 109–115, 2001.

[63] S. Bredikhin, K. Maeda, and M. Awano, "NO decomposition by an electrochemical cell with mixed oxide working electrode," *Solid State Ionics*, vol. 144, pp. 1–9, 2001.

[64] S. Bredikhin, K. Maeda, and M. Awano, "Low current density electrochemical cell for NO decomposition," *Solid State Ionics*, vol. 152–153, pp. 727–733, 2002.

[65] S. Bredikhin, K. Hamamoto, Y. Fujishiro, and M. Awano, "Electrochemical reactors for NO decomposition. Basic aspects and a future," *Ionics*, vol. 15, pp. 285–299, 2009.

[66] K. Matsuda, S. Bredikhin, K. Maeda, and M. Awano, "Optimization of an electrochemical cell for NO decomposition by compositional control of the electro-catalytic electrode," *Solid State Ionics*, vol. 156, pp. 223–231, 2003.

[67] S. Bredikhin, K. Matsuda, K. Maeda, and M. Awano, "Novel low voltage electrochemical cell for NO decomposition," *Solid State Ionics*, vol. 149, pp. 327–333, 2002.

[68] S. Bredikhin, G. Abrosimova, a. Aronin, K. Hamamoto, Y. Fujishiro, S. Katayama, and M. Awano, "Pt-YSZ cathode for electrochemical cells with multilayer functional electrode," *Journal of The Electrochemical Society*, vol. 151, no. 12, pp. J95–J99, 2004.

[69] M. Awano, "NO_x decomposition by electrochemical reactor with electrochemically assembled multilayer electrode," *Solid State Ionics*, vol. 175, no. 1–4, pp. 605–608, 2004.

[70] K. Hamamoto, T. Hiramatsu, Þ. Shiono, Þ. Katayama, Y. Fujishiro, and S. Bredikhinþ, "Microstructure controlled high selective $DeNO_x$ electrochemical reactor," *Journal of the Ceramic Society of Janpan*, vol. 112, no. 5, pp. 1071–1074, 2004.

[71] K. Hamamoto, Y. Fujishiro, and M. Awano, "Intermediate temperature electrochemical reactor for NO_x decomposition," *Journal of The Electrochemical Society*, vol. 153, no. 11, p. D167–D170, 2006.

[72] K. Hamamoto, Y. Fujishiro, and M. Awano, "Low-temperature NO_x decomposition using an electrochemical reactor," *Journal of The Electrochemical Society*, vol. 155, no. 8, pp. E109–E111, 2008.

[73] K. Hamamoto, T. Suzuki, Y. Fujishiro, and M. Awano, "Tubular solid oxide electrolysis cell for NO_x decomposition," *Journal of The Electrochemical Society*, vol. 158, no. 8, pp. B1050–B1053, 2011.

[74] Y. Yoshinobu, Y. Tsuda, H. Ueda, Y. Nakanishi, and J. Gong, "Simultaneous reduction of NO_x and PM in diesel exhaust based on electrochemical reaction," *SAE Technical Paper 2010-01-0306*.

[75] M. L. Traulsen and K. Kammer Hansen, "Improvement of LSM15-CGO10 electrodes for electrochemical removal of NO_x by KNO_3 and MnO_x impregnation," *Journal of The Electrochemical Society*, vol. 158, no. 12, pp. P147–P161, 2011.

[76] M. L. Traulsen, F. Bræstrup, and K. K. Hansen, "NO_x conversion on porous LSF15–CGO10 cell stacks with KNO_3 or K_2O impregnation," *Journal of Solid State Electrochemistry*, vol. 16, no. 8, pp. 2651–2660, 2012.

[77] M. L. Traulsen, K. B. Andersen, and K. K. Hansen, "NO_x conversion on LSM15-CGO10 cell stacks with BaO impregnation," *Journal of Materials Chemistry*, vol. 22, no. 23, pp. 11792–11800, 2012.

[78] F. Rohr, I. Grißtede, A. Sundararajan, and W. Müller, "Diesel NO_x-storage catalyst systems for Tier 2 BIN5 legislation," *SAE Technical Paper series*, 2008–01–0766.

[79] Factsage 6.2. Thermmfact and GTT-Technologies.

[80] I. Rickardsson, L. Jo, and C. Nyberg, "Influence of surface topology on NO adsorption: NO on Ni(100) and Ni(510)," *Surface Science*, vol. 414, pp. 389–395, 1998.

[81] W. a. Brown, R. Kose, and D. a. King, “Femtomole adsorption calorimetry on single-crystal surfaces,” *Chemical reviews*, vol. 98, pp. 797–832, 1998.

[82] R. Lindsay, A. Theobald, T. Gießel, O. Schaff, A. . Bradshaw, N. . Booth, and D. . Woodruff, “The structure of NO on Ni(111) at low coverage,” *Surface Science*, vol. 405, pp. L566–L572, 1998.

[83] A. D. Karmazyn, V. Fiorin, and D. a. King, “Calorimetric studies of NO on Ni{211}: criteria for switching from dissociative to molecular adsorption,” *Surface Science*, vol. 547, pp. 184–192, 2003.

[84] K. Hamamoto, Y. Fujishiro, and M. Awano, “Reduction and reoxidation reaction of catalytic layers in electrochemical cells for NO_x decomposition,” *Journal of The Electrochemical Society*, vol. 154, no. 9, pp. F172–F175, 2007.

[85] S. C. Singhal and K. Kendall, Eds., *High temperature solid state fuel cells: Fundamentals, design and applications*, Oxford, Elsevier Advanced Technology, 2003, pp. 119–143.

[86] J. Mizusaki, “A chemical diffusion-controlled electrode reaction at the compact $La_{1-x}Sr_xMnO_3$/stabilized zirconia interface in oxygen atmospheres,” *Journal of The Electrochemical Society*, vol. 143, no. 10, pp. 3065–3073, 1996.

[87] S. Carter, A. Selcuk, R. J. Chater, and J. Kajda, “Oxygen transport in selected nonstoichiometric perovskite-structure oxides,” *Solid State Ionics*, vol. 53–56, pp. 597–605, 1992.

[88] C. H. Kim, G. Qi, K. Dahlberg, and W. Li, “Strontium-doped perovskites rival platinum catalysts for treating NO_x in simulated diesel exhaust,” *Science*, vol. 327, no. 5973, pp. 1624–1627, 2010.

[89] B. Dalslet, P. Blennow, P. V. Hendriksen, N. Bonanos, D. Lybye, and M. Mogensen, “Assessment of doped ceria as electrolyte,” *Journal of Solid State Electrochemistry*, vol. 10, no. 8, pp. 547–561, 2006.

[90] M. Mogensen, “Physical, chemical and electrochemical properties of pure and doped ceria,” *Solid State Ionics*, vol. 129, no. 1–4, pp. 63–94, 2000.

[91] L. Lietti, P. Forzatti, I. Nova, and E. Tronconi, “NO_x Storage Reduction over Pt−Ba/γ-Al2O3 Catalyst,” *Journal of Catalysis*, vol. 204, no. 1, pp. 175–191, 2001.

[92] J. H. Kwak, D. H. Kim, T. Szailer, C. H. F. Peden, and J. Szanyi, “NO_x uptake mechanism on $Pt/BaO/Al_2O_3$ catalysts,” *Catalysis Letters*, vol. 111, no. 3–4, pp. 119–126, 2006.

[93] H. Ohtsuka, “The selective catalytic reduction of nitrogen oxides by methane on noble metal-loaded sulfated zirconia,” *Applied Catalysis B: Environmental*, vol. 33, no. 4, pp. 325–333, 2001.

[94] H. Ohtsuka and T. Tabata, “Roles of palladium and platinum in the selective catalytic reduction of nitrogen oxides by methane on palladium–platinum-loaded sulfated zirconia,” *Applied Catalysis B: Environmental*, vol. 29, pp. 177–183, 2001.

[95] S. Salasc, M. Skoglundh, and E. Fridell, “A comparison between Pt and Pd in NO_x storage catalysts,” *Applied Catalysis B: Environmental*, vol. 36, no. 2, pp. 145–160, 2002.

[96] T. Kobayashi, T. Yamada, and K. Kayano, “Study of NO_x trap reaction by thermodynamic calculation,” *SAE Technical Paper series*, 970745.

[97] W. S. Epling, G. C. Campbell, and J. E. Parks, “The effects of CO_2 and H_2O on the NO_x destruction performance of a model NO_x storage/reduction catalyst,” *Catalysis Letters*, vol. 90, no. 1–2, pp. 45–56, 2003.

[98] S. Erkfeldt, E. Jobson, and M. Larsson, “The effect of carbon monoxide and hydrocarbons on NO_x storage at low temperature,” *Topics in Catalysis*, vol. 16/17, pp. 127–131, 2001.

[99] F. Rodrigues, L. Juste, C. Potvin, J. F. Tempère, G. Blanchard, and G. Djéga-mariadassou, “NO_x storage on barium-containing three-way catalyst in the presence of CO_2,” *Catalysis Letters*, vol. 72, no. 1–2, pp. 59–64, 2001.

[100] G. W. Graham, H. Jen, W. Chun, H. P. Sun, X. Q. Pan, and R. W. Mccabe, “Coarsening of Pt particles in a model NO_x trap,” *Catalysis Letters*, vol. 93, pp. 129–134, 2004.

[101] J. Li, J. Theis, W. Chun, C. Goralski, R. Kudla, J. Ura, W. Watkins, M. Chattha, and R. Hurley, “Sulfur poisoning and desulfation of the lean NO_x trap,” *SAE Technical Paper*, 2001–01–2503.

[102] Zview 3.2c. Scribner Associates, Inc.

[103] *Model 42i High Level Instruction Manual-Chemiluminescence NO-NO_2-NO_X analyzer*. Thermo Scientific, USA, 2007.

[104] R. Burch, J. P. Breen, and F. C. Meunier, “A review of the selective reduction of NO_x with hydrocarbons under lean-burn conditions with non-zeolitic oxide and platinum group metal catalysts,” *Applied Catalysis B: Environmental*, vol. 39, no. 4, pp. 283–303, 2002.

[105] K. Hamamoto, “Influence of NO_x absorbent on NO_x decomposition propertiy of Gd doped CeO_2 based electrochemical cells,” *Journal of the Ceramic Society of Japan*, vol. 119, no. 2, pp. 89–92, 2011.

[106] K. Matsuda, S. Bredikhin, and K. Maeda, “Optimization of a composite working electrode for a new family of electrochemical cell for NO decomposition,” *Journal of the American Ceramic Society*, vol. 58, no. 7, pp. 1155–1158, 2003.

[107] S. Bredikhin, G. Abrosimova, A. Aronin, and M. Awano, “Electrochemical cells with multilayer functional electrodes,” *Ionics*, vol. 12, no. 1, pp. 33–39, 2006.

[108] S. Shibata and M. P. Sumino, “Growth of oxide layers on platinum electrodes in molten alkali nitrates,” *Electrochimica Acta*, vol. 20, pp. 871–876, 1975.

[109] Y. Xiong, K. Yamaji, H. Kishimoto, M. E. Brito, T. Horita, and H. Yokokawa, “Deposition of Platinum particles at LSM/ScSZ/Air three-phase boundaries using a platinum current collector,” *Electrochemical and Solid-State Letters*, vol. 12, no. 3, pp. B31–B33, 2009.

[110] J. Shao and K. K. Hansen, “Optimization of an electrochemical cell with an adsorption layer for NOx removal,” *Journal of Solid State Electrochemistry*, vol. 16, no. 10, pp. 3331–3340, 2012.

[111] T. Campbell, “Atomic and molecular oxygen adsorption on Ag(111),” *Surface Science*, vol. 157, pp. 43–60, 1985.

[112] W.-X. Li, C. Stampfl, and M. Scheffler, “Insights into the function of silver as an oxidation catalyst by ab initio atomistic thermodynamics,” *Physical Review B*, vol. 68, no. 16, p. 165412, 2003.

[113] J. Wang, M. Liu, and M. Lin, “Oxygen reduction reactions in the SOFC cathode of Ag/CeO_2,” *Solid State Ionics*, vol. 177, no. 9–10, pp. 939–947, 2006.

[114] E. Barsoukov and J. R. Macdonald, *Impedance spectroscopy-theory, experiment, and applications*, Second Edi. Hoboken, New Jersey, John Wiley & Sons, Inc., 2005, p. 37.

[115] T. Jacobsen, B. Zachau-Chistensen, L. Bay, and S. Skaarup, *Proceedings 17th Risø international symposium on materials science*. Risø national laboratory, Roskilde, Denmark, 1996, p. 32.

[116] M. J. Jørgensen and M. Mogensen, “Impedance of solid oxide fuel cell LSM/YSZ composite cathodes,” *Journal of The Electrochemical Society*, vol. 148, no. 5, pp. A433–A442, 2001.

[117] J. E. Bauerle, “Study of solid electrolyte polarization by a complex admittance method,” *Journal of Physics and Chemistry of Solids*, vol. 30, pp. 2657–2670, 1969.

[118] N. L. Robertson and J. N. Michaels, “Double layer capscitance of porous Platinum electrodes in zirconia electrochemical cells,” *Journal of The Electrochemical Society*, vol. 138, no. 5, pp. 1494–1499, 1991.

[119] A. J. A. Winnubst, A. H. A. Scharenborg, and A. J. Burggraaf, “The electrode resistance of ZrO_2-Y_2O_3-(Bi_2O_3) electrolytes with Pt electrodes,” *Solid State Ionics*, vol. 14, pp. 319–327, 1984.

[120] S. Primdahl and M. Mogensen, “Gas conversion impedance: a test geometry effect in characterization of solid oxide fuel cell anodes,” *Journal of The Electrochemical Society*, vol. 145, no. 7, pp. 2431–2438, 1998.

[121] E. Xue, K. Seshan, and J. Ross, "Roles of supports, Pt loading and Pt dispersion in the oxidation of NO to NO_2 and of SO_2 to SO_3," *Applied Catalysis B: Environmental*, vol. 11, no. 1, pp. 65–79, 1996.

[122] L. Olsson, B. Westerberg, H. Persson, E. Fridell, M. Skoglundh, and B. Andersson, "A kinetic study of oxygen adsorption/desorption and NO oxidation over Pt/Al_2O_3 catalysts," *Journal of Physical Chemistry B*, vol. 103, pp. 10433–10439, 1999.

[123] L. Olsson, H. Persson, E. Fridell, M. Skoglundh, and B. Andersson, "A kinetic study of NO oxidation and NO_x storage on Pt/Al_2O_3 and $Pt/BaO/Al_2O_3$," *Journal of Physical Chemistry B*, vol. 105, pp. 6895–6906, 2001.

[124] B. Westerberg and E. Fridell, "A transient FTIR study of species formed during NO_x storage in the $Pt/BaO/Al_2O_3$ system," *Journal of Molecular Catalysis A: Chemical*, vol. 165, pp. 249–263, 2001.

[125] I. Nova, L. Castoldi, L. Lietti, E. Tronconi, and P. Forzatti, "On the dynamic behavior of 'NO_x-storage/reduction' $Pt–Ba/Al_2O_3$ catalyst," *Catalysis Today*, vol. 75, pp. 431–437, 2002.

[126] W. Bögner, M. Krämer, B. Krutzsch, S. Pischinger, D. Voigtländer, G. Wenninger, F. Wirbeleit, M. S. Brogan, R. J. Brisley, and D. E. Webster, "Removal of nitrogen oxides from the exhaust of a lean-tune gasoline engine," *Applied Catalysis B: Environmental*, vol. 7, pp. 153–171, 1995.

[127] M. L. Traulsen and K. K. Hansen, "Diffuse reflectance infrared fourier transform study of NO_x adsorption on CGO10 impregnated with K_2O or BaO," *Journal of Physical Chemistry A*, vol. 116, pp. 2497–2505, 2012.

[128] M. H. Miles, G. E. Mcmanis, and A. N. Fletcher, "Reactions involving silver ions and silver metal in molten nitrates," *Journal of The Electrochemical Society*, vol. 131, no. 9, pp. 2075–2081, 1984.

[129] A. Conte and M. D. Ingram, "Corrion of silver in fused nitrate: application of E/pO_2- diagram*," *Electrochimica Acta*, vol. 13, pp. 1551–1557, 1968.

[130] T.-J. Huang and C.-H. Wang, "Effect of O_2 concentration and voltage on nitric oxide decomposition over $(LaSr)MnO_3–(Ce,Gd)O_{2-x}$ cathode of solid oxide fuel cell," *Journal of The Electrochemical Society*, vol. 158, no. 12, pp. B1515–B1522, 2011.

[131] G. Reinhardt, H. D. Wiemhöfer, and W. Göpel, "Electrode reactions of $La_{0.8}Sr_{0.2}MnO_{3\pm\delta}$-electrodes on stabilized zirconia with oxygen and the nitrogen oxides NO and NO_2," *Ionics*, vol. 1, pp. 32–39, 1995.

[132] J. Shao and K. K. Hansen, "Enhancement of NO_x removal performance for $(La_{0.85}Sr_{0.15})_{0.99}MnO_3/Ce_{0.9}Gd_{0.1}O_{1.95}$ electrochemical cells by NO_x storage/reduction adsorption layers," *Electrochimica Acta*, vol. 90, pp. 482–491, 2013.

[133] J. Shao and K. K. Hansen, "NO_x Reduction on Ag Electrochemical Cells with a $K\text{-}Pt\text{-}Al_2O_3$ Adsorption Layer," *Journal of the Electrochemical Society*, vol. 160, no. 6, pp. H294–H301, 2013.

[134] A. Tarancón, J. Peña-Martínez, D. Marrero-López, A. Morata, J. C. Ruiz-Morales, and P. Núñez, "Stability, chemical compatibility and electrochemical performance of $GdBaCo_2O_{5+x}$ layered perovskite as a cathode for intermediate temperature solid oxide fuel cells," *Solid State Ionics*, vol. 179, no. 40, pp. 2372–2378, 2008.

[135] C. Gaudillère, L. Olivier, P. Vernoux, C. Zhang, Z. Shao, and D. Farrusseng, "Alternative perovskite materials as a cathode component for intermediate temperature single-chamber solid oxide fuel cell," *Journal of Power Sources*, vol. 195, no. 15, pp. 4758–4764, 2010.

[136] J. H. Kim, M. Cassidy, J. T. S. Irvine, and J. Bae, "Electrochemical investigation of composite cathodes with $SmBa_{0.5}Sr_{0.5}Co_2O_{5+\delta}$ cathodes for intermediate temperature-operating solid oxide fuel cell," *Chemistry of Materials*, vol. 22, no. 3, pp. 883–892, 2010.

[137] Z. Duan, Y. Min, A. Yan, Z. Hou, Y. Dong, M. Cheng, and W. Yang, "$Ba_{0.5}Sr_{0.5}Co_{0.8}Fe_{0.2}O_{3-\delta}$ as a cathode for IT-SOFCs with a GDC interlayer," *Journal of Power Sources*, vol. 160, pp. 57–64, 2006.

[138] H. Zhao, D. Teng, X. Zhang, C. Zhang, and X. Li, "Structural and electrochemical studies of $Ba_{0.6}Sr_{0.4}Co_{1-y}Ti_yO_{3-\delta}$ as a new cathode material for IT-SOFCs," *Journal of Power Sources*, vol. 186, no. 2, pp. 305–310, 2009.

[139] S. S. Bhella and V. Thangadurai, "Sintering effects on proton conductivity of Ta-doped $Ba_2(CaNb)_2O_6$ and its reactivity with SOFC cathodes," *Journal of The Electrochemical Society*, vol. 156, no. 5, pp. B634–B642, 2009.

[140] C. Jin, J. Liu, and J. Sui, "Sintering behavioral and electrochemical performances of LSM-BSB composite cathode for IT-SOFCs," *Journal of Electroceramics*, vol. 26, no. 1–4, pp. 74–77, 2011.

[141] K.-Z. Fung and T.-Y. Chen, "Cathode-supported SOFC using a highly conductive lanthanum aluminate-based electrolyte," *Solid State Ionics*, vol. 188, no. 1, pp. 64–68, 2011.

[142] T. Tzvetkoff and A. Girginov, "Corrosion of nickel , iron , cobalt and their alloys in molten salt electrolytes," *Journal of Materials Science*, vol. 30, pp. 5561–5575, 1995.

[143] J. Shao and K. K. Hansen, "Electrochemical NO_x reduction on an LSM/CGO symmetric cell modified by NO_x adsorbents," *Journal of Materials Chemistry A*, DOI: 10.1039/c3ta10901a, 2013.